The Role of Recurrently Observed Aneuploidy in Tumorigenesis

A Dissertation Presented By

Asad Aziz Lakhani

BA Honors, Biochemistry

University of Cambridge

Submitted to

The Cold Spring Harbor Laboratory School of Biological Sciences

In Partial Fulfillment of the Requirements for the

Degree of Doctor of Philosophy

in

Biological Sciences

Cold Spring Harbor Laboratory

March 2023

Dedicated to my harshest critic and most ardent supporter. Thank you for your endless encouragement of my scientific pursuits, and for going out of your way to get me the best education possible. Couldn't have gotten here without you, dad.

Summary

Nearly 90% of human tumors exhibit aneuploidy, an alteration in the copy number of whole chromosomes or chromosomal arms. Despite a century since the preliminary observation of aneuploidy in cancer, the exact mechanisms by which chromosomal variability contributes to tumorigenesis remain unclear. The simultaneous alteration in the dosage of hundreds of genes on the aneuploid chromosome means that identifying dosage-sensitive driver genes is difficult. This is further complicated by the technical challenge of inducing targeted chromosomal arm gain or loss, and of distinguishing the phenotypic effects of the aneuploid chromosome from effects of genomic instability.

To navigate these challenges, we developed a suite of tools called ReDACT: Restoring Disomy in Aneuploid cells using CRISPR Targeting. These chromosomal engineering techniques enable the elimination of specific aneuploidies from cancer genomes. Using ReDACT, we created a panel of isogenic cells that have or lack common aneuploidies across diverse cancer backgrounds. We engineered loss of trisomy 1q in models of ovarian (A2780) and gastric cancer (AGS), as well as mammary epithelial cells (MCF10A); loss of trisomy 8q in colorectal cancer cells (HCT116, RKO); and loss of trisomies 1q, 7p and 8q in melanoma (A2058) cells.

While loss of the aneuploid chromosome only had a mild effect on cellular proliferation, the aneuploidy-loss populations formed both fewer and smaller colonies under conditions of anchorage-independent growth in soft agar assays – a key hallmark of cancer. This effect was more severe for loss of 1q than for loss of 7p or 8q aneuploidy. A2780 and A2058 cells disomic for chromosome 1q failed to form tumors following subcutaneous xenografts in nude mice. However, we observed 1q regain in both *in vitro* proliferation assays and following xenografts, indicating an evolutionary pressure to re-establish aneuploidy

dosage. Furthermore, 1q loss impaired malignant transformation of MCF10A cells: 1q trisomic cells transduced with *HRAS*^{G12V} formed tumors, whereas 1q disomic cells did not.

Strikingly, HCT116 cells disomic for chromosome 8q showed a greater deficit in colony formation compared to loss of the oncogenic *KRAS*^{G13D} and *CTNNB1*^{pS45del} alleles. Similarly, RKO 8q-loss clones also exhibited a greater deficit in colony formation compared to loss of the two *BRAF*^{V600E} alleles. In fact, we observed chr12 gain in HCT116 8q disomy xenografts, which served to amplify *KRAS*^{G13D} and compensate for 8q loss. These results collectively highlight the importance of aneuploid chromosomes towards cancer phenotypes.

To identify dosage-sensitive genes present on chromosome 1q that may be driving 1q aneuploidy, we transcriptionally downregulated several candidates in parental, 1q trisomic cells, and identified the genes whose inhibition resulted in a proliferative defect. Of these, overexpression of *MDM4* and *MCL1* in 1q disomic cells resulted in a partial rescue of the colony-deficit phenotype. Our results suggest *MDM4* and *MCL1* act in a dosage-sensitive manner to downregulate *TP53* pathway activity and inhibit apoptosis respectively, thereby partially accounting for the oncogenic benefits of a 1q trisomy. Furthermore, we identify targeting of *UCK2*, a gene involved in the pyrimidine salvage pathway, as a therapeutic vulnerability in 1q aneuploid cells.

Overall, we demonstrate that specific aneuploidies play essential roles in tumorigenesis, raising the possibility that targeting these "aneuploidy addictions" could represent a novel approach for cancer treatment.

Acknowledgements

Foremost, I would like to thank my thesis advisor, Jason Sheltzer, for guiding me through this PhD. Your enthusiasm for this project, your willingness to explore new and interesting ideas, and your constructive feedback have all been critical to our collective success. Thank you for supporting my professional growth, especially outside academic bounds. I am also grateful to all members of the Sheltzer lab, past and present, who have provided advice, challenged hypotheses, and generally offered help and support. Special thanks to Erin Sausville and Kate Long for the many late-night meals and mid-TC conversations.

I would like to express my profound gratitude to Rob Martienssen for not only serving as the chair of my thesis committee, but also for providing a terrific lab environment and resources to continue my PhD at CSHL over the past year and a half. Thank you to all members of the Martienssen lab who have been extremely welcoming and supportive. I have tremendously enjoyed the camaraderie you have provided, and have been privileged to work alongside you.

I am also indebted to members of my thesis committee. Thank you to Dave Tuveson for being an excellent academic mentor – your pep talks have always left me highly motivated. And thank you to Chris Vakoc for your superb insights into my work – I have truly appreciated the refreshing perspective you bring to cancer biology. Thanks also to Neil Ganem for generously taking the time to serve as the external examiner for this thesis.

It would be remiss to overlook the contributions of everyone who has been helpful every time I have encountered hurdles, especially over the past couple of years. I am deeply grateful to the CSHL School of Biological Sciences for the incredible support you provide for all students. It has been a source of comfort to know I can drop by Urey at any time, and

someone will be available to help out. Special thanks to Alex Gann for having my back, and to Alyson Kass-Eisler for having answers to all things CSHL. And thank you to Sydney Gary for helping minimize any disruptions to my work during the Sheltzer lab's move to Yale. I am grateful to Ken Chang and his lab for allowing me to continue my tissue culture work in Cairns. Thanks also to the Dos Santos lab, especially Mike Ciccone, for always being available to resolve any logistical issues I have encountered during periods of nomadic existence in between labs and storage spaces. And thank you to Tobias Janowitz, for your informal mentorship and refreshingly honest discussions on all things academia.

Over the past couple of years, I have been incredibly lucky to work with a truly remarkable group of people towards improving access to biotech. I am grateful to all members of Nucleate New York leadership for the generosity of your time and effort in making such a unique program work, and I am privileged to work alongside you. Thanks also to members of BEC leadership, and to the Office of DEI, for your assistance in bringing such programs to CSHL.

Long Island can be a bit isolating, especially for someone who grew up in a sprawling metropolis like Karachi. Thank you to Khatidja Merchant for being my link to the comforts of home, and for providing an endless supply of lovingly home-cooked meals. Thanks also to my extended family in Dallas for regularly checking in, and for always having their doors open to me. And thank you to the lads: Rizwaan Mohammed, Hashi Ibrahim-Hashi, and Will Clare. I still marvel at our hours long conversations (even if they're 85% football), and am very grateful for your friendship. I look forward to more ambitious adventures in far flung corners of the globe.

To all my classmates who made the transition to life on Long Island fun: it has been reassuring to have gone through our PhD journeys together, and to share not only in

accomplishments, but more importantly in struggles. Special thanks to Teri Cheng – classmate, landlord, house mate, and lab mate – for being a brotherly companion through it all, and for making an excellent effort at refining my tastes, be they in classical music, food, or cologne. And of course, I am deeply indebted to Alexa Pagliaro. You have not only been a provider of remarkably sage advice, but also an incredible friend and confidante. Thank you for doing your darndest to fix my poor culinary and procrastination habits, and for being an amazing source of care and support.

I wouldn't be here without the unconditional love and support of my family. Thank you, mom, for checking in every day, even when we have little new to share. Thank you, Sara, for remaining the atypical little sister: your brusque honesty and deep empathy are a rare combination, and one I highly appreciate. And thank you dad, for remaining a steadfast source of support, even when I may disappoint you. To my grandparents, uncles, aunts, and cousins, it is a true pleasure to visit you every chance I get. I will remain eternally grateful for all your love and support. Thank you.

Table of Contents

Commonly Used Abbreviations

BUTTE:	Bounds of Time Until Expansion
CIN:	Chromosomal Instability
CRISPR:	Clustered Regularly Interspaced Short Palindromic Repeats
CRISPRi:	CRISPR Interference
CRISPRa:	CRISPR Activation
EPO-GEMM:	Electroporation-based Genetically Engineered Mouse Model
GSEA:	Gene Set Enrichment Analysis
HAC:	Human Artificial Chromosome
HSV-TK:	Herpes Simplex Virus Thymidine Kinase
MACHETE:	Molecular Alteration of Chromosomes with Engineered Tandem Elements
MMCT:	Microcell Mediated Chromosome Transfer
ORF:	Open Reading Frame
ReDACT:	Restoring Disomy in Aneuploid Cells using CRISPR Targeting
ReDACT-NS:	ReDACT-Negative Selection
ReDACT-TR:	ReDACT-Telomere Replacement
ReDACT-CO:	ReDACT-CRISPR Only
SAC:	Spindle Assembly Checkpoint
SCNA:	Somatic Copy Number Alteration
SMASH:	Short Multiply Aggregated Sequence Homologies
SNP:	Single Nucleotide Polymorphism
TALEN:	Transcription Activator-Like Effector Nuclease
TCGA:	The Cancer Genome Atlas
WGD:	Whole Genome Duplication
WGS:	Whole Genome Sequencing

Figures and Tables

Chapter 1: Introduction

“Nothing in life makes sense except in the light of evolution”
Theodosius Dobzhansky

Overview

David Hansemann first observed mitotic chromosomal mis-segregation in epithelial cancers more than 130 years ago (Hansemann 1890), but it was another 24 years before Theodor Boveri and Marcella O'Grady postulated that this chromosomal variability drove tumor development (McKusick 1985; Bignold et al. 2006). Still, a century later, the functional causes and consequences of aneuploidy in cancer development, maintenance, and metastasis remain elusive.

It is important to distinguish the study of aneuploidy from overall changes in ploidy and from chromosomal instability (CIN). Polyploidy refers to the gain of an equal set of all chromosomes. While such whole genome doubling events may also be the starting point for generation of aneuploid karyotypes (Lens and Medema 2019), the term "aneuploidy" refers to an unbalanced gain or loss of either whole chromosomes or chromosomal arms (Ben-David and Amon 2020). CIN, meanwhile, is an elevated rate of chromosomal mis-segregation during cell division. While CIN can lead to aneuploidy, not all aneuploid cells exhibit CIN (Gordon et al. 2012), as the aneuploid karyotype may nevertheless remain stable.

Several excellent reviews have recently covered the various facets of aneuploidy biology, including its causes and consequences (Gordon et al. 2012; Santaguida and Amon 2015; Knouse et al. 2017; Chunduri and Storchová 2019), its context-dependent role (Ben-David and Amon 2020; Vasudevan et al. 2021), and the interplay and distinctions between chromosomal instability (CIN) and aneuploidy (van Jaarsveld and Kops 2016; Lukow and Sheltzer 2022). The history of aneuploidy research has included diverse model systems, beginning with the study of sea urchin embryos (Bignold et al. 2006) and encompassing yeast, chicken, and mouse cells (Chunduri and Storchová 2019; Ben-David and Amon 2020; Vasudevan et al. 2021). While studies in all model systems have offered tremendous insight

into the underlying biology, this thesis is focused on recurrently observed aneuploidy in human cancer.

Aneuploidy in Cancer

Aneuploidy affects a greater percentage of the cancer genome than any other somatic genetic alteration (Taylor et al. 2018). While somatic copy-number alterations (SCNAs) are present in 99% of tumors (Watkins et al. 2020), the most frequent individual focal copy number alterations (MYC amplifications and CDKN2A/B deletions) are observed in just 14% of cancer specimens (Beroukhim et al. 2010). Meanwhile, an analysis of patient datasets from The Cancer Genome Atlas (TCGA) revealed the most frequent chromosomal arm alterations were present in over 33% of tumors (chromosome 8p and 17p loss, chromosome 8q gain) (Figure 1), and 88% of all tumors exhibited aneuploidy (Taylor et al. 2018). A typical tumor possesses a median of 3 gains and 5 losses of chromosomal arms (Ben-David and Amon 2020). This means aneuploidy is observed at 30 times the expected frequency when assessed by an inverse length distribution compared to focal SCNAs, and affects 25% of the genome in a typical cancer sample – only 10% is affected by SCNAs (Beroukhim et al. 2010). Thus, not only does aneuploidy play a critical role in shaping the cancer genome, but tumors must also select for favorable aneuploid karyotypes, and chromosomal gain or loss must provide a fitness advantage beyond that provided by focal amplifications or deletions (Davoli et al. 2013).

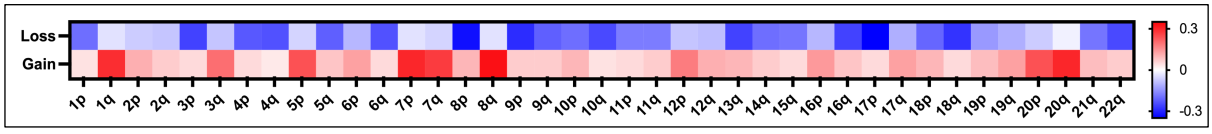

Figure 1: Chromosomal Arm Level Alterations Across Patient Tumor Samples
This figure was adapted from Taylor et al. 2018. The study used data from 10,522 genomes from TCGA to assess changes in chromosomal copy number across 33 subtypes of cancer.

This is reflected in the tumor type distribution of aneuploidy (Figure 2). Gain of chromosome 12p is observed across the vast majority of germ cell tumors (Taylor-Weiner et al. 2016), as is chromosome 7 gain and chromosome 10 loss in glioblastomas without IDH mutations (Taylor et al. 2018). Aneuploidy of chromosome 1q, meanwhile, marks multiple myeloma and is also frequently observed in breast, lung, and liver tumors (Schmidt et al. 2021), and an extra copy of chromosome 8 is often found in leukemia and myelodysplastic syndrome (Cuneo et al. 1998; Oudat et al. 2001). Moreover, arm losses from chromosomes 1, 2, 11 and 18 are recurrently observed in pituitary adenomas (Bi et al. 2017). Not only can different cancer types be identified by their aneuploidy profiles (Patkar et al. 2021), but copy number alterations also harbor significantly greater prognostic power than mutational profiles (Shukla et al. 2020; Smith and Sheltzer 2022).

Remarkably, aneuploidy can also serve as a biomarker for therapeutic response. Low grade gliomas marked by co-deletion of chromosomes 1p and 19q have been found to respond better to specific chemotherapy regimens (Cairncross et al. 2013), and we recently reported trisomy of chromosome 1q could serve as a biomarker for use of *UCK2*-targeting drugs (Chapter 2) (Girish*, Lakhani* et al. 2023). A retrospective analysis of melanoma patients treated with immune checkpoint blockade showed a negative correlation between SCNA burden and patient response, suggesting SCNAs could be used as biomarkers for therapeutic efficacy (Davoli et al. 2017). Co-occurring patterns of arm alterations can also identify potential synthetic lethality and resistance mechanisms (Shukla et al. 2020). Aneuploidy can thereby not only be used for characterization of tumor type and grade, but also serve as an indicator of patient response to therapy.

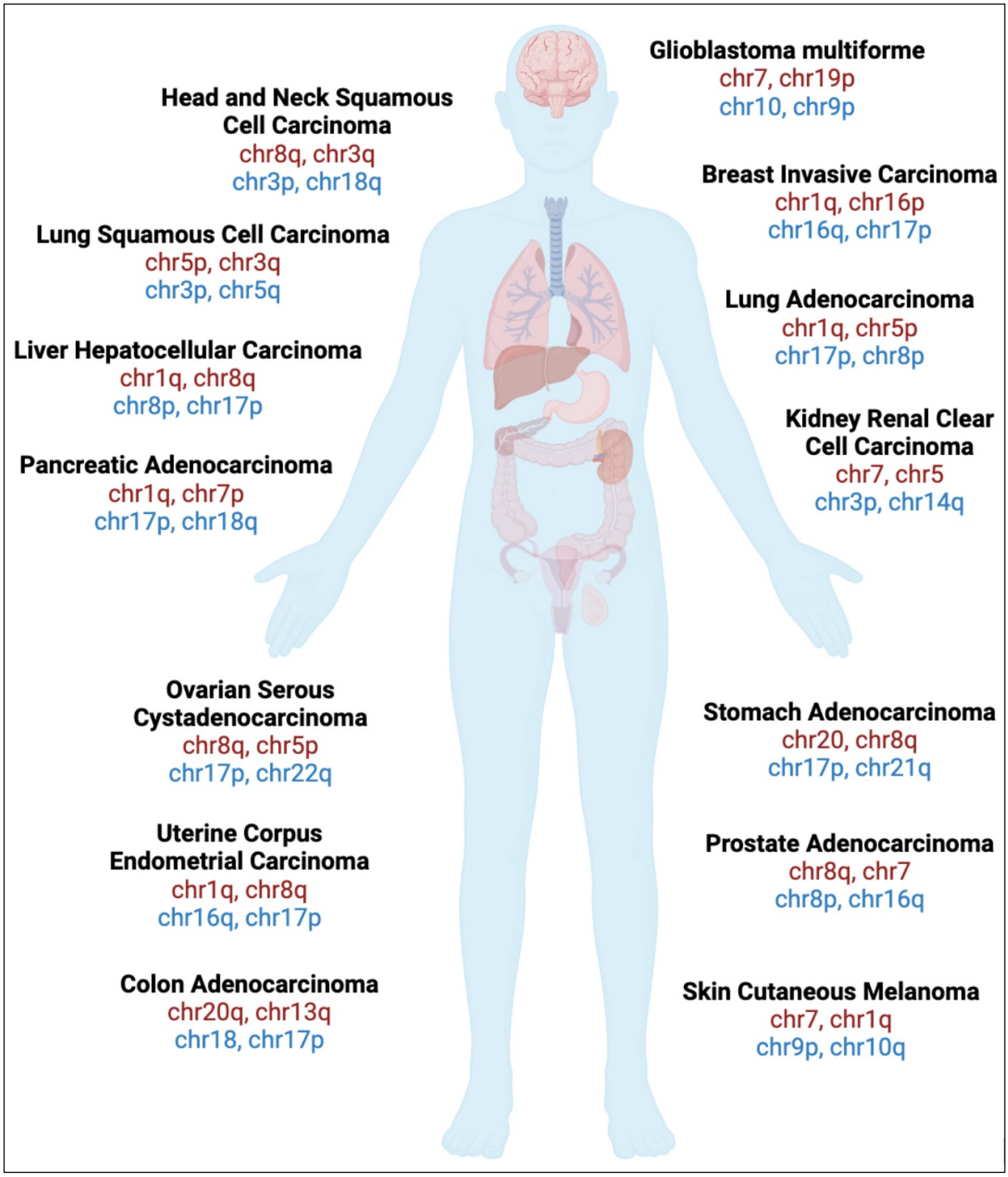

Figure 2: Frequently Observed Aneuploidies Across Human Cancer
The two most frequently observed chromosomal gains (red) and losses (blue) across 14 different cancer types are highlighted. The data for this figure was obtained from Taylor et al. 2018. The study analyzed 10,522 genomes from The Cancer Genome Atlas (TCGA) to assess changes in chromosomal copy number across 33 subtypes of cancer.

When Does Aneuploidy Arise?

Karyotypic dissection at distinct tumor grades has helped reveal early and late arising copy number changes. A recent study of nearly 400 multi-sampled tumors across 22 cancer types interrogated the evolutionary timescale of SCNAs (Watkins et al. 2020). Loss of 17p13.1, the locus harboring *TP53*, was found to occur early in 9 out of 13 tumors, suggesting this alteration was necessary for both tumorigenesis and tolerance of subsequent whole genome duplication. Similarly, gain of the loci harboring *ERBB2* and *EGFR* in $HER2^+$ breast cancer and lung adenocarcinoma respectively, was also found to occur early. Loss of the *CDKN2A* locus occurred early in ER^+ and $HER2^+$ breast cancer, but late in renal clear cell carcinoma. Meanwhile, losses of *TP53* and *STK11* loci in lung adenocarcinoma were found to both occur early and persist into metastasis, suggesting these alterations define the tumors' metastatic potential (Watkins et al. 2020).

Aneuploid chromosomes are also gained or lost within defined periods of tumor evolution, with early gains suggestive of a fundamental role in driving tumor progression. Gain of chromosome 3q is frequently observed in advanced cervical cancer, and marks the transition from severe dysplasia to invasive carcinoma (Heselmeyer et al. 1996, 1997). Meanwhile, chromosome 3p deletion is observed across the respiratory tract in the earliest stages of lung cancer pathogenesis (Sundaresan et al. 1992; Hung 1995). In fact, the frequency and length of genomic deletion was found to scale with severity of histopathological preneoplastic changes (Wistuba et al. 2000). Similarly, gains of chromosomes 8q, 13q and 20q, and loss of chromosomes 18q and 17p, are frequently observed in colorectal cancer (Bomme et al. 1994; Muleris et al. 1994), and found to be more frequent in carcinomas compared to adenomas (Meijer et al. 1998). Indeed, a subtype of breast cancer is defined by chromosome 1q gain and 16q loss (Dutrillaux et al. 1990; Pandis et al. 1992), which have been implicated in

the genesis of both ductal and lobular carcinomas (Privitera et al. 2021). The progression from Barret's esophagus to esophageal carcinoma is also associated with aneuploidy (Ross-Innes et al. 2015), and trisomy of chromosome 5 may promote metastasis by inducing a partial epithelial-to-mesenchymal transition (Vasudevan et al. 2020). Thus, aneuploidy can exert a profound influence on the tumor genome during the earliest stages of cancer development, and karyotypic alterations are associated with increased tumor invasiveness and aggressiveness.

Recently developed computational frameworks analyzing hundreds of tumors have supplemented these findings. An analysis of over 2600 tumors, for example, suggested early oncogenesis is defined by mutations and copy number alterations in a constrained set of genes or chromosomes (PCAWG Evolution & Heterogeneity Working Group et al. 2020). Single copy gains of chromosomes 7, 19, or 20 in glioblastoma, which are observed in over 90% of patients, occur within the first 10% of molecular time, and loss of chromosomes 2, 6, 11 and 16 precedes *MEN1* and *DAXX* driver mutations in pancreatic neuroendocrine tumors (PCAWG Evolution & Heterogeneity Working Group et al. 2020). A separate method for assessing chromosomal alterations before or after population expansion confirmed chromosome 5q was gained early in colorectal adenocarcinoma, thereby amplifying *APC*, while chromosome 1q gain amplifying *AKT3* also occurred early in breast cancer (Wang et al. 2022). These findings support a model whereby specific aneuploid chromosomes can be drivers for tumorigenesis, and chromosomal gains occur in punctuated bursts at similar molecular times, resulting in beneficial karyotypes for clonal population growth (PCAWG Evolution & Heterogeneity Working Group et al. 2020).

As mentioned above, whole genome duplication (WGD) can elevate rates of aneuploidy. Over 30% of tumors exhibit WGD (Bielski et al. 2018), and WGD is associated

with a higher rate of every other type of SCNA (Zack et al. 2013). WGD can also mark a shift in bias from chromosomal gain to chromosomal loss (Shukla et al. 2020). This suggests chromosomal gain is preferred very early on during tumor development, and chromosomal loss occurs following WGD, when multi-gene deletion can be better tolerated in a polyploid background (Shukla et al. 2020). Combined, these observations highlight the crucial role of aneuploidy in tumorigenesis, with early chromosomal gains driving malignancy, and later chromosomal gains and losses further optimizing the karyotypic landscape for tumor expansion.

Dosage-Sensitive Genes

SCNAs and aneuploidy, by definition, simultaneously alter the expression of multiple genes. The introduction of extra chromosomes into diploid cells, however, is not always beneficial for cancer cell fitness (Stingele et al. 2012; Sheltzer et al. 2017), disrupting both the transcriptome and proteome (Torres et al. 2008). The prevalence of SCNAs and aneuploidy in cancer therefore suggests that the simultaneous gain or loss of multiple genes must not only compensate for the negative consequences of having an aneuploid karyotype, but also provide an additional fitness advantage. Two recent experimental examples illustrate this point well. First, a 4 Mb deletion within a mouse model, syntenic to human 17p13.1 (locus of tumor suppressor gene *TP53*), accelerated lymphoma and leukemia development compared to deletion of *Trp53* (homologue to human *TP53*) alone (Liu et al. 2016). Second, deletion of the *CKDN2A* cluster on chr9p in a syngeneic mouse model of pancreatic cancer mitigated suppression of proliferation, while co-deletion of the neighboring *IFN* cluster also facilitated immune evasion, thus synergizing to evade both cell intrinsic and extrinsic tumor suppressor

mechanisms (Barriga et al. 2022). Therefore, multiple dosage-sensitive genes are responsible for the gain or loss of a SCNA.

The same is also true for aneuploidy. Deletions of mouse orthologues of human genes present on chromosome 8p in a model of hepatocellular carcinoma showed multiple genes cooperatively inhibit tumorigenesis, and their deletion can synergistically promote tumor development (Xue et al. 2012). Deletion of chromosome 9p in low grade gliomas was also attributed to several genes, which in turn can serve as subtype-specific prognostic biomarkers for tumor aggressiveness and patient survival (Roy et al. 2016). The simultaneous copy number gain of *RAD21* alongside *MYC* in *EWS-FLI1* driven Ewing sarcomas was found to be crucial for the oncogenic benefits of trisomy 8, as *RAD21* dampened replication stress caused by the fusion oncoprotein (Su et al. 2021). Remarkably, human *MYC* expression from mouse chromosome 6 in a model of T cell lymphoma altered the acquired karyotype. While chromosome 15 gain (syntenic to human chromosome 8q) during tumor development was attributed to the presence of *MYC*, transgenic *MYC* expression from chromosome 6 resulted in its gain. However, chromosome 15 aneuploidy was still observed, and attributed to the presence of *RAD21 (*Trakala et al. 2021*)*. These results suggest that while aneuploidies may be partially driven by oncogenes or tumor suppressors, changes in expression of multiple dosage-sensitive genes on aneuploid chromosomes are required to fully explain the observed phenotypes.

That idea is supported by correlational analyses of oncogenes, tumor suppressors, essential genes, and aneuploidy. A study analyzing over 8000 tumor-normal pairs showed the complex patterns of aneuploidy observed in cancers could be attributed to the interplay between haploinsufficiency and triplosensitivity, i.e. genes whose dual copy expression is essential for viability but whose copy number gain may introduce a significant fitness cost

(Davoli et al. 2013). It should be noted, however, that numerous significantly recurrent SCNAs do not harbor known oncogenes or tumor suppressors (Zack et al. 2013), and the same is true for frequently observed aneuploidy. This may partially be explained by co-occurrence and mutual exclusivity relationships between aneuploid chromosomes and somatic mutations. For example, loss of chromosome 3q and gain of chromosome 16p co-occurs in WGD^- colon cancers, but was found to be mutually exclusive in WGD^+ samples. Meanwhile, chromosome 1p loss and chromosome 5p gain co-occurs in WGD^+ glioblastoma, but is mutually exclusive in WGD^- tumors (Prasad et al. 2022). Chromosome 1q gain and *TP53* mutation, and *KRAS* mutation and chromosome 18q gain, are both mutually exclusive as well (Chapter 2) (Girish*, Lakhani* et al. 2023). While interrogation of patient datasets has allowed such patterns to be well documented, they are nevertheless correlational. Experimentally validated examples of SCNA or aneuploidy co-occurrence and mutual exclusivity are still very limited. Investigations focused on the experimental dissection of these relationships – in particular the necessity, sufficiency, and developmental timing of a SCNA/aneuploidy and its interplay with other cancer alterations – are needed to better understand the molecular underpinnings of these correlational patterns.

Experimental Manipulation of Chromosomes

The standard tools of molecular genetics have been successfully used to evaluate the functional role of oncogenes and tumor suppressors over the past few decades. Invariably, a thorough demonstration of gene functionality involves its downregulation to assess necessity for an observed phenotype, and its upregulation to assess sufficiency. Downregulation has been accomplished through genetic, transcriptional and proteomic manipulation, for example using homologous recombination (Shirasawa et al. 1993) or CRISPR/Cas9 (Cong et al. 2013),

RNA (Hannon and Rossi 2004) or CRISPR interference (Larson et al. 2013), and PROTACs (Zhou et al. 2000) (Li et al. 2022) or small molecule drugs (Zhong et al. 2021) respectively. Meanwhile, upregulation has been accomplished through introduction of overexpression constructs, either virally into DNA (Siwko et al. 2008), through transient expression of cDNA or ORFs (Hu and Zhang 2016; Sack et al. 2018), or more recently using CRISPR activation (Joung et al. 2022). Application of similar techniques to aneuploid chromosomes in human cells, however, has remained technically challenging due to the sheer size of genomic manipulation required. Regardless, several techniques have historically been used to assess contributions of aneuploidy to tumorigenic processes. Recently, the repertoire for targeted chromosomal manipulation of human chromosomes has significantly expanded (Figure 3, Table 1).

Models of Chromosomal Gain

Microcell-mediated chromosome transfer (MMCT) was developed in the 1970s by combining the technologies of microcell formation and cell fusion to introduce chromosomes from donor to recipient cells (Ege and Ringertz 1974; Veomett et al. 1974). At first, this allowed the introduction of a few chromosomes into exogenous cells through fusion of mouse (Fournier and Ruddle 1977) or chicken (Dieken and Fournier 1996) microcells with Chinese hamster ovary (CHO) or human HeLa cells. A major advance in studying clinically-relevant aneuploidy came at the turn of the century with the development of a library of mouse A9 cell hybrids containing single copies of human chromosomes (Inoue et al. 2001). This, in turn, facilitated the generation of isogenic human cell lines that differed in the copy number of a single aneuploid chromosome, which have since allowed examination of the oncogenic and tumor suppressive contributions of aneuploid chromosomes (Stingele et al. 2012; Passerini et

al. 2016; Sheltzer et al. 2017; Kneissig et al. 2019). The history of MMCT and its current practice have been further reviewed elsewhere (Doherty and Fisher 2003; Suzuki et al. 2020).

However, it should be noted that exogenous introduction of an extra chromosome into a cellular background that hasn't adapted to aneuploidy is not necessarily reflective of aneuploidy evolution within tumors. Numerous studies have recently described the consequences of chromosomal sequestration within micronuclei and their subsequent integration into the parent genome, including massive chromosomal rearrangements and chromothripsis (Soto et al. 2018; Kneissig et al. 2019), and activation of immunostimulatory cGAS-STING signaling (Mackenzie et al. 2017; Bakhoum et al. 2018). Therefore, the interpretation of phenotypic consequences of aneuploidy using MMCT-derived models should be undertaken with careful consideration of these effects.

The isolation of aneuploid cells from individuals affected by disease or developmental abnormalities provides another avenue for assessing the consequences of aneuploidy. For example, isolation of trisomy 13, 18 and 21 cells from individuals affected by Patau, Edwards or Down Syndrome respectively, has provided insights into cellular processes affected by the extra chromosome (Kimura et al. 2005; Hwang et al. 2019; Zhu et al. 2019). Similarly, a comparison between aneuploid and non-aneuploid cell lines and tumors from cancer patients has revealed common patterns of genomic, transcriptional and proteomic dysregulation (Davoli et al. 2013; Taylor et al. 2018; Schukken and Sheltzer 2022). However, only the three autosomal trisomies mentioned above are embryonically tolerated, and a lack of matched genetic controls devoid of the aneuploid chromosome introduces many confounding variables into any analysis.

Inducing Chromosomal Mis-segregation

Induction of chromosomal mis-segregation is another useful technique for the generation of aneuploid populations. Various components of the spindle machinery have historically been manipulated to trigger mis-segregation, including microtubules (Cimini et al. 1999; Thompson and Compton 2008), and topoisomerase II (Clarke et al. 1998). However, the prolonged mitotic arrest caused by spindle disruption can cause DNA damage, confounding any assessment of the consequences of aneuploidy (Orth et al. 2012). To minimize DNA damage, transient inhibition of Mps1, occasionally preceded by inhibition of CENP-E, has been recently used for chromosomal mis-segregation (Qian et al. 2010; Sheltzer et al. 2017; Soto et al. 2018; Lukow et al. 2021; Ippolito et al. 2021). These methods generate random aneuploidies, which can subsequently be isolated through single cell cloning and further interrogated for phenotypic consequences.

Within the past year, a number of new methods have been devised for targeted chromosomal mis-segregation. Broadly, they rely on altering the forces acting on chromosomes during mitosis by targeting chromosome-specific sequences. KaryoCreate, for example, utilizes sgRNAs targeting unique centromeric α-satellite repeats to recruit dCas9 fused to a mutant kinetochore scaffold protein. This alters the normal error-correction process mediated by Aurora B and PP1, resulting in targeted chromosomal mis-segregation (Bosco et al. 2022). Meanwhile, dCas9 fused to either the kinetochore-nucleating domain of CENP-T (Tovini et al. 2022) or *Physcomitrella patens's* Kinesin14VIb motor protein (Truong et al. 2022), and targeted to repetitive endogenous arrays present on chromosomes 1 and 9, also achieved mis-segregation of those chromosomes. These techniques therefore offer the ability to isolate clonal populations of cells that either gain or lose the mis-segregated chromosomal arm.

Targeted Chromosomal Arm Loss

Deletion of large genomic fragments has been facilitated by the development of technologies for creation of dsDNA breaks at precise loci, in particular TALENs and CRISPR/Cas9. In turn, this has allowed induction of targeted chromosomal arm loss. For example, chromosome 8p loss of heterozygosity was engineered in mammary epithelial cells using two pairs of TALENs to induce loss of a 33 Mb segment (Cai et al. 2016). Provision of an artificial telomere to cap a CRISPR-induced dsDNA break subsequently facilitated both telomere truncation of chromosome 21 (Uno et al. 2017) and targeted deletion of chromosome 3p (Taylor et al. 2018). Recently, it was reported that chromosomal loss could be a consequence of CRISPR/Cas9 induced DNA breaks in embryonic stem cells (Zuccaro et al. 2020; Papathanasiou et al. 2021). This led to CRISPR use for the explicit purpose of inducing chromosomal arm loss in clonal populations of cells (Adell et al. 2022). We expanded the suite of tools through the introduction of three new techniques collectively called ReDACT: Restoring Disomy of Aneuploid cells using CRISPR Targeting (Chapter 2) (Girish*, Lakhani* et al. 2023). Arm loss was induced by creating dsDNA breaks at centromere-proximal regions, either using CRISPR by itself (ReDACT-CO), alongside an artificial telomere (ReDACT-TR), or by selecting against an integrated drug selection marker (ReDACT-NS). This allowed generation of isogenic populations of cells differing in aneuploidies of chromosomes 1q, 7p and 8q, and subsequent assessment of the phenotypic consequences of aneuploidy loss (Chapter 2) (Girish*, Lakhani* et al. 2023).

Technique Description	Intended Consequence	Reference(s)
Microcell-Mediated Chromosome Transfer (MMCT): fusion of mouse A9 cells containing individual human chromosomes with human cells	Chromosome gain	(Inoue et al. 2001; Stingele et al. 2012)
KaryoCreate: dCas9-KNL1$^{RVSF/AAAA}$ targeted to centromeric α-satellite repeats using chromosome-specific sgRNAs	Arm gain or loss	(Bosco et al. 2022)
dCas9 fused to CENP-TΔC or Kinesin14VIb, targeted to repetitive endogenous arrays on chromosomes 1 & 9	Arm gain or loss	(Tovini et al. 2022; Truong et al. 2022)
Two pairs of TALENS spanning intended deletion	Arm loss	(Cai et al. 2016)
Chromosome truncation using an artificial telomere	Arm loss	(Uno et al. 2017; Taylor et al. 2018; Girish*, Lakhani* et al. 2023)
Negative selection of aneuploid chromosome	Arm loss	(Girish*, Lakhani* et al. 2023)
CRISPR-induced dsDNA break at centromere-proximal location	Arm loss	(Zuccaro et al. 2020; Adell et al. 2022; Girish*, Lakhani*, et al. 2023)

Table 1: Summary of Methods for Targeted Chromosomal Manipulation in Human Cells

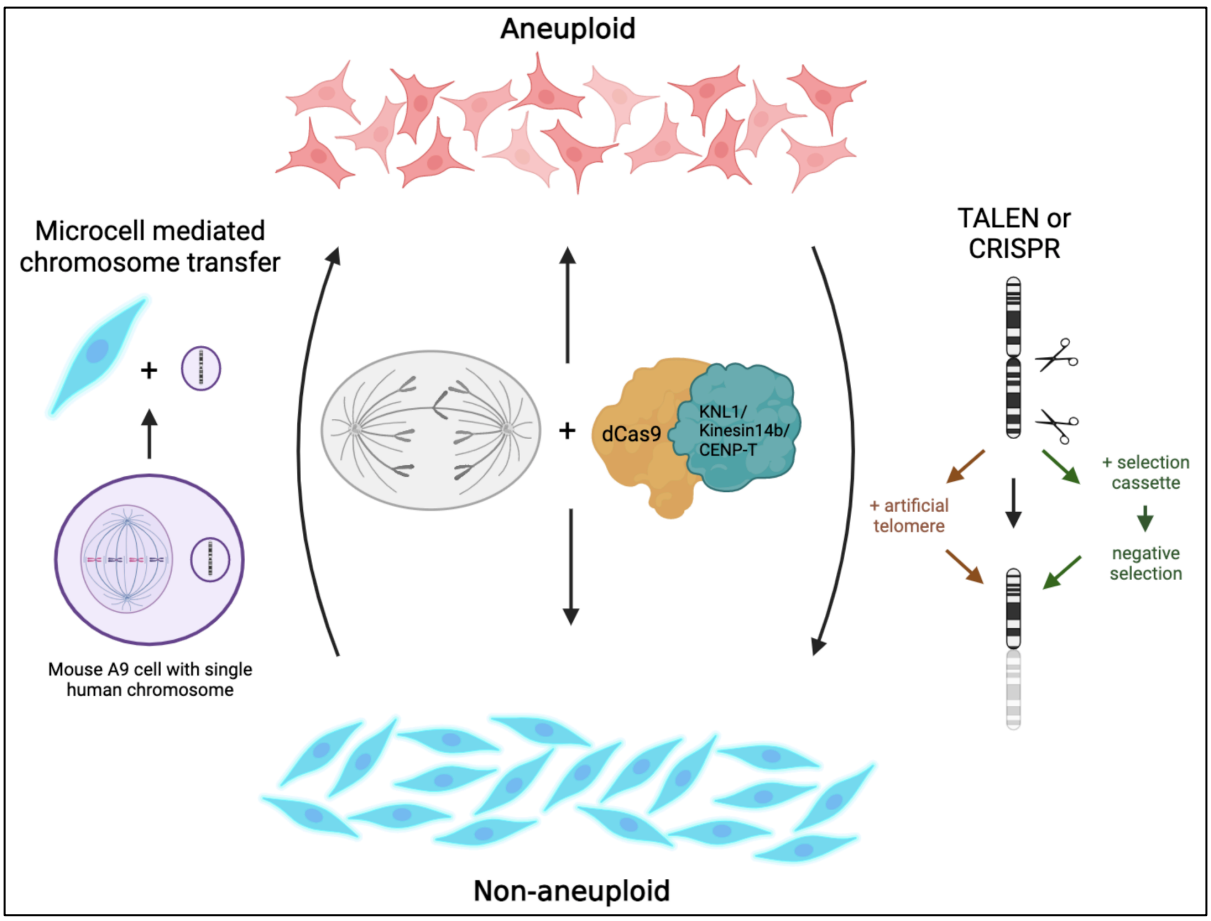

Figure 3: Methods for Targeted Chromosomal Gain or Loss
Extra chromosomes can be introduced into cells using microcell mediated chromosome transfer (MMCT). TALENs and CRISPR/Cas9 can be used to induce targeted chromosomal arm deletions, which may be facilitated by artificial telomeres or negative selection cassettes. dCas9 fused to a component of the mitotic machinery and targeted to unique chromosomal repeats can induce mis-segregation. All techniques can be used for the generation of genetically-matched lines differing in an aneuploid chromosome.

These methods combined offer the opportunity, for the first time, to dissect the contribution of each aneuploid chromosome to any cancer phenotype. While a comprehensive study of all clinically relevant aneuploid chromosomes – either individually or in commonly observed combinations – will undoubtedly require a monumental effort, there is tremendous potential for discovery of new cancer biology.

Thesis Outline

This thesis addresses three key facets of aneuploidy in cancer. Foremost is the development of novel tools for the targeted elimination of individual chromosomal arms to generate isogenic lines that differ in a single aneuploid chromosome. Second is the assessment of phenotypic consequences upon loss of an aneuploid chromosome. Third is the identification of dosage-sensitive genes that may drive chromosomal gain.

Chapter 2 is reprinted from a bioRxiv preprint (Girish*, Lakhani*, et al. 2023). In it, we show recurrently observed aneuploidy exhibits characteristics similar to oncogenes in cellular models of cancer. Chromosome 1q is gained early in tumor development, and an investigation of patient datasets highlights mutual exclusivity relationships between aneuploidy and driver oncogene mutations (Figure 1). We report a new suite of tools called ReDACT: Restoring Disomy in Aneuploid cells using CRISPR Targeting, which allow the targeted deletion of chromosome 1q in diverse cancer backgrounds, and show this results in compromised tumorigenicity (Figure 2). We also delete chromosomes 7p and 8q (Figure 3), and demonstrate not all aneuploidies are created equal – loss of trisomy 1q hampers malignancy to a greater extent compared to loss of trisomy 7p or 8q. This is also reflected in the likelihood of aneuploidy regain, in both *in vitro* and *in vivo* settings (Figure 4). We trace the loss of trisomy 1q phenotype to *MDM4*, a negative regulator of *TP53* present on chromosome 1q, and show trisomy 1q is mutually exclusive with *TP53* mutation (Figure 5). Finally, we identify increased sensitivity to *UCK2* targeting drugs in trisomy 1q (Figure 6), suggesting 1q aneuploidy may serve as a biomarker for therapeutic response.

Chapter 3 expounds on results shown in Chapter 2. I show trisomy 1q is able to outcompete disomy 1q in cellular competition assays (Figure 2), and present dosage-sensitive drivers for 1q gain other than *MDM4* (Figure 2). I also highlight the distinction between

exogenous and endogenous chromosomal regain, and demonstrate that endogenous regain is sufficient to rescue the 1q loss growth deficit (Figure 3). Then, I report results from another 8q-loss model – RKO – which highlights the complexities of researching aneuploidy (Figure 4). I also directly compare loss of aneuploidy to deletion of key oncogenic drivers (Figure 5). Finally, I identify heretofore unreported dosage-sensitive drivers for 8q trisomy in colon cancer cells (Figure 6). These results thereby lay the groundwork for future investigations.

Chapter 4 offers a summary of the experimental results shown in Chapters 2 and 3, and suggests future directions for study. I also recap the history of the oncogene addiction paradigm, and place our results in that context, thereby lending credence to our suggestion of "aneuploidy addiction" as a novel framework for assessing cancer-related aneuploidy.

Attribution

With the exceptions highlighted below, all work reported here is my own.

Chapter 2 was a collaborative effort (all authors are listed on page 33). I was the sole contributor for Figures 3E-H, 4G-H and 6E-F, as well as Supplementary Figures S3C, S4C, S5, S6C, S6E, S7B-C, S8D-E, S9C, and S10C. I also contributed to Figures 2A-D, 3A, 5I, 5L, and 5N, as well as Supplementary Figures S3A, S6B, S8A, and S14F.

For Chapter 3, Vishruth Girish and Sarah Thompson contributed to Table 1, and Vishruth Girish and Erin Sausville contributed to Figures 2a-c. All other work is my own.

Chapter 2: Oncogene-Like Addiction to Aneuploidy in Human Cancers

Chapter 2 is reproduced, with minor modifications, from Girish*, Lakhani* et al., bioRxiv, 2023 http://biorxiv.org/lookup/doi/10.1101/2023.01.09.523344

Supplementary Tables are available online

Oncogene-like addiction to aneuploidy in human cancers

Vishruth Girish[1,2*], Asad A. Lakhani[3*], Christine M. Scaduto[3†], Sarah L. Thompson[1†], Leanne M. Brown[1], Ryan A. Hagenson[1], Erin L. Sausville[3], Brianna E. Mendelson[1], Devon A. Lukow[1], Monet Lou Yuan[3], Pranav K. Kandikuppa[1], Eric C. Stevens[1], Sophia N. Lee[1], Barbora Salovska[1], Wenxue Li[1], Joan C. Smith[1], Alison M. Taylor[4], Robert A. Martienssen[3,5], Yansheng Liu[1], Ruping Sun[6], Jason M. Sheltzer[1#]

1. Yale University School of Medicine, New Haven, CT 06511

2. Johns Hopkins University School of Medicine, Baltimore, MD 21205

3. Cold Spring Harbor Laboratory, Cold Spring Harbor, NY 11724

4. Columbia University School of Medicine, New York, NY 10032

5. Howard Hughes Medical Institute, Cold Spring Harbor Laboratory, Cold Spring Harbor, NY, USA

6. Department of Laboratory Medicine and Pathology, University of Minnesota, Minneapolis, MN 55455

* Equal contribution

† Equal contribution

To whom correspondence may be addressed. Email: Jason.Sheltzer@yale.edu.

Abstract

Most cancers exhibit aneuploidy, but its functional significance in tumor development is controversial. Here, we describe ReDACT (Restoring Disomy in Aneuploid cells using CRISPR Targeting), a set of chromosome engineering tools that allow us to eliminate specific aneuploidies from cancer genomes. Using ReDACT, we created a panel of isogenic cells that have or lack common aneuploidies, and we demonstrate that trisomy of chromosome 1q is required for malignant growth in cancers harboring this alteration. Mechanistically, gaining chromosome 1q increases the expression of *MDM4* and suppresses *TP53* signaling, and we show that *TP53* mutations are mutually-exclusive with 1q aneuploidy in human cancers. Thus, specific aneuploidies play essential roles in tumorigenesis, raising the possibility that targeting these "aneuploidy addictions" could represent a novel approach for cancer treatment.

Introduction

Chromosome copy number changes, otherwise known as aneuploidy, are a ubiquitous feature of tumor genomes (Taylor et al. 2018; Gordon et al. 2012). While the pervasiveness of aneuploidy in cancer has been known for over a century (Boveri 2008; Hardy and Zacharias 2005), the role of aneuploidy in tumor development has remained controversial (Vasudevan et al. 2021; Ben-David and Amon 2020; Sheltzer and Amon 2011; Weaver and Cleveland 2006). Chromosome gains have been proposed to serve as a mechanism for increasing the dosage of tumor-promoting genes that are found within altered regions (Davoli et al. 2013; Sack et al. 2018). However, proof of this hypothesis is lacking, and it has alternately been suggested that aneuploidy could arise as a result of the loss of checkpoint control that frequently occurs in advanced malignances (Zimonjic et al. 2001). Indeed, individuals with Down syndrome, which is caused by the triplication of chromosome 21, have a significantly decreased risk of developing most solid cancers, suggesting that in certain cases aneuploidy may actually have tumor-suppressive properties (Satgé et al. 1998; Hasle et al. 2016).

Our ability to directly interrogate the role of aneuploidy in cancer has historically been limited by the experimental difficulties involved in manipulating entire chromosome arms. Over the past 40 years, cancer researchers have used the standard tools of molecular genetics, including gene over-expression, knockdown, and mutagenesis, to develop a deep understanding of many individual oncogenes and tumor suppressors (Bister 2015; O'Loughlin and Gilbert 2019). For instance, the biological functions of genes like *KRAS* and *TP53* were elucidated in part by creating and analyzing isogenic cell lines that express or lack these genes (Bunz et al. 1998; Shirasawa et al. 1993). However, existing approaches for single-gene manipulations are insufficient to interrogate the chromosome-scale changes that commonly occur in tumors and that affect hundreds or thousands of genes simultaneously.

The consequences of eliminating specific aneuploid chromosomes from human cancer cells have not previously been established.

Studies of individual cancer driver genes led to the discovery of a phenomenon called "oncogene addiction", in which loss or inhibition of a single oncogene is sufficient to induce cancer regression (Weinstein 2002). For example, mutations in *KRAS* cause the development of pancreas cancer, and genetically ablating *KRAS* in a "*KRAS*-addicted" pancreas tumor blocks growth and triggers apoptosis (Waters and Der 2018). The principle of oncogene addiction also underlies the efficacy of cancer targeted therapies: drugs that inhibit "addictions" like *EGFR* and *BRAF* can result in sustained clinical responses in tumors that are driven by these oncogenes (Sharma and Settleman 2007; Ono et al. 2004; Chapman et al. 2011).

Previous cancer genome sequencing projects have revealed that the aneuploidy patterns observed in human tumors are non-random, and specific chromosome gain events occur significantly more often than expected by chance (Taylor et al. 2018; Knouse et al. 2017; Beroukhim et al. 2010; Zack et al. 2013). We speculated that these recurrent aneuploidies could themselves represent a novel type of cancer "addiction", analogous to the concept of oncogene addictions. Eliminating these "aneuploidy addictions" could similarly block cancer growth and suppress malignant phenotypes. To investigate this hypothesis, we developed a set of computational and functional techniques to explore the similarities between aneuploidy and oncogenes and to uncover the phenotypic consequences of eliminating recurrent aneuploid chromosomes from established cancers.

Results

Specific chromosome gains recurrently occur early in cancer development

Somatic mutations in oncogenes typically arise early in tumor evolution, consistent with their recognized roles as drivers of cancer development (McGranahan et al. 2015). We recently developed a novel computational approach to leverage multi-sample tumor sequencing data to determine the relative timing of somatic copy number gains in cancer evolution (Wang et al. 2022). We applied this tool to investigate the timing of aneuploidy events in a cohort of breast cancer (BRCA) and melanoma (MEL) patients (Yates et al. 2017; Hayward et al. 2017). We found that specific chromosome copy number changes are consistently observed early in tumor development (Fig. 1A-B). Notably, we found that chromosome 1q gains are recurrently the first copy number alteration that occurs in breast cancer evolution, and these gains are also among the first alterations in melanoma evolution. In general, we observed that common aneuploidies arose earlier in tumor development than less-common aneuploidies, in agreement with the assumption that early somatic alterations are likely to be fitness-driving events (Fig. 1C) (Paterson et al. 2020). However, the correlation between frequency and timing was not maintained across all chromosomes. For instance, in breast cancer, chromosome 8q gains and chromosome 1q gains occur with similar frequencies, but we found that 1q gains consistently arose earlier during tumor development than 8q gains. We conclude that, as previously observed with oncogenic point mutations, specific chromosome gains occur in a defined temporal order, and we speculate that aneuploidies that are consistently gained early during tumorigenesis may enhance cancer fitness.

[THIS PAGE INTENTIONALLY LEFT BLANK]

Figure 1 (page 40): Specific chromosome gains arise early in tumor development and are mutually-exclusive with driver gene mutations.

(A) The inferred timing of somatic copy number gains in the evolution of two tumors. A breast tumor is shown on the left and a melanoma on the right. Copy number (CN) states along the genome are shown on the left in each panel and color coded. The plot visualizes the time fraction of somatic evolution from germline to the most recent common ancestor (MRCA) of the patient tumor sample. For each copy number segment, the inferred timing is shown as a rectangle (exactly solved timing) or an arrow (upper bounds of timing when the timing solutions are not unique) with the same color-coding as its CN. The top panel shows the cumulative distribution (CDF) of the timing. Genome doubling (GD) can be observed as the punctuated gains occurring in a narrow time window and chromosome 1q gains appear to be extremely early and preceding GD in these two tumors.

(B) Recurrent early gains of chromosome 1q in BRCA and MEL. For each tumor type, we converted the timing of gains into ranks for genomic bins within a patient and computed the rank sums across patients for each bin. The normalized rank sums for each genomic bin are shown for BRCA and MEL, respectively. The large negative values indicate recurrent early initiating gains. We used the normalized rank sums to test against the null hypothesis (no regions show recurrent early gain across patients). Bins from chromosome 1q reject this null for both tumor types (with 90% confidence level).

(C) The timing of a gain compared to the frequency of its occurrence in BRCA and MEL. The points on the plots show the timing of gain of a genomic bin versus its frequency of copy number gain. Colors represent chromosomal arms, and color darkness indicates the density of points. Both the timings and frequencies are transformed into normalized rank sums (see Methods).

(D) A pan-cancer analysis of mutual exclusivity between mutations in 25 commonly-mutated cancer genes and chromosome arm gain events. The complete results of this analysis are included in Table S1.

(E) Mutual exclusivity and co-occurrence patterns between one representative chromosome gain (+13q, orange bars at the top), and point mutations in several different cancer driver genes.

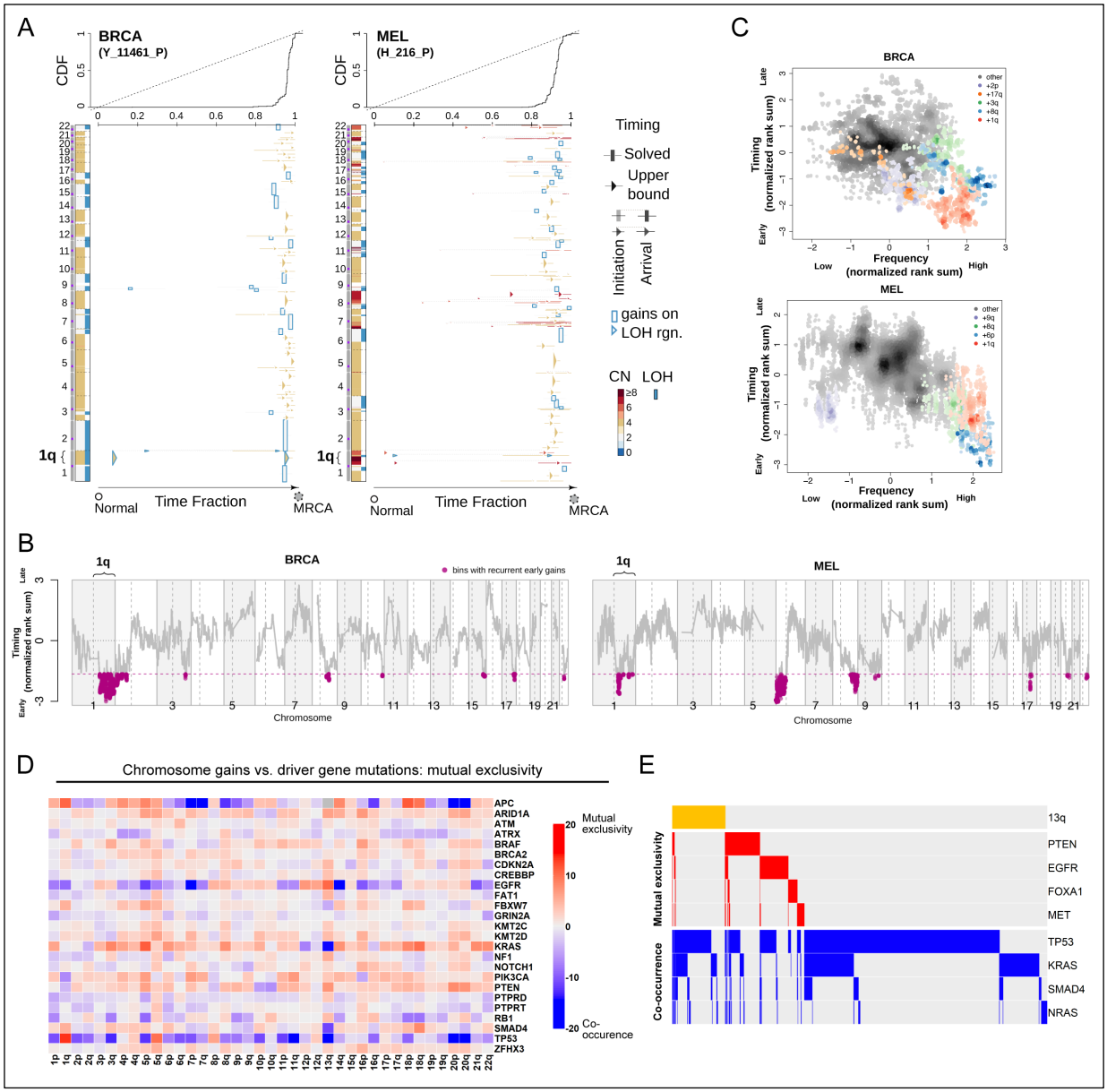

Figure 1: Specific chromosome gains arise early in tumor development and are mutually-exclusive with driver gene mutations.

Specific chromosome gains are associated with altered mutational patterns and with cancer progression

In instances where two oncogenes converge to activate the same pathway, cancers frequently acquire mutations in either gene but not both (Cisowski and Bergo 2017; El Tekle et al. 2021). For example, melanomas can develop mutations in *BRAF* or *NRAS* that drive MAPK signaling, but co-mutation of both genes is redundant and rarely observed (Gorden et al. 2003). If chromosome gains play an oncogene-like role supporting cancer growth, then specific aneuploidies may also be expected to exhibit mutual exclusivity with individual oncogenic mutations. To investigate this possibility, we calculated patterns of mutual exclusivity between chromosome arm gains and mutations across 23,544 cancer patients (Nguyen et al. 2022). We detected several hundred instances in which aneuploidies and mutations co-occur less often than expected by chance both within individual cancer types and in a pan-cancer analysis (Fig. 1D-E, S1, and Table S1). For instance, *KRAS* mutations are mutually exclusive with chromosome 18q gains in pancreatic cancer, while *BRAF* mutations are mutually exclusive with chromosome 20q gains in colorectal cancer (Fig. S1 and Table S1). These results are consistent with our hypothesis that specific chromosome gains can play an oncogene-like role in cancer, thereby making the acquisition of certain oncogenic mutations redundant in the presence of that aneuploidy.

High levels of aneuploidy are generally associated with poor cancer patient outcomes (Stopsack et al. 2019; Hieronymus et al. 2018; Lukow et al. 2021). However, it is less clear whether specific copy number changes drive tumor progression, or whether the aneuploid state itself represents a universal risk factor. We calculated the association between patient outcome and copy number gains affecting every chromosome band across 10,884 patients and 33 cancer types from The Cancer Genome Atlas (TCGA). We discovered that certain copy

number alterations were commonly prognostic across multiple cancer types, particularly gains affecting chromosome 1q (Fig. S2A-C and Table S2A). The strong association between 1q gains and disease progression was robust to the inclusion of multiple clinical variables, including patient age, sex, tumor stage, and tumor grade (Fig. S2D and Table S2B). 1q copy number correlated with hallmarks of aggressive disease in genetically-diverse cancer types, including with Gleason score in prostate adenocarcinoma and with thrombocytopenia in acute myeloid leukemia (Fig. S2E). We performed a similar analysis for cancer-associated mutations, and we found that the only gene for which mutations were prognostic in more than four cancer types is TP53 (Fig. S2A and S2D). These results illustrate that specific chromosome gain events, particularly involving regions of chromosome 1q, are robust pan-cancer markers for the risk of disease progression.

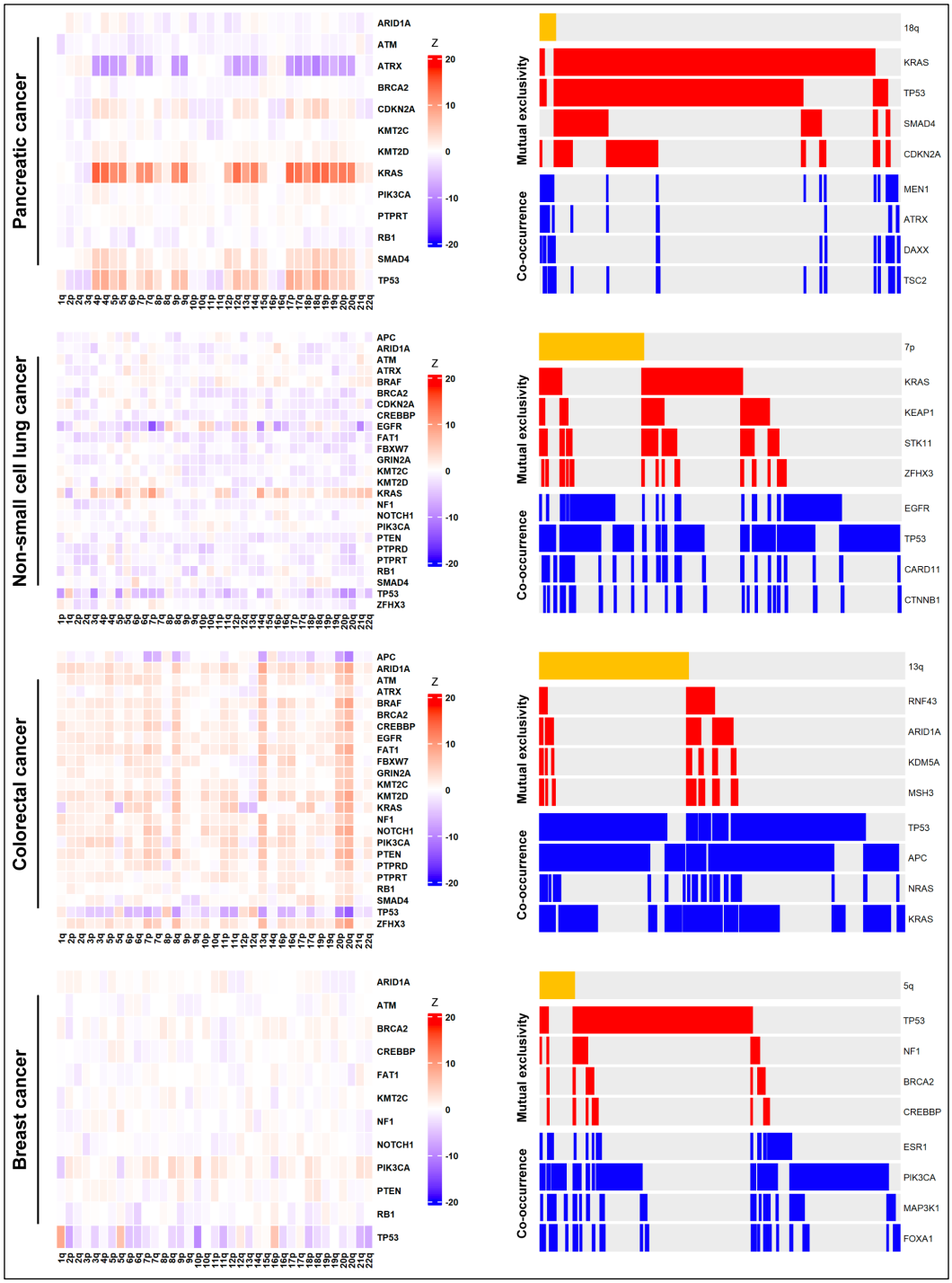

Figure S1. Mutual exclusivity between chromosome arm gains and mutations in cancer driver genes in individual cancer types. (Left) Heatmaps are displayed demonstrating mutual exclusivity (in red) and co-occurrence patterns (in blue) between chromosome arm gains and mutations in common cancer driver genes within four individual cancer types: pancreatic cancer, non-small cell lung cancer, colorectal cancer, and breast cancer. (Right) Oncoprint panels highlighting mutual exclusivity and co-occurrence patterns within individual cancer types for specific chromosome gain events. The complete results of this analysis are included in Table S1.

[THIS PAGE INTENTIONALLY LEFT BLANK]

Figure S2 (page 46): Specific copy number gains, particularly involving chromosome 1q.21, are associated with disease progression and patient death.

(A) A scatterplot displaying the relationship between copy number gains for each chromosome band (left) and mutations (right) and patients outcomes across 32 cancer types from the TCGA (Smith and Sheltzer 2022). Significance was determined by calculating univariate Cox proportional hazards regression models for each data type. The complete results for this analysis are presented in Table S2A.

(B) Kaplan-Meier plots displaying the relationship between 1q.21 copy number gains and disease progression in prostate adenocarcinoma, rectal adenocarcinoma, and renal clear cell carcinoma.

(C) A forest plot showing hazard ratios and 95% confidence intervals for Cox proportional hazards regression between 1q.21 copy number and patient outcome for each of the indicated cancer types. The hazard ratios plotted in red represent those that are significant at a $p < 0.05$ threshold.

(D) A scatterplot displaying the relationship between copy number gains for each chromosome band (left) and mutations (right) and patients outcomes across 32 cancer types from the TCGA (Smith and Sheltzer 2022). Significance was determined by calculating multivariate Cox proportional hazards regression models for each data type, adjusting each model for patient age and sex, and tumor stage and grade. The complete results for this analysis are presented in Table S2B.

(E) Chromosome 1q.21 gains are associated with hallmarks of disease progression risk in various cancer types.

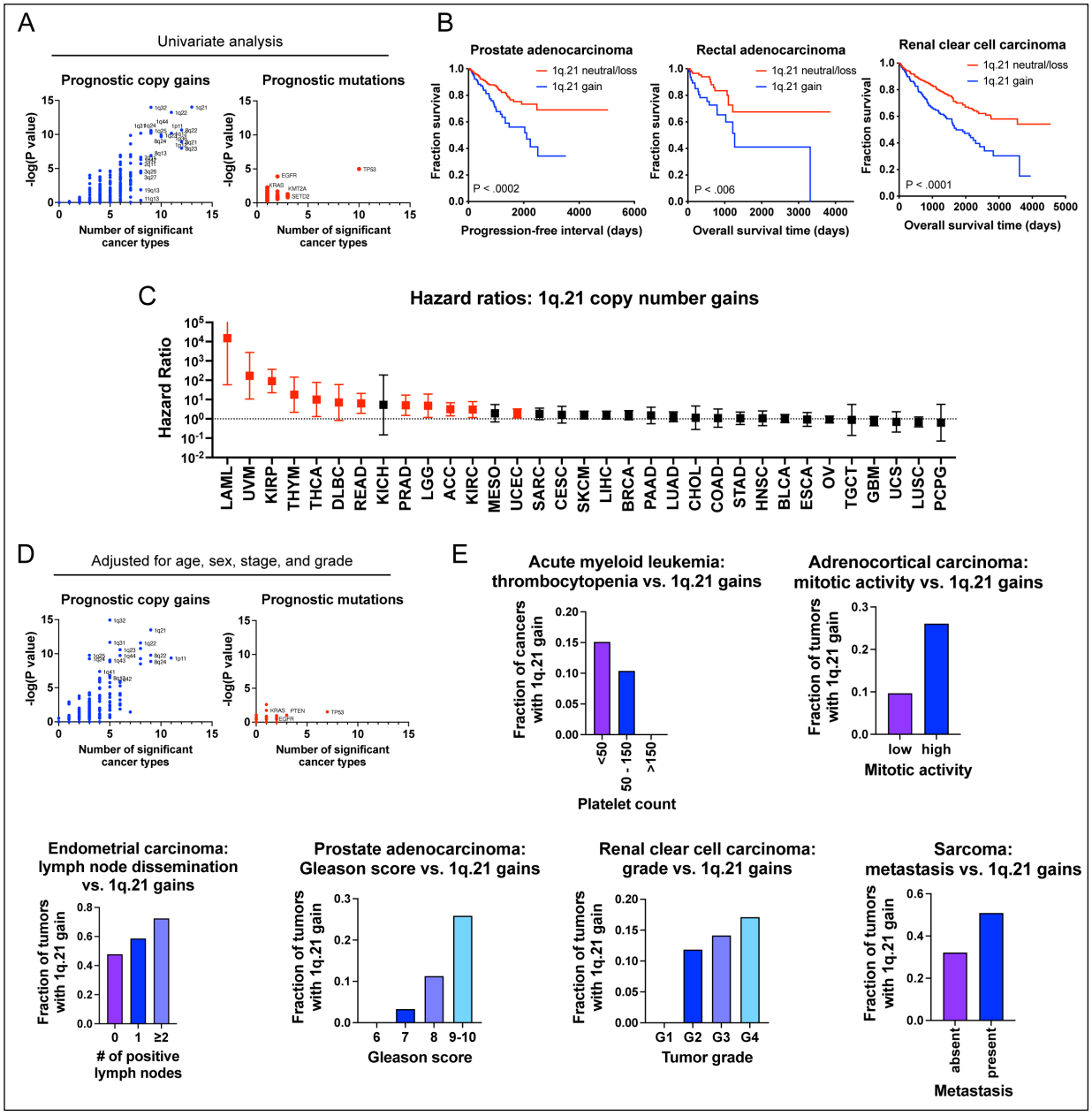

Figure S2: Specific copy number gains, particularly involving chromosome 1q.21, are associated with disease progression and patient death.

Loss of trisomy 1q blocks malignant growth in human cancers

The computational analyses described above highlighted several similarities between chromosome copy number gains and driver mutations, raising the possibility that these aneuploidies could represent oncogene-like cancer addictions. The oncogene addiction paradigm was first established by developing genetic techniques to eliminate individual genes from established cancer cell lines (Shirasawa et al. 1993; Weinstein 2002; Luo et al. 2009). In order to conduct comparable assays with aneuploidy, we created a set of approaches collectively called ReDACT (Restoring Disomy in Aneuploid cells using CRISPR Targeting) (Fig. 2A). In the first approach, called ReDACT-NS (Negative Selection), we integrate a single copy of herpesvirus thymidine kinase (HSV-TK) onto an aneuploid chromosome of interest. Then, the cells are transfected with a gRNA that cuts between the integrant and the centromere and treated with ganciclovir, which is toxic to cells that express HSV-TK (Fillat et al. 2003). Loss of the aneuploid chromosome harboring HSV-TK allows cells to survive ganciclovir selection. In the second approach, called ReDACT-TR (Telomere Replacement), cells are co-transfected with a gRNA that cuts near the centromere of an aneuploid chromosome and a cassette encoding ~100 repeats of the human telomere seed sequence (Uno et al. 2017). CRISPR cleavage coupled with integration of the telomeric seed sequence leads to loss of an aneuploid chromosome arm and formation of a *de novo* telomere. In the third approach, called ReDACT-CO (CRISPR Only), we took advantage of prior reports demonstrating that in rare circumstances CRISPR cleavage by itself is sufficient to trigger chromosome loss (Zuccaro et al. 2020; Papathanasiou et al. 2021), and we transfected cells with a gRNA targeting an aneuploid chromosome arm without any other selection markers. We successfully applied all three approaches to create clones derived from human cell lines that had lost specific aneuploid chromosomes.

We first focused on aneuploidies of chromosome 1q, as we found that 1q gains were an early event in multiple cancer types and were strongly associated with disease progression (Fig. 1 and S2). We targeted the 1q trisomy in the A2058 melanoma cell line, AGS gastric cancer cell line, and A2780 ovarian cancer cell line. We generated multiple independent derivatives of each line in which a single copy of chromosome 1q had been eliminated, thereby producing cell lines that were disomic rather than trisomic for chromosome 1q. We verified loss of the 1q trisomy and the absence of any other chromosome copy number changes using SMASH-Seq, a sequencing-based approach to determine DNA copy number (Wang et al. 2016), and by G-banding analysis of metaphase spreads (Fig. 2B, S3-S4, and Table S3). Loss of the 1q trisomy decreased the expression of genes encoded on chromosome 1q by an average of 26% at the RNA level and 21% at the protein level (Fig. 2C). These results suggest that chromosome loss causes a substantial downregulation of genes encoded on an aneuploid chromosome, though these effects can be buffered to some extent by cellular dosage compensation (Schukken and Sheltzer 2022; McShane et al. 2016).

Next, we tested whether losing the 1q trisomy affects malignant growth in cancer cells. Toward that end, we quantified anchorage-independent colony formation, an *in vitro* proxy for malignant potential (Shin et al. 1975; Hamburger and Salmon 1977), in the 1q-trisomic and 1q-disomic cells. While 1q-trisomic A2058, A2780, and AGS cells displayed robust colony formation, multiple independent 1q-disomic clones derived from each cell line exhibited minimal anchorage-independent growth (Fig. 2D). We then performed contralateral subcutaneous injections with each cell line to test whether aneuploidy-loss affected tumor growth *in vivo*. Consistent with our colony formation assays, we observed that 1q-trisomic A2058 and A2780 cells rapidly formed large tumors, while 1q-disomic cells displayed minimal tumor growth (Fig. 2E). At the end of these assays, the trisomic cells had formed

tumors that were on average 25-fold larger than the tumors formed by the 1q-disomic cells. For the AGS cancer cell line, neither the trisomic nor the disomic cells formed tumors following subcutaneous injection (Fig. S5). Finally, we performed proliferation assays to measure the doubling time of the 1q-trisomic and the 1q-disomic cells in culture (Fig. S6A-C). The aneuploidy-loss clones divided more slowly *in vitro* compared to the 1q-trisomic cells, though the difference in doubling time (~35%) was substantially less than the differences observed in the soft agar and xenograft assays. In total, these results suggest that multiple human cancer cell lines are dependent on the presence of a third copy of chromosome 1q to support malignant growth, and elimination of this aneuploid chromosome compromises their tumorigenic potential. Furthermore, we note that this phenotypic pattern, in which aneuploidy loss causes a moderate effect on *in vitro* doubling but a severe effect on anchorage-independent growth and xenograft formation, resembles the previously-reported consequences of eliminating *bona fide* oncogene addictions (Shirasawa et al. 1993; Chin et al. 1999).

Loss of trisomy 1q prevents malignant transformation

We discovered that 1q gains were commonly the first copy number alteration to occur during breast tumor development (Fig. 1A-C). We therefore hypothesized that, in addition to being required for cancer growth, aneuploidy of chromosome 1q may directly promote cellular transformation. To test this, we performed chromosome engineering in MCF10A, an immortal but non-tumorigenic mammary epithelial cell line (Soule et al. 1990). SMASH-Seq revealed that this cell line harbors a trisomy of chromosome 1q, and we successfully applied ReDACT-CO and ReDACT-TR to generate derivatives of MCF10A with two copies rather than three copies of 1q (Fig. 2F, S3D, and Table S3). We then attempted to transform the 1q-

trisomic and 1q-disomic cells by transducing them with a retrovirus encoding the *HRAS*^{G12V} oncogene. *HRAS*^{G12V} expression was sufficient to transform trisomic MCF10A, as these cells were able to form colonies in soft agar and grow as xenografts in nude mice (Fig. 2G-H). In contrast, 1q-disomic MCF10A clones expressing *HRAS*^{G12V} exhibited impaired colony formation and were unable to produce tumors *in vivo*, demonstrating that loss of the trisomic chromosome prevented cellular transformation. These results are consistent with our finding that 1q gains are an early event during breast cancer development and demonstrate that specific aneuploidies can cooperate with oncogenes to transform non-malignant cells.

Figure 2 (page 52): Phenotypic effects of losing chromosome 1q-aneuploidy.
(A) Chromosomal engineering strategies for the targeted deletion of chromosome arms: (1) ReDACT-NS: using CRISPR-Cas9 homology-directed repair, we integrated a positive-negative selection cassette encoding a fluorescent reporter, a positive selection marker, and a negative selection marker (HSV thymidine kinase) at a centromere-proximal region on chromosome 1q. We induced arm loss by generating a dsDNA break centromere-proximal to the cassette with Cas9, and isolated clonal populations of cells that were ganciclovir-resistant. (2) ReDACT-TR: We induced arm loss by generating a dsDNA break at a centromere-proximal location with Cas9 while providing cells with an ectopic telomere seed sequence for repair. (3) ReDACT-CO: We induced arm loss by generating a dsDNA break at a centromere-proximal location with Cas9, and isolated clonal populations of cells. For all three approaches, we screened clonal populations of cells for targeted chromosome loss through TaqMan CNV assays and validated their karyotypes through SMASH sequencing.

(B) Representative SMASH karyotypes of the 1q-disomic clones generated from the 1q-trisomic cancer cell lines A2780, AGS, and A2058. Chromosome 1q is highlighted in blue. A complete list of aneuploidy-loss clones is included in Table S3.

(C) 1q-disomic clones display decreased RNA expression and protein expression of genes encoded on chromosome 1q. RNA expression data was obtained through bulk RNA-seq and represents the average expression of genes by chromosome arm across multiple 1q-disomic clones for each cell line. Protein expression data was obtained through mass spectrometry, and representative data from one 1q-disomic clone is shown for each cell line. Data are log2 transformed, normalized to the parental cell line, and adjusted so that the mean expression across all chromosomes is 0.

(D) 1q-disomic clones exhibit decreased anchorage-independent growth. The micrographs display representative images of colony formation for 1q-trisomic and 1q-disomic clones.

(E) 1q-disomic clones exhibit impaired xenograft growth *in vivo*. 1q-trisomic and 1q-disomic cells were injected contralaterally and subcutaneously into immunocompromised mice. The graphs display the mean ± SEM for each trial. Representative mice are shown on the right.

(F) SMASH karyotype of a 1q-disomic clone generated from the mammary epithelial cell line MCF10A. Chromosome 1q is highlighted in blue.

(G) 1q-disomic MCF10A clones transduced with $HRAS^{G12V}$ exhibit decreased anchorage-independent growth relative to 1q-trisomic MCF10A cells.

(H) 1q disomic MCF10A clones transduced with $HRAS^{G12V}$ clones exhibit impaired xenograft growth *in vivo*. 1q-trisomic and 1q-disomic cells were injected contralaterally and subcutaneously into immunocompromised mice. The graphs display the mean ± SEM for each trial. Representative mice are shown below.

For anchorage-independent growth assays in D and G, the boxplots represent the 25th, 50th, and 75th percentiles of colonies per field, while the whiskers represent the 10th and 90th percentiles. Unpaired t-test, n = 15 fields of view, data from representative trial. Representative images are shown below. $^{**}p < 0.005$, $^{***}p < 0.0005$

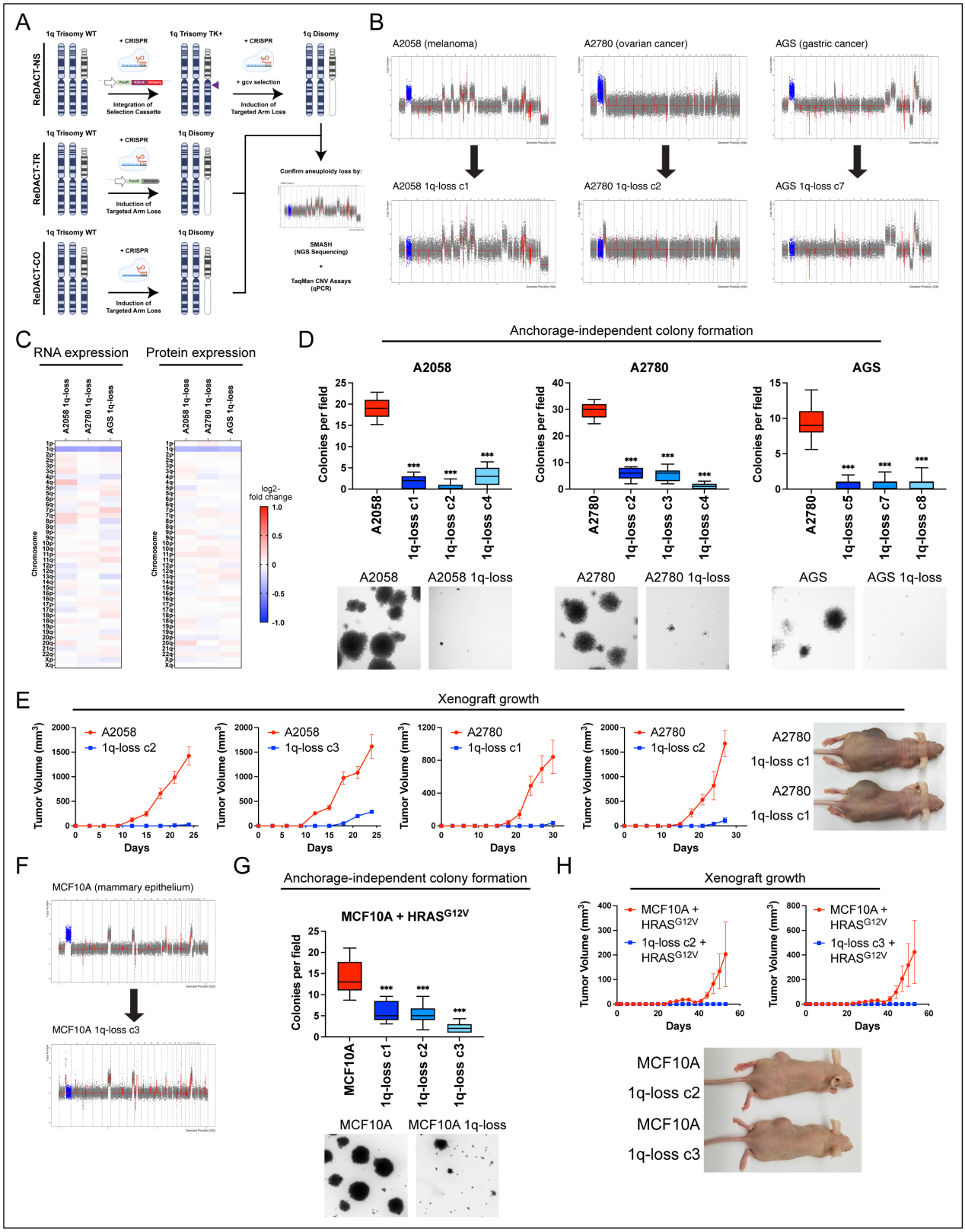

Figure 2: Phenotypic effects of losing chromosome 1q-aneuploidy.

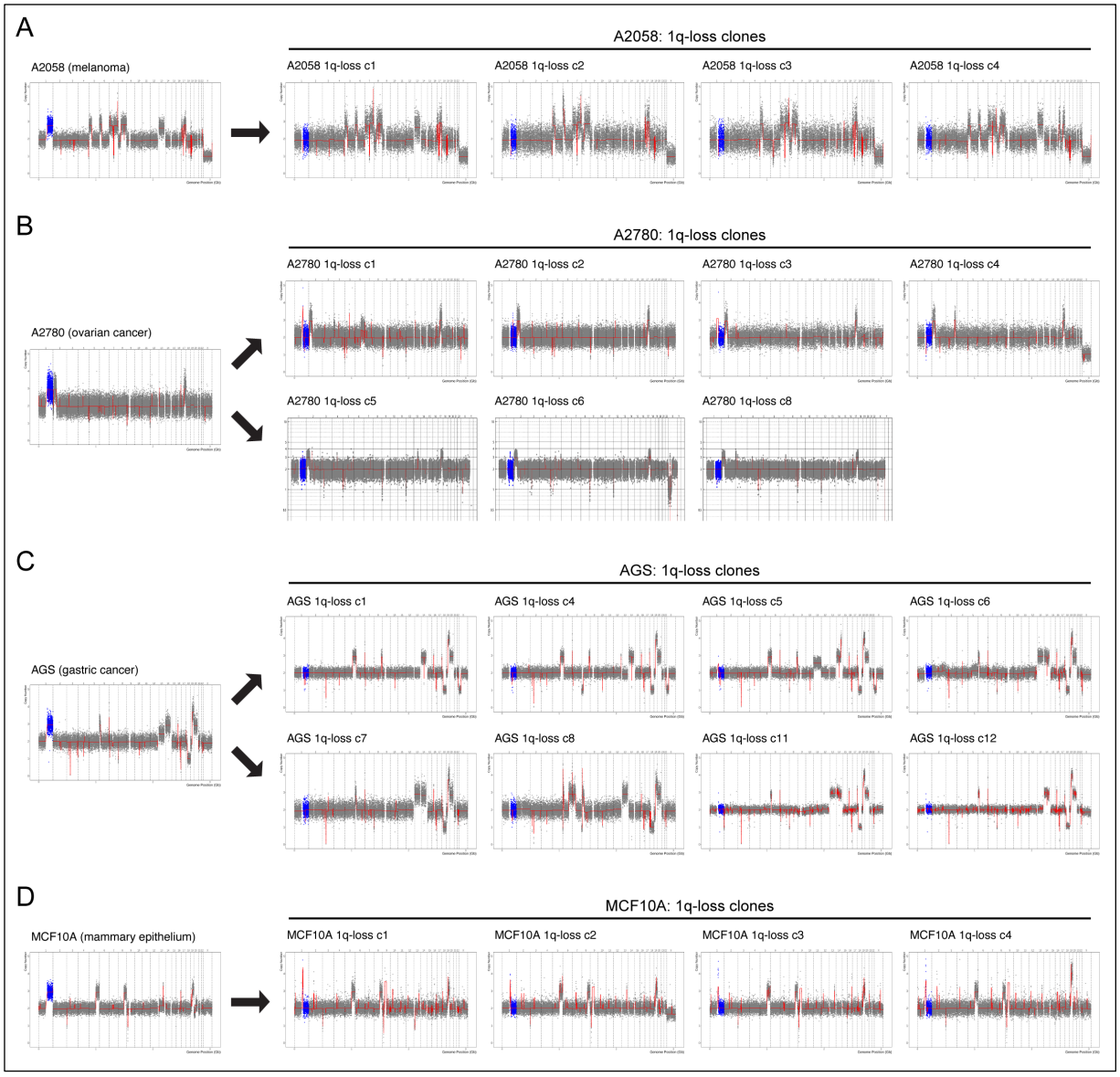

Figure S3. Additional karyotypes of 1q-disomic clones.
(A) SMASH karyotypes of 1q-disomic clones generated from the 1q-trisomic cancer cell line A2058. (B) SMASH karyotypes of 1q-disomic clones generated from the 1q-trisomic cancer cell line A2780. (C) SMASH karyotypes of 1q-disomic clones generated from the 1q-trisomic cancer cell line AGS. (D) SMASH karyotypes of 1q-disomic clones generated from the 1q-trisomic immortalized mammary epithelial cell line MCF10A. For all karyotypes in A-D, chromosome 1q is highlighted in blue. A complete list of aneuploidy-loss clones is included in Table S3.

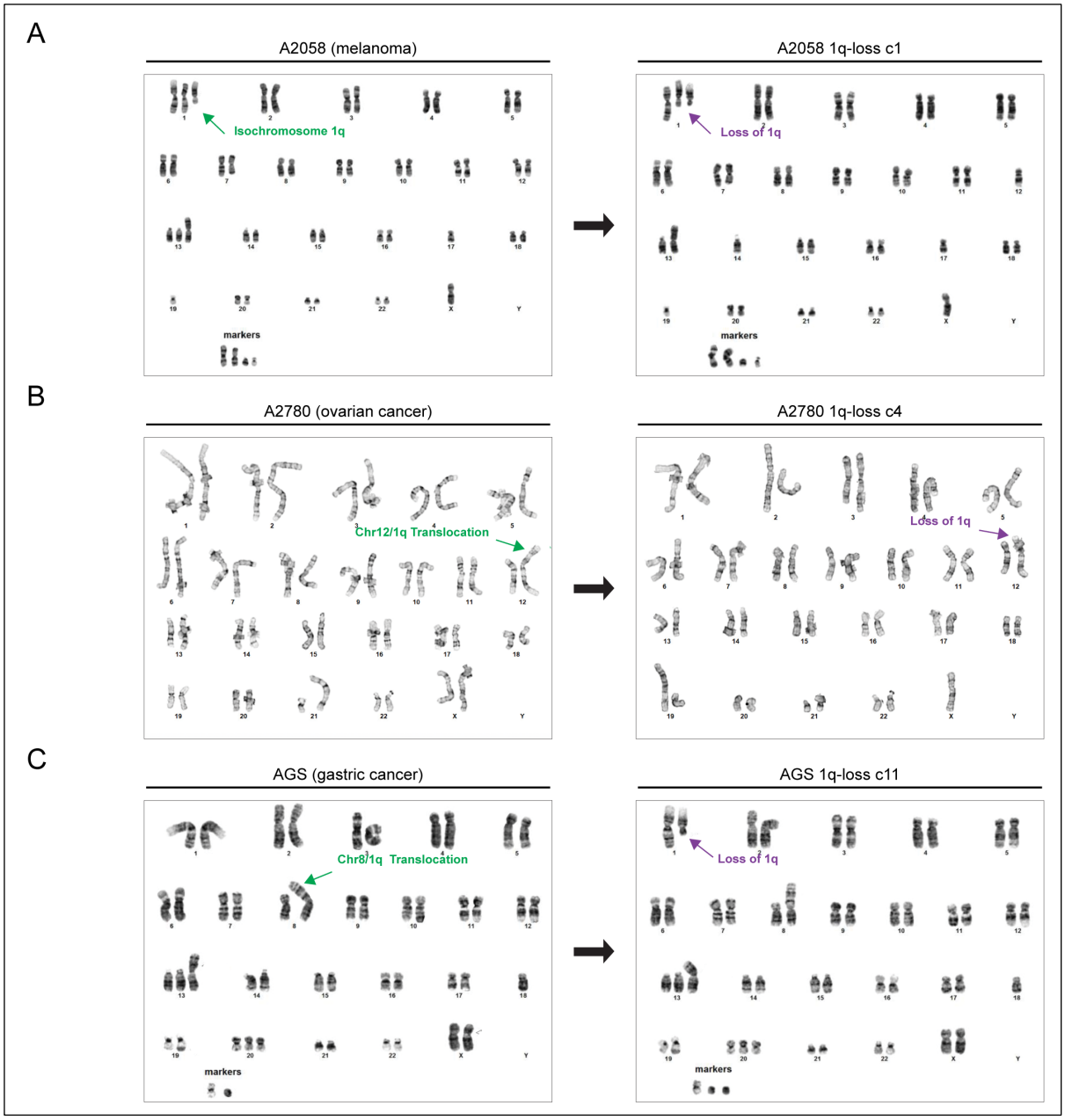

Figure S4. G-banded karyotypes of 1q-disomic clones.
(A) G-banded karyotypes of A2058 and a 1q-disomic A2058 clone. The third copy of chromosome 1q in A2058 is present as an isochromosome [chr 1, iso(1q), del(1q)], and 1q-disomic clone has lost a copy of 1q from the intact chromosome 1. (B) G-banded karyotypes of A2780 and a 1q-disomic A2780 clone. The third copy of chromosome 1q in A2780 is translocated to chromosome 12q, and the 1q-disomic clone has lost this translocated copy of 1q. (C) G-banded karyotypes of AGS and a 1q-disomic AGS clone. The third copy of chromosome 1q in AGS is translocated to chromosome 8p, and the 1q-disomic clone has lost a copy of 1q from an intact chromosome 1. For all G-banded karyotypes in A-C, green arrows indicate the extra copy of chromosome 1q in parental cells and purple arrows indicate the deletion in the 1q-disomic clones.

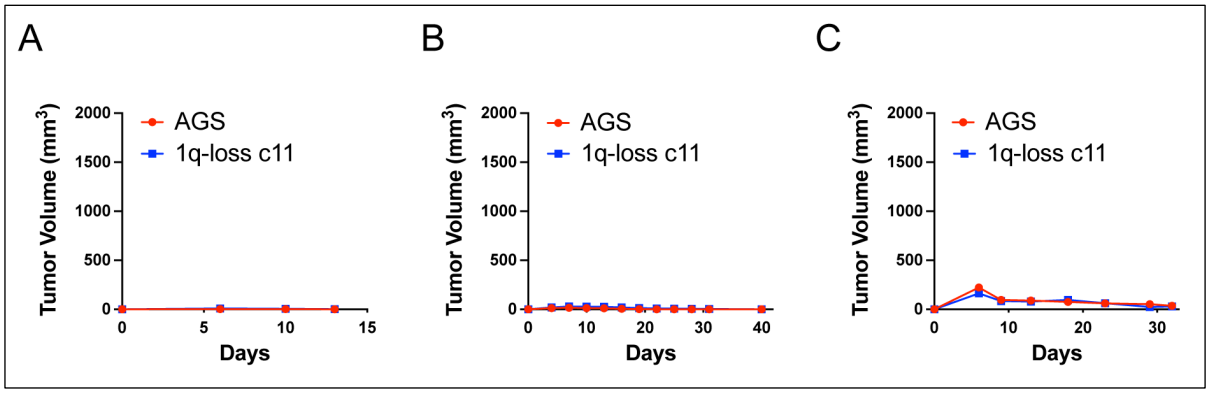

Figure S5. Wild-type AGS cells fail to grow as subcutaneous xenografts.
(A) 5 million 1q-trisomic or 1q-disomic AGS cells were suspended in PBS and injected subcutaneously and contralaterally into 5-week-old female Nu/J mice. No tumor formation was observed. (B) 4 million 1q-trisomic or 1q-disomic AGS cells were suspended in PBS and injected subcutaneously and contralaterally into 6-week-old female NSG mice. No tumor formation was observed. (C) 15 million 1q-trisomic or 1q-disomic AGS cells were suspended in a 1:1 mixture of PBS and Matrigel and injected subcutaneously and contralaterally into 6-week-old female J:NU mice. No tumor formation was observed.

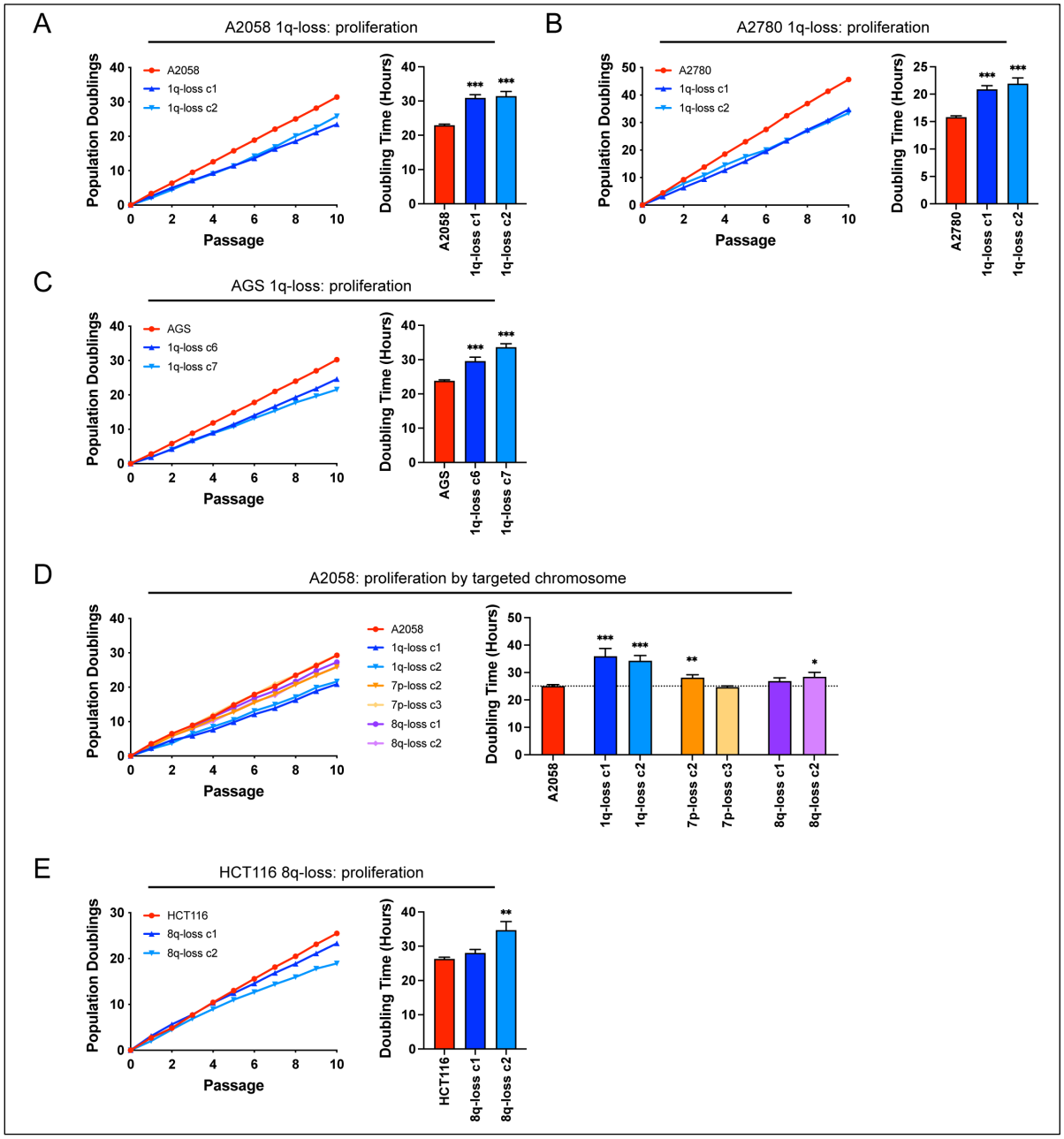

Figure S6. Elimination of trisomy-1q causes a moderate decrease in 2D cell proliferation. (A) Proliferation assays in 1q-trisomic and 1q-disomic A2058 cells. (B) Proliferation assays in 1q-trisomic and 1q-disomic A2780 cells. (C) Proliferation assays in 1q-trisomic and 1q-disomic AGS cells. (D) Proliferation assays in parental and 1q-disomic, 7p-disomic, or 8q-disomic A2058 cells. (E) Proliferation assays in 8q-trisomic and 8q-disomic HCT116 cells. For all proliferation assays in A-E, cumulative population doublings are shown on the left, and the doubling time calculated from these assays is shown on the right. Data are the mean ± SEM, n=10 passages. Data were analyzed by unpaired t-test. *p < 0.05, **p < 0.005, ***p < 0.0005

Robust anchorage-independent growth in human cancer cell lines subjected to CRISPR cutting and ganciclovir selection

In order to confirm that our findings were a specific consequence of aneuploidy loss, we generated and tested a series of control clones subjected to various CRISPR manipulations that did not induce loss of the 1q trisomy (Fig. S7 and S8A). These control clones included:

1) Cell lines harboring a CRISPR-mediated integration of the HSV-TK cassette that were not subjected to selection for 1q-loss
2) Cell lines in which the HSV-TK cassette was deleted by transfecting cells with two gRNAs targeting immediately upstream and downstream of the integrant coupled with ganciclovir selection, which resulted in a segmental deletion of the cassette while leaving the rest of 1q unaffected
3) Cell lines subjected to CRISPR-mediated cutting with a 1q-targeting gRNA, in which the lesion was repaired without inducing chromosome loss
4) Cell lines subjected to CRISPR-mediated cutting with a gRNA targeting the non-coding Rosa26 locus (Irion et al. 2007)
5) Cell lines in which dual CRISPR guides were used to generate segmental deletions on chromosome 1q of genes encoding non-expressed olfactory receptors
6) Cell lines in which CRISPR was used to delete a terminal segment on chromosome 1q, eliminating the telomere and decreasing the copy number of 26 out of 968 protein-coding genes on the chromosome

We performed SMASH-Seq on each control clone that we generated and we confirmed that each clone retained an extra copy of chromosome 1q (Fig. S7). We then measured the effects of these manipulations on anchorage-independent growth. We found that every

control clone maintained the ability to form colonies in soft agar, with some variability between independent clones. Across the three cancer cell lines and 28 different control clones, we observed that the 1q-disomic clones exhibited significantly worse anchorage-independent growth than every control clone that we generated (Fig. S8B-E). These results indicate that the deficiencies in malignant growth exhibited by the 1q-disomic clones are not a result of our use of CRISPR or ganciclovir selection (discussed in more detail below and in Supplemental Text 1).

Figure S7. Karyotypes of control clones subjected to various CRISPR manipulations. (A) SMASH karyotypes of the control clones generated from the 1q trisomic cancer cell line A2058, with all clones maintaining 1q trisomy. (B) SMASH karyotypes of the control clones generated from the 1q trisomic cancer cell line A2780, with all clones maintaining 1q trisomy. (C) SMASH karyotypes of the control clones generated from the 1q trisomic cancer cell line AGS, with all clones maintaining 1q trisomy. For all karyotypes in A-C, chromosome 1q is highlighted in blue. Additional information on how these clones were generated is presented in Figure S8.

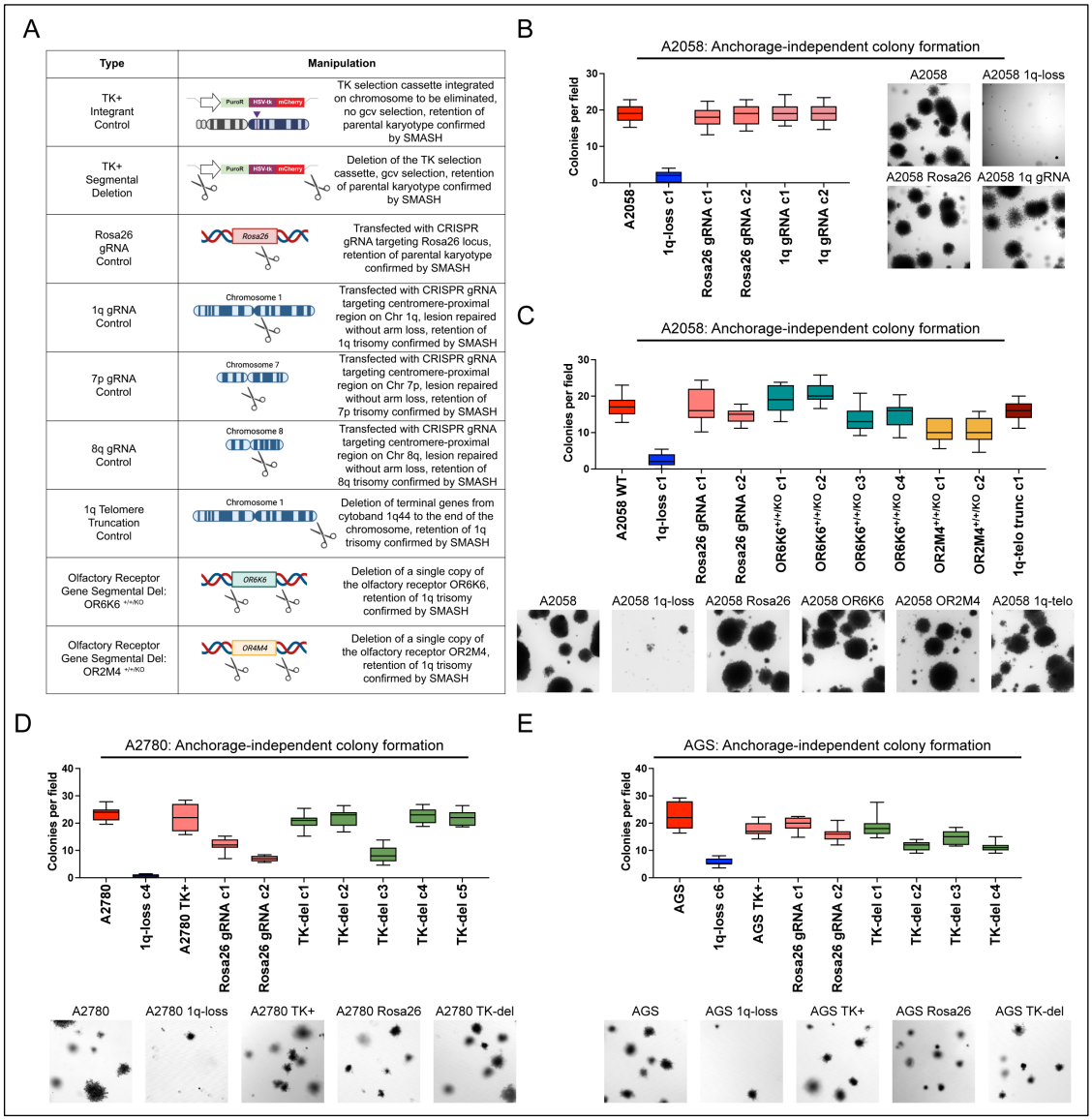

Figure S8. 1q-disomic cancer cells exhibit uniformly worse growth in soft agar compared to control clones subjected to various CRISPR manipulations. (A) A schematic of the various strategies used to generate the control clones tested in this work. Note that the 7p and 8q gRNA control clones are tested in Figure S10. (B) A 1q-disomic clone exhibits worse anchorage-independent growth compared to Rosa26 gRNA and 1q gRNA control clones in A2058. (C) A 1q-disomic clone exhibits worse anchorage-independent growth compared to Rosa26 gRNA, olfactory receptor deletion, and 1q-telo truncation control clones in A2058. (D) A 1q-disomic clone exhibits worse anchorage-independent growth compared to TK+ integrant, Rosa26 gRNA, and TK-segmental deletion control clones in A2780. Note that these control clones display some variation in anchorage-independent growth, but every control clone grew better than a 1q-disomic clone. (E) A 1q-disomic clone exhibits worse anchorage-independent growth compared to TK+ integrant, Rosa26 gRNA, and TK-segmental deletion control clones in AGS. For anchorage-independent growth assays in B-D, boxes represent the 25th, 50th, and 75th percentiles of colonies per field, while the whiskers represent the 10th and 90th percentiles. Data are from n = 15 fields of view, and a representative trial is shown for each experiment.

Eliminating different cancer aneuploidies produces unique phenotypic consequences

We investigated two alternate possibilities to explain the loss of malignant potential that we observed following elimination of the 1q trisomy. First, we considered the possibility that the poor growth of the 1q-disomic clones was a consequence of some aspect of the ReDACT approach that was not fully captured by the control clones tested above. Second, while we initially focused on aneuploidy of chromosome 1q due to its occurrence early in cancer development and its association with poor prognosis (Fig. 1A-C and S2), we considered the possibility that the loss of any clonal aneuploid chromosome from a cancer cell line could have identical phenotypic effects. To further investigate the consequences of inducing aneuploidy-loss, we took advantage of the A2058 melanoma cell line, which harbors multiple trisomic chromosomes. We previously described the consequences of eliminating trisomy 1q from this cell line (Fig. 2); we subsequently used the same ReDACT techniques to generate derivatives of this cell line that had lost either the trisomy of chromosome 7p or the trisomy of chromosome 8q. SMASH-Seq confirmed the desired aneuploidy-loss events without other karyotypic changes (Fig. 3A, S9A-B, and Table S3).

As expected, loss of either trisomy 7p or trisomy 8q resulted in a significant decrease in the expression of genes encoded on the affected chromosomes (Fig. 3B). Next, we tested anchorage-independent growth in these aneuploidy-loss clones. If the poor growth of the 1q-disomic clones is a non-specific effect of ReDACT, then we would expect that all aneuploidy-loss clones would exhibit similar phenotypes. While 7p-disomic and 8q-disomic clones exhibited impaired anchorage-independent growth compared to a panel of control clones, we observed that this defect was not as severe as the defect observed among 1q-disomic clones (Fig. 3C and S10). Loss of trisomy-1q resulted in a 92% decrease in colony formation relative to the parental A2058 cells, compared to decreases of 49% and 47% for 7p-loss and 8q-loss,

respectively. *In vitro* doubling times were also closer to wild-type levels for 7p-disomic and 8q-disomic cells compared to 1q-disomic cells (Fig. S6D). Finally, we measured tumor growth following subcutaneous injections of the 7p-disomic and the 8q-disomic cells in nude mice. Loss of either the 7p or the 8q trisomy resulted in a moderate decrease in tumor growth (Fig. 3D). At the end of the assay, the wild-type tumors were on average two-fold larger than the tumors formed by either 7p-disomic or 8q-disomic cells, compared to a 30-fold difference between A2058 wild-type and 1q-disomic tumors (Fig. 2E). In total, these results indicate that A2058 melanoma cells exhibit a greater degree of "addiction" to the 1q-trisomy compared to the trisomies of chromosome 7p or 8q.

To explore the consequences of losing chromosome 8q aneuploidy in a distinct cancer type, we eliminated the 8q-trisomy from the colorectal cancer cell line HCT116 (Fig. 3E-F, S9C and Table S3). Consistent with our observations in A2058, loss of the 8q trisomy significantly decreased but did not fully prevent anchorage-independent growth in HCT116 (Fig. 3G). We then tested xenograft formation in the HCT116 8q-disomic cells, and we observed that one 8q-loss clone exhibited a moderate defect in tumor growth while a second clone was able to form tumors at levels comparable to the trisomic parental line (Fig. 3H). These results demonstrate that eliminating aneuploid chromosomes has variable effects, depending on the identity of the chromosome and the genetic background of the cancer.

Figure 3 (page 64): Variable degrees of addiction to aneuploidy of chromosome 1q, 7p, and 8q.

(A) Representative SMASH karyotypes of the 1q-disomic, 7p-disomic, and 8q-disomic clones generated from the melanoma cell line A2058. Trisomy of chromosomes 1q, 7p, and 8q are highlighted in blue in the parental cell line on the left, and the respective targeted chromosome loss is highlighted in blue in the derived clones on the right. A complete list of aneuploidy-loss clones is included in Table S3.

(B) 1q-disomic, 7p-disomic, and 8q-disomic clones in A2058 exhibit decreased RNA expression of genes encoded on the targeted chromosome. RNA expression data was obtained through bulk RNA-seq and represents the average expression of genes by chromosome arm across multiple aneuploidy-loss clones for each targeted chromosome. Data are log2 transformed, normalized to the parental cell line, and adjusted so that the mean expression across all chromosomes is 0.

(C) 7p-disomic and 8q-disomic clones in A2058 exhibit a milder deficit in anchorage-independent growth as compared to 1q-disomic clones. The micrographs display representative images of colony formation for the indicated cell lines.

(D) 7p-disomic and 8q-disomic clones in A2058 exhibit a moderate defect in xenograft growth. Wild-type (7p-trisomic and 8q-trisomic) cells and either 7p-disomic or 8q-disomic cells were injected contralaterally and subcutaneously into immunocompromised mice. The graphs display the mean ± SEM for each trial. Representative mice are shown on the right.

(E) SMASH karyotype of an 8q-disomic clone generated from the colorectal cancer cell line HCT116. Chromosome 8q is highlighted in blue.

(F) 8q-disomic clones in HCT116 exhibit decreased RNA expression of genes encoded on chromosome 8q. RNA expression data was obtained through bulk RNA-seq and represents the average expression of genes by chromosome arm across multiple aneuploidy-loss clones for each cell line. Data are log2 transformed, normalized to the parental cell line, and adjusted so that the mean expression across all chromosomes is 0.

(G) 8q-disomic clones in HCT116 exhibit decreased anchorage-independent growth. The micrographs display representative images of colony formation for the indicated cell lines.

(H) 8q-disomic clones in HCT116 exhibit variable xenograft growth. 8q-trisomic and 8q-disomic cells were injected contralaterally and subcutaneously into immunocompromised mice. The graphs display the mean ± SEM for each trial. Representative mice are shown below the graphs.

For anchorage-independent growth assays in C and G, boxes represent the 25th, 50th, and 75th percentiles of colonies per field, while the whiskers represent the 10th and 90th percentiles. Unpaired t-test, n = 15 fields of view, data from representative trial. Representative images are shown below.

***$p < 0.0005$

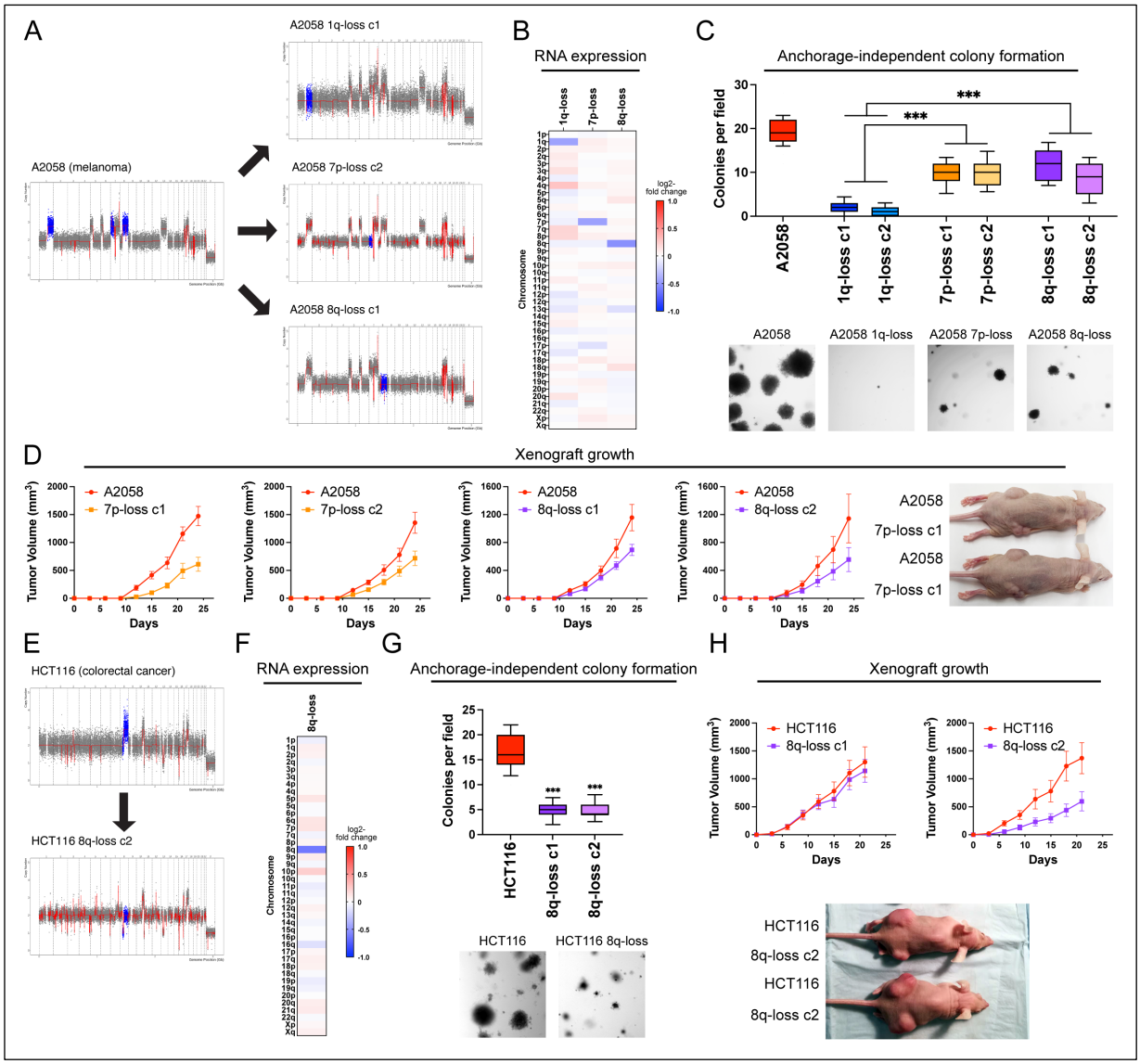

Figure 3: Variable degrees of addiction to aneuploidy of chromosome 1q, 7p, and 8q.

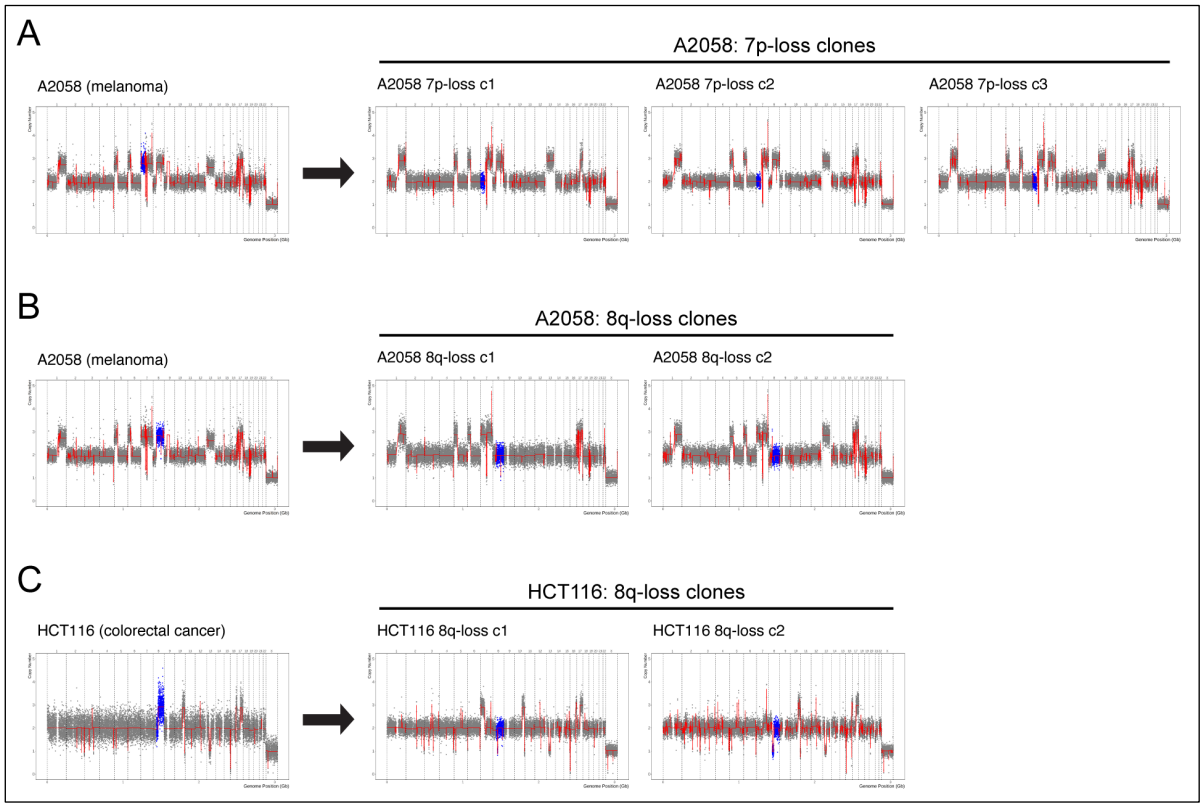

Figure S9. Additional karyotypes of 7p-disomic and 8q-disomic clones.
(A) SMASH karyotypes of 7p-disomic clones generated from the 7p-trisomic cancer cell line A2058. Chromosome 7p is highlighted in blue. (B) SMASH karyotypes of 8q-disomic clones generated from the 8q-trisomic cancer cell line A2058. Chromosome 8q is highlighted in blue. (C) SMASH karyotypes of 8q-disomic clones generated from the 8q-trisomic cancer cell line HCT116. Chromosome 8q is highlighted in blue.

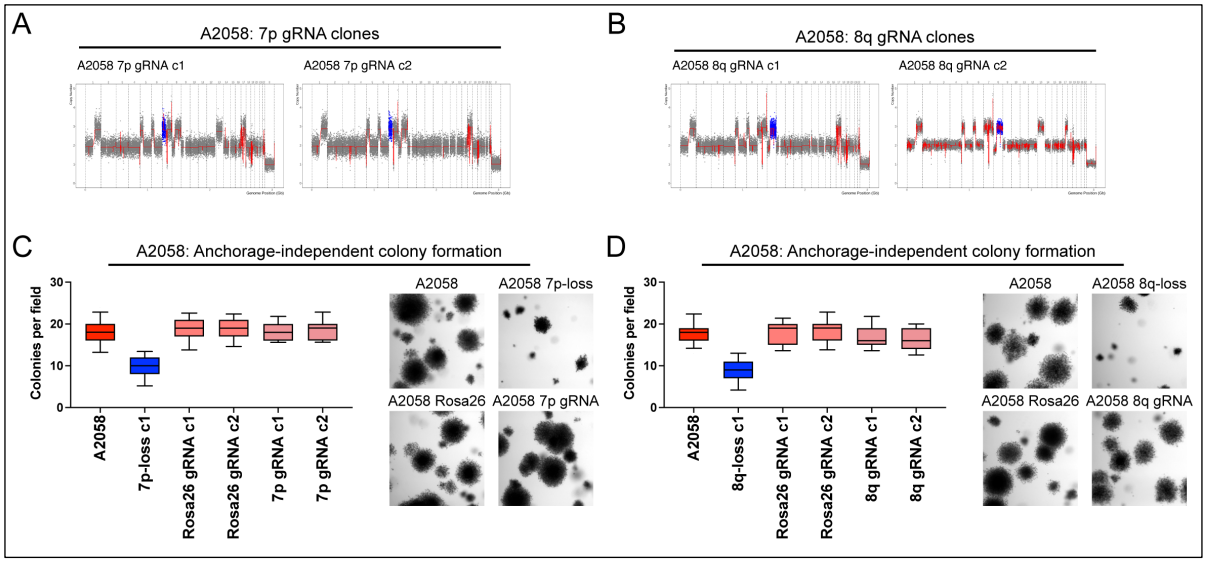

Figure S10. Karyotypes and anchorage-independent growth of A2058 7p and 8q control clones

(A) SMASH karyotypes of control clones generated by transfecting cells with the same CRISPR gRNA used to produce the 7p-disomic clones. Clones were selected that maintain the 7p trisomy. Chromosome 7p is highlighted in blue. (B) SMASH karyotypes of control clones generated by transfecting cells with the same CRISPR gRNA used to produce the 8q-disomic clones. Clones were selected that maintain the 8q trisomy. Chromosome 8q is highlighted in blue. (C) A 7p-disomic clone exhibits worse anchorage-independent growth compared to Rosa26 gRNA and 7p gRNA control clones in A2058. (D) An 8q-disomic clone exhibits worse anchorage-independent growth compared to Rosa26 gRNA and 8q gRNA control clones in A2058. For anchorage-independent growth assays in C-D, boxes represent the 25th, 50th, and 75th percentiles of colonies per field, while the whiskers represent the 10th and 90th percentiles. Unpaired t-test, n = 15 fields of view, data from representative trial. Representative images are shown next to each graph.

Karyotype evolution and 1q trisomy restoration after aneuploidy loss

A hallmark of oncogene addictions is that loss or inhibition of a driver oncogene results in strong and rapid selection to re-establish oncogenic signaling (Torti and Trusolino 2011). For instance, when *EGFR*-driven lung cancers are treated with an *EGFR* inhibitor, these cancers evolve to acquire specific mutations, including $EGFR^{T790M}$ (which restores *EGFR* activity) and $KRAS^{G13D}$ (which activates a parallel oncogenic pathway) (Westover et al. 2018). We sought to investigate whether elimination of an "aneuploidy addiction" would also result in evolutionary pressure to restore the lost aneuploidy. We injected 1q-disomic A2058 cells into nude mice and then determined the copy number of chromosome 1q in the resulting xenografts using qPCR (Fig. 4A). We discovered that 65 out of 82 1q-disomic xenografts re-acquired an extra copy of chromosome 1q, demonstrating strong selective pressure to regain the initial 1q aneuploidy. We subjected 20 of these post-xenograft clones to SMASH-Seq, and we found that chromosome 1q-regain was the only detectable chromosome-scale copy number change (Fig. 4B and S11A). No gross karyotypic changes were observed when the parental 1q-trisomic cells were grown as xenografts (Fig. 4B and S11B). If loss of the chromosome 1q trisomy compromises malignant potential, then we would expect that regaining 1q aneuploidy would restore cell fitness. Consistent with this hypothesis, we found that cells that had re-acquired the 1q trisomy exhibited increased clonogenicity compared to the 1q-disomic cells when grown under anchorage-independent conditions (Fig. 4C).

Next, we assessed karyotype evolution following *in vivo* growth of A2058 7p-disomic and 8q-disomic clones. Interestingly, 17 out of 68 7p-disomic xenografts and 17 out of 63 8q-disomic xenografts were found to exhibit 7p- and 8q-trisomy regain, respectively (Fig. 4D-E). These rates of chromosome re-gain were significantly lower than the rates that we observed for chromosome 1q ($P < .0001$, chi-square test; Fig. 4F). These results suggest that there is

moderate selective pressure to restore 7p and 8q trisomies and stronger selective pressure to restore 1q trisomy in A2058. We then sought to determine whether we could observe evolutionary pressure to restore chromosome 1q aneuploidy when 1q-disomic cells were grown *in vitro*. Toward that end, we passaged A2058, A2780, and AGS 1q-trisomic and 1q-disomic cancer cell lines for thirty days in culture and then we assessed their karyotypes. Similar to our *in vivo* results, we uncovered multiple instances in which 1q-disomic cells independently regained an extra copy of chromosome 1q over the course of the assay (Fig. S12).

Finally, we assessed karyotype evolution in xenografts produced by 8q-disomic HCT116 cells (Fig. 4G). Interestingly, we found that 0 out of 13 tumors regained the trisomy of chromosome 8q, but 7 out of 13 tumors gained a *de novo* trisomy of chromosome 12. HCT116 cells are driven by a heterozygous $KRAS^{G13D}$ mutation (Shirasawa et al. 1993), and KRAS is encoded on chromosome 12. Sanger sequencing analysis revealed that every chromosome 12-trisomic tumor had amplified the copy of chromosome 12 harboring the mutant $KRAS^{G13D}$ allele (Fig. 4G). Increasing dosage of mutant KRAS has previously been associated with enhanced tumor fitness (Burgess et al. 2017; Mueller et al. 2018), and we observed that these chromosome 8q-disomic/chromosome 12-trisomic cells exhibited superior anchorage-independent growth relative to the chromosome 8q-disomic/chromosome 12-disomic pre-xenograft population (Fig. 4H). In total, these results suggest that aneuploidy loss creates strong selective pressure for karyotype evolution, and the effects of aneuploidy loss can be suppressed *in cis* (by regaining the lost chromosome) or *in trans* (by acquiring a beneficial secondary alteration).

Figure 4 (page 70): Cancers rapidly recover chromosome 1q aneuploidy.

(A) A2058 1q-disomic cells frequently evolve to recover a third copy of chromosome 1q during xenograft growth.

(B) Representative SMASH karyotypes of A2058 wildtype and 1q-disomic tumors. The initial karyotypes for these lines prior to the xenograft assay are shown on the left, and karyotypes of tumors following the xenograft assay are shown on the right. Chromosome 1q is highlighted in blue.

(C) 1q-disomic clones that have evolved to regain 1q-trisomy following xenograft growth exhibit increased anchorage-independent growth relative to the pre-xenograft 1q-disomic parental cells.

(D) Variable evolution of 7p-disomic cells to recover a third copy of chromosome 7p during xenograft growth.

(E) Variable evolution of 8q-disomic cells to recover a third copy of chromosome 8q during xenograft growth.

(F) Regain of trisomy 1q occurs more frequently than regain of trisomy 7p or trisomy 8q. Tumors were classified as exhibiting regain if the mean copy number of the targeted chromosome was ≥ 2.5, as determined through TaqMan copy number assays. n = 213 tumors, chi-squared test.

(G) HCT116 8q-disomic clones evolve to gain a copy of chromosome 12 during xenograft assays, resulting in the acquisition of an extra copy of the $KRAS^{G13D}$ allele. Cell lines were rederived from tumors harvested at the endpoint of xenograft assays, and subjected to SMASH karyotyping and Sanger sequencing of KRAS. The xenograft growth curve is shown on the left, and representative SMASH karyotype profiles and Sanger sequencing chromatograms pre- and post-xenograft are shown on the right. Chromosome 8q is highlighted in blue and chromosome 12 is highlighted in green.

(H) 8q-disomic clones that have evolved to acquire trisomy of chromosome 12 following xenograft growth exhibit increased anchorage-independent growth relative to the pre-xenograft 8q-disomic parental cells.

For copy number profiling in A, D, and E, cell lines were rederived from tumors at the endpoint of the xenograft assays, and chromosome copy number was determined through TaqMan copy number assays. Mean ± SEM, n = 3 probes on targeted chromosome, data from representative trials are shown. The corresponding xenograft assays are shown on the left.

For the anchorage-independent growth assays in C and H, the boxes represent the 25th, 50th, and 75th percentiles of colonies per field, while the whiskers represent the 10th and 90th percentiles. Unpaired t-test, n = 15 fields of view, data from representative trial. Representative images are shown on the right.

***$p < 0.0005$

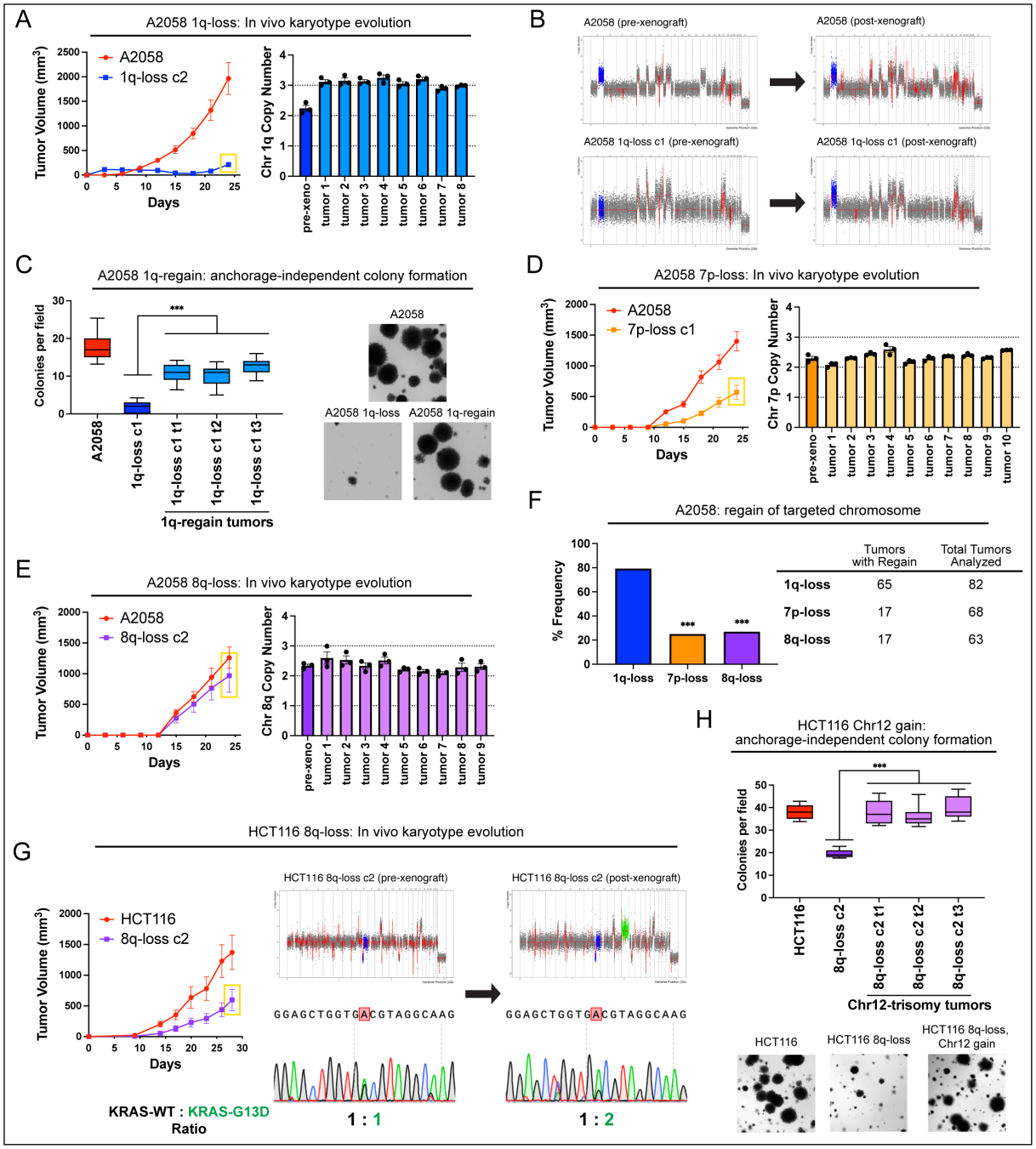

Figure 4: Cancers rapidly recover chromosome 1q aneuploidy.

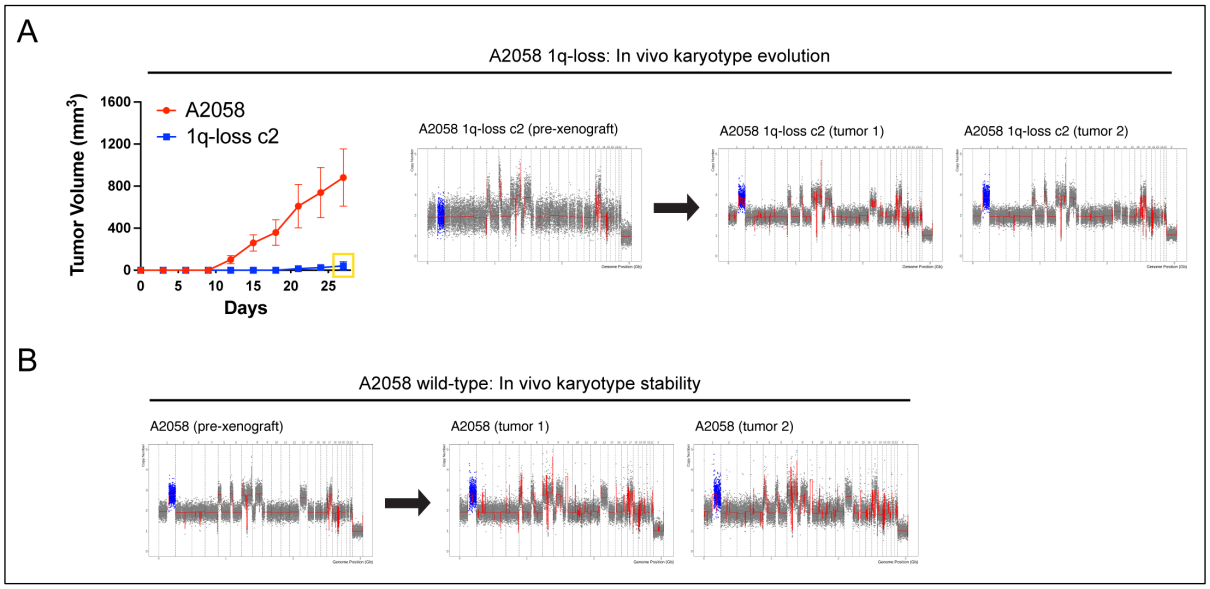

Figure S11. Karyotype analysis of additional 1q-trisomic and 1q-disomic A2058 xenografts

(A) 1q-disomic cells frequently evolve to recover a third copy of chromosome 1q during xenograft growth. (B) A2058 wildtype tumors exhibit karyotypic stability during xenograft growth. For the data shown in A-B, initial karyotypes for these lines prior to xenograft assays are shown on the left, and karyotypes of tumors following the xenograft assays are shown on the right. Chromosome 1q is highlighted in blue.

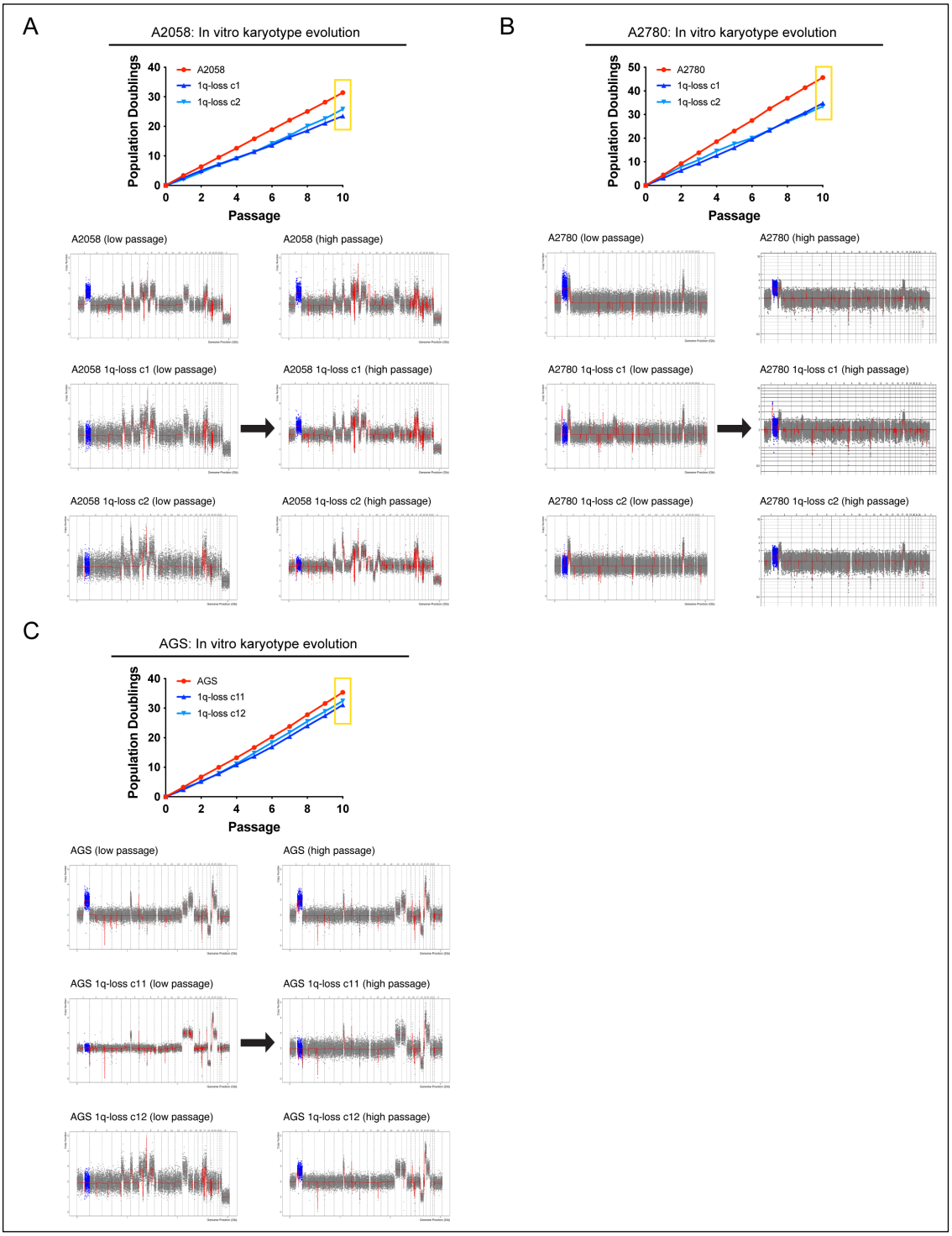

Figure S12. Karyotype evolution of 1q-disomic cancer cells following serial passaging in vitro. (A) Regain of the 1q-trisomy during prolonged *in vitro* passaging of A2058 1q-disomic clones. (B) Regain of the 1q-trisomy during prolonged *in vitro* passaging of A2780 1q-disomic clones. (C) Regain of the 1q-trisomy during prolonged *in vitro* passaging of AGS 1q-disomic clones. For A-C, cells were harvested at the start of the proliferation assay and after 10 passages at the conclusion of the assay, and subject to SMASH karyotyping. Karyotypes are shown below, with chromosome 1q highlighted in blue.

Chromosome 1q aneuploidy suppresses p53 signaling by increasing MDM4 expression

We sought to uncover the biological mechanism underlying the addiction to chromosome 1q aneuploidy. RNA-seq analysis of A2780 cells revealed that elimination of the 1q-trisomy causes significant upregulation of tumor suppressor p53 target genes (Fig. 5A-B). Western blotting confirmed that 1q-disomic clones exhibit increased phosphorylation of p53 at serine-15 and increased expression of the canonical p53 target p21 (Fig. 5C) (Fischer 2017). These results were not a by-product of CRISPR mutagenesis, as A2780 cells harboring a CRISPR-mediated integration of HSV-TK did not display evidence of p53 activation (Fig. 5B-C). Additionally, 1q-disomic cells exhibited a delay in the G1 phase of the cell cycle and increased levels of senescence-associated beta-galactosidase staining, both of which are associated with p53-mediated tumor suppression (Fig. S13) (Sugrue et al. 1997, 53). These results suggest that the chromosome 1q trisomy inhibits p53 signaling, and elimination of this trisomy antagonizes malignant growth at least in part by triggering p53 activation.

To explore whether p53 inhibition is a common consequence of chromosome 1q gains, we examined our prior analysis of aneuploidy-mutation mutual exclusivity in cancer genomes (Table S1). Interestingly, out of 14,383 aneuploidy-gene mutation pairs, the single strongest instance of mutual exclusivity was between 1q gains and *TP53* mutations (Fig. 5D). Put differently, while chromosome 1q gains and *TP53* mutations are separately very common in cancer, individual tumors develop both 1q gains and *TP53* mutations significantly less often than expected by chance ($P < 10^{-39}$, Fisher's exact test; Table S1). Next, we applied a recently-described classification algorithm capable of predicting cancers that lack p53 function based on their transcriptional profiles (Fito-Lopez et al. 2022). As expected, cancers from the TCGA with non-synonymous *TP53* mutations scored significantly higher with this classifier than cancers with wild-type *TP53* (Fig. 5E). Considering only tumors with wild-type

TP53, we calculated the association between the p53 status classifier and every possible chromosome arm gain in the TCGA. Across all chromosomes, 1q gains exhibited the strongest correlation with the p53-loss signature (Fig. 5F-G). Among tumors with wild-type *TP53*, gains of chromosome 1q were associated with significantly lower expression of the p53 target genes *CDKN1A* (p21), *GADD45A*, and *RRM2B* (Fig. 5H) (Fischer 2017). In total, these results indicate that gaining chromosome 1q phenocopies the effects of p53 mutations and suppresses p53 activity in human tumors.

We sought to discover the gene(s) on chromosome 1q responsible for inhibiting p53 signaling. We noted that *MDM4*, a known negative regulator of p53 activity, is located on 1q32 (Karni-Schmidt et al. 2016). *MDM4* expression increased with chromosome 1q copy number and higher *MDM4* expression correlated with the p53-loss transcriptional signature (Fig. S14A-B). To uncover whether *MDM4* is directly responsible for the 1q-aneuploidy addiction observed in A2780, we first used CRISPR-interference (CRISPRi) to downregulate *MDM4* expression without fully ablating it (Gilbert et al. 2014; Horlbeck et al. 2016). In A2780 competition assays, we observed that downregulating MDM4 impaired cell fitness relative to A2780 cells in which *AAVS1* or *PIP5K1A*, an unrelated gene on chromosome 1q, were downregulated (Fig. 5I) (Girish and Sheltzer 2020). Next, we used a two-guide strategy to delete a single copy of *MDM4* in an otherwise trisomic background (Fig. 5J-K and S14C-D). We found that the subsequent A2780 $MDM4^{+/+/KO}$ clones downregulated MDM4 and upregulated TP53 target genes, comparable to the effects observed in cells lacking the entire 1q trisomy (Fig. 5L and S14E). We then tested the colony formation ability of $MDM4^{+/+/KO}$ clones, and we discovered that losing a single copy of *MDM4* significantly decreased anchorage-independent growth (Fig. 5M). Subsequently, we performed the converse experiment: we cloned *MDM4* cDNA under the control of a doxycycline-inducible promoter

and transduced the construct into both 1q-trisomic and 1q-disomic cells. Remarkably, we found that moderate (1.7-fold) overexpression of *MDM4* was sufficient to cause a significant increase in anchorage-independent growth in the 1q-disomic cells, while this same treatment did not affect the 1q-trisomic cells (Fig. 5N and S14F).

Finally, to investigate the role of p53 as a mediator of 1q-aneuploidy addiction from an orthogonal approach, we used CRISPR to delete the *TP53* gene in A2780 1q-disomic and 1q-trisomic cells (Fig. S15A). SMASH-Seq confirmed that these cells did not acquire any secondary chromosomal copy number changes during clonal derivation (Fig. S15B). We discovered that loss of *TP53* rescued the G1 delay and significantly enhanced anchorage-independent growth in 1q-disomic cells (Fig. S15C-D). The magnitude of the increase in colony formation was significantly greater in the 1q-disomic cells compared to the 1q-trisomic cells (4-fold vs. 1.5-fold; $P < .0001$, t-test) (Fig. S15D). In total, these results indicate that chromosome 1q gains represent a mechanism by which p53-wildtype cancers can suppress p53 activity, and this suppression occurs due to the increased expression of *MDM4*. Nonetheless, we note that deleting *TP53* and overexpressing *MDM4* increased fitness in the 1q-disomic clones but did not fully restore fitness to wild-type levels. Thus, there are likely other dosage-sensitive fitness genes on chromosome 1q, and those genes may contribute to selection for 1q-gains in p53-mutant backgrounds.

[This Page Intentionally Left Blank]

Figure 5 (page 78): A single extra copy of *MDM4* suppresses *TP53* signaling and contributes to the 1q-trisomy addiction.

(A) GSEA analysis of A2780 RNA-seq data reveals upregulation of the p53 pathway in the 1q-disomic clones, relative to the parental trisomy.
(B) A heatmap displaying the upregulation of 10 p53 target genes in A2780 1q-disomic clones. The TK+ clone indicates a clone that harbors the CRISPR-mediated integration of the HSV-TK transgene but that was not treated to induce chromosome 1q-loss.
(C) Western blot analysis demonstrating activation of p53 signaling in 1q-disomic clones. *GAPDH* was analyzed as a loading control. The TK+ clone indicates a clone that harbors the CRISPR-mediated integration of the HSV-TK transgene but that was not treated to induce chromosome 1q-loss.
(D) A waterfall plot highlighting the most-significant instances of mutual exclusivity between chromosome arm gains and mutations in cancer-associated genes. The complete dataset for mutual exclusivity and co-occurrence is included in Table S1.
(E) Boxplots displaying the *TP53*-mutation phenocopy signature (Fito-Lopez et al. 2022) in cancers from the TCGA, split based on whether the cancers harbor a non-synonymous mutation in *TP53*.
(F) A scatterplot comparing the association between chromosome arm gains and the *TP53*-mutation phenocopy signature (Fito-Lopez et al. 2022) in TP53-wildtype cancers from TCGA. Cancers with chromosome 1q gains are highlighted in blue.
(G) Boxplots displaying the *TP53*-mutation phenocopy signature (Fito-Lopez et al. 2022) in cancers from the TCGA, split based on whether tumors harbor a gain of chromosome 1q. Only *TP53*-wildtype cancers are included in this analysis.
(H) Boxplots displaying the expression of three p53 target genes – *CDKN1A* (p21), *RRM2B*, and *GADD45A* – in cancers from TCGA split based on the copy number of chromosome 1q. Only *TP53*-wildtype cancers are included in this analysis.
(I) A CRISPRi competition assay demonstrates that gRNAs targeting *MDM4* drop out over time in A2780 cells. In contrast, gRNAs targeting *AAVS1* and *PIP5K1A*, another gene encoded on chromosome 1q, exhibit minimal depletion.
(J) A schematic displaying the strategy for using paired CRISPR gRNAs to delete a single copy of *MDM4* in a cell line with a trisomy of chromosome 1q.
(K) SMASH karyotype demonstrating maintenance of the chromosome 1q trisomy in an $MDM4^{+/+/KO}$ clone. Chromosome 1q is highlighted in blue.
(L) 1q-disomic clones and $MDM4^{+/+/KO}$ clones in A2780 exhibit comparable upregulation of p53 transcriptional targets, as determined through TaqMan gene expression assays.
(M) $MDM4^{+/+/KO}$ clones exhibit decreased anchorage-independent growth relative to the $MDM4^{+/+/+}$ parental cell line.
(N) Induction of *MDM4* cDNA in 1q-disomic clones in A2780 increases anchorage-independent growth.

For the graphs in E, G, H, M, and N, the boxplots represent the 25th, 50th, and 75th percentiles of the indicated data, while the whiskers represent the 10th and 90th percentiles of the indicated data. For the soft agar experiments in M and N, the data are from n = 15 fields of view, and a representative trial is shown. ***$p < 0.0005$

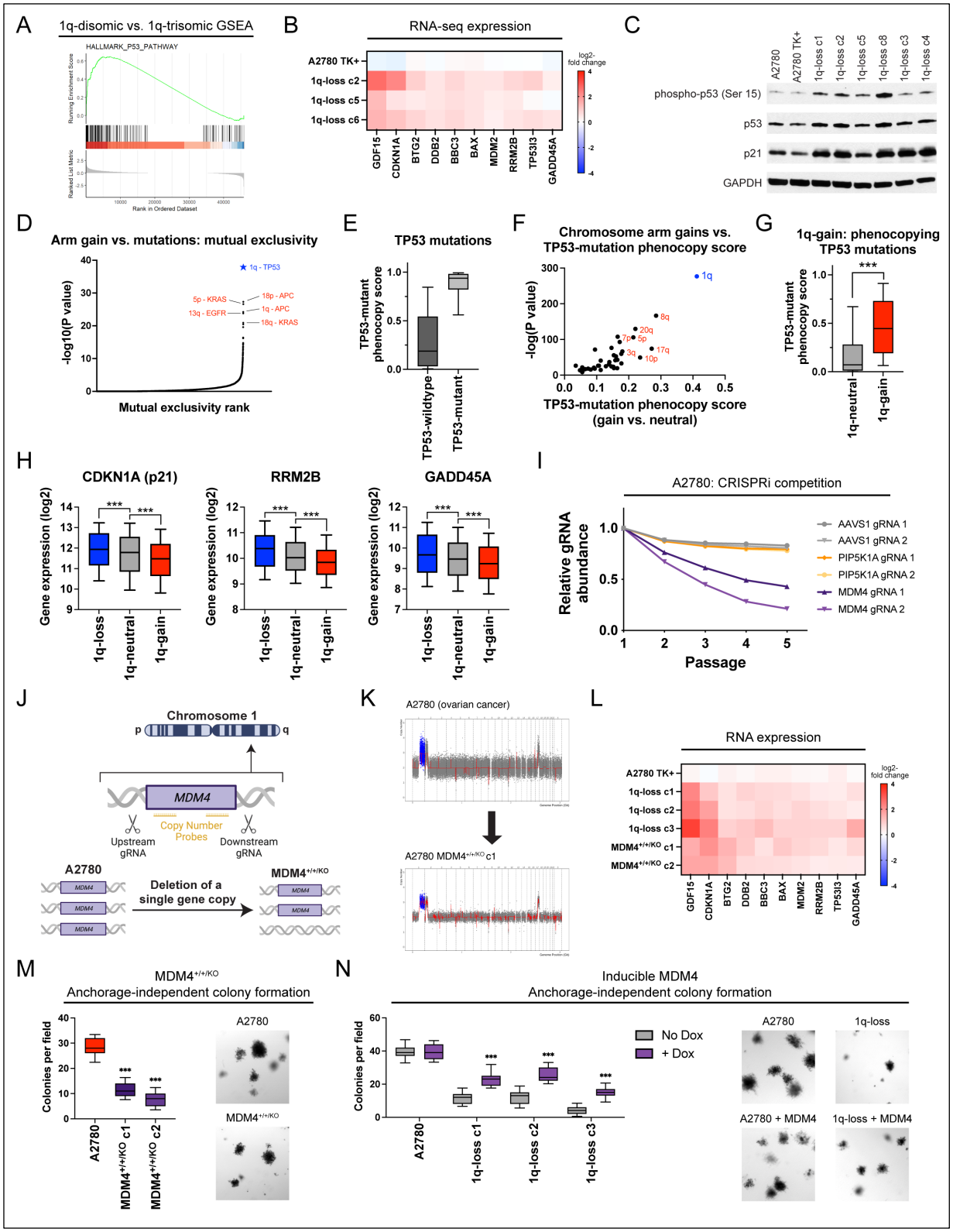

Figure 5: A single extra copy of *MDM4* suppresses *TP53* signaling and contributes to the 1q-trisomy addiction.

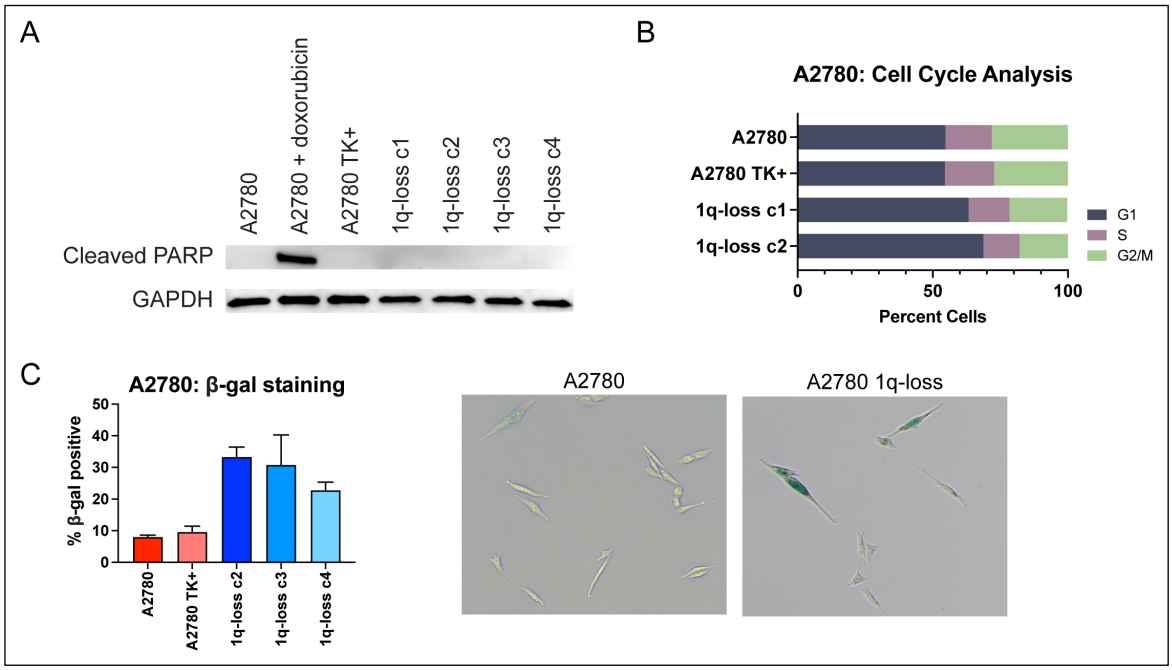

Figure S13. Elimination of the 1q trisomy causes a G1 delay and an increase in senescence.

(A) Levels of cleaved *PARP1* were assessed using western blotting to determine whether aneuploidy-loss induces apoptosis. As a positive control, wild-type cells were treated with the DNA-damaging agent doxorubicin. *GAPDH* was analyzed as a loading control. (B) Cell cycle analysis of A2780 and A2780 1q-disomic clones, determined via propidium iodide staining. (C) A2780 and A2780 1q-disomic clones were stained for beta-galactosidase expression to assess the levels of senescence in each population.

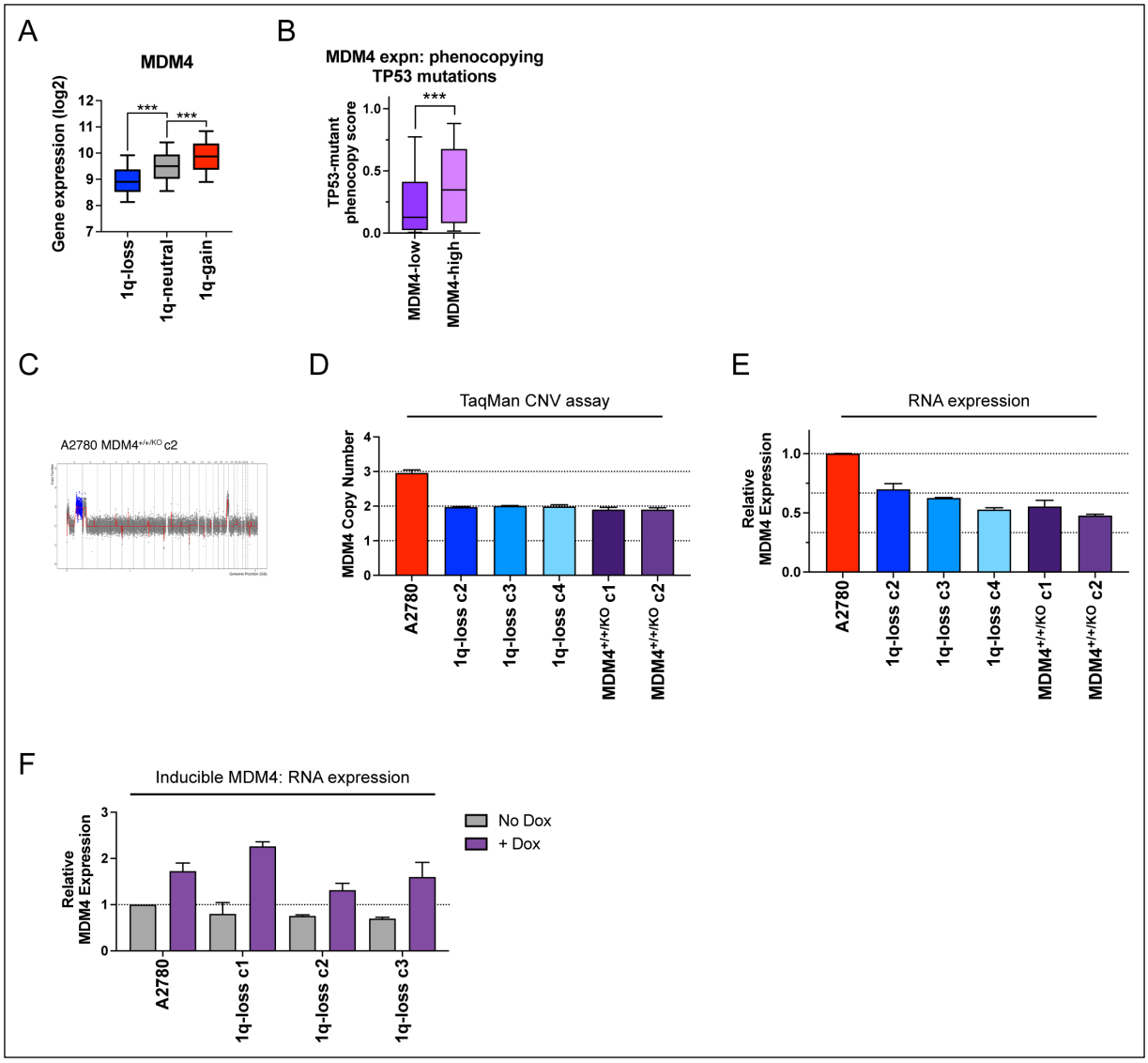

Figure S14. *MDM4* expression in human tumors and *MDM4* genetic manipulations in A2780 cells.

(A) Boxplots displaying the expression of *MDM4* in human cancers from TCGA split based on the copy number of chromosome 1q. (B) Boxplots displaying the *TP53*-mutation phenocopy signature (Fito-Lopez et al. 2022) in cancers from the TCGA, split based on the expression of *MDM4*. Only TP53-wildtype cancers are included in this analysis. (C) SMASH karyotype demonstrating maintenance of the chromosome 1q trisomy in an *MDM4*$^{+/+/KO}$ clone. Chromosome 1q is highlighted in blue. (D) TaqMan copy number verification of the deletion of a single copy of *MDM4* in A2780 cells. Mean ± SEM, n=2 probes for MDM4. (E) *MDM4*$^{+/+/KO}$ and 1q-disomic clones exhibit decreased expression of *MDM4*, as determined through TaqMan gene expression assays. Data are normalized to parental A2780. (F) Expression of *MDM4* in 1q-trisomic and 1q-disomic cells harboring *MDM4* under the control of a doxycycline-inducible promoter. *MDM4* expression was measured using qRT-PCR.
***p < 0.0005

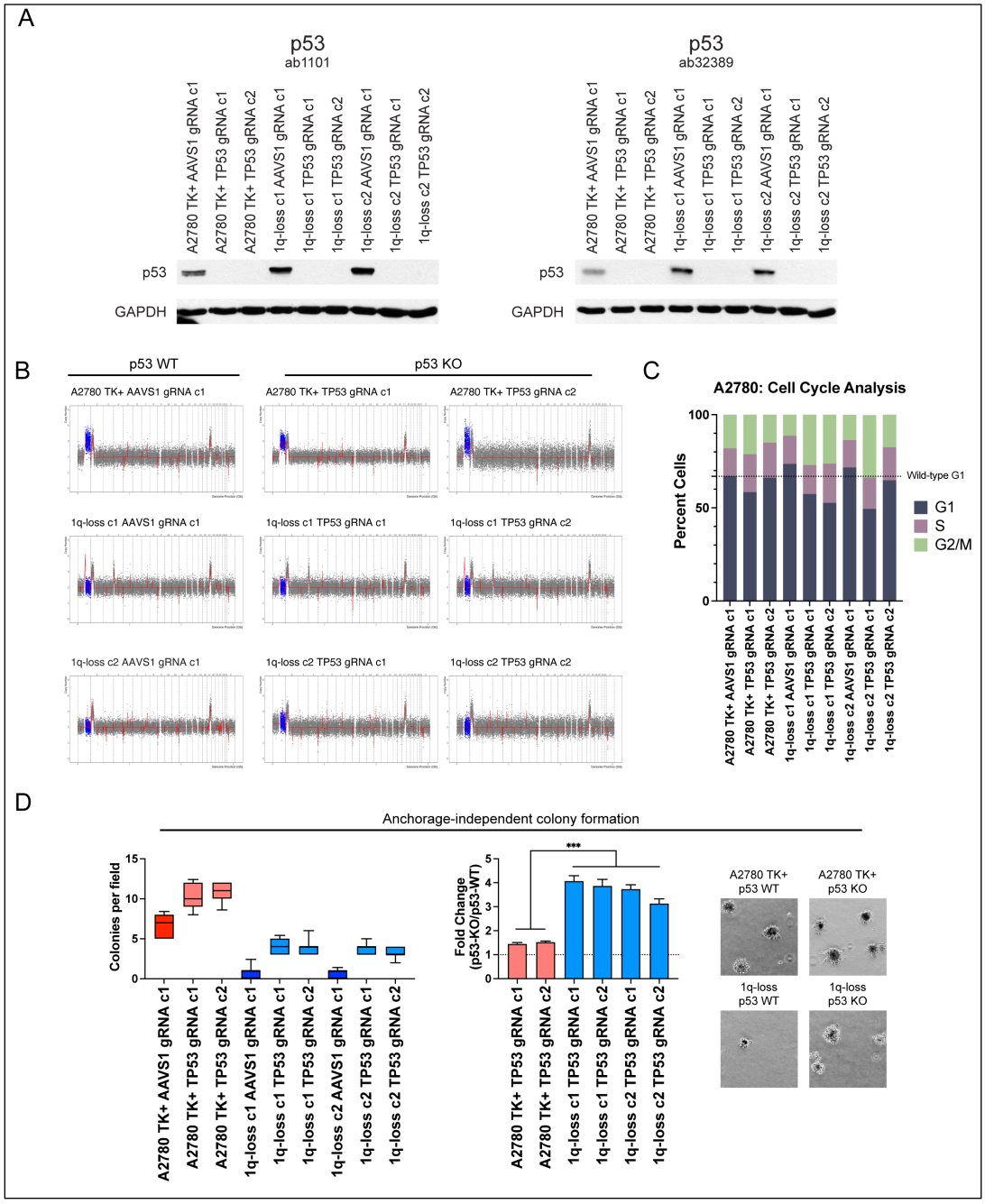

Figure S15. Deletion of *TP53* selectively increases the fitness of 1q-disomic cells.
(A) Western blot validation of p53-KO with two different antibodies. *AAVS1* gRNA clones serve as isogenic p53-WT controls. *GAPDH* was used as a loading control. (B) SMASH karyotypes of p53-KO and p53-WT clones. TK+ integrant clones maintain the 1q-trisomy, 1q-disomic clones maintain the 1q-disomy, and no other karyotypic alterations are observed. Chromosome 1q is highlighted in blue. (C) Cell cycle analysis of p53-KO and p53-WT clones in A2780 TK+ and 1q-disomic lines, determined via propidium iodide staining. (D) Deletion of TP53 increases anchorage independent growth by ~1.5-fold in 1q-trisomic clones and by ~4-fold in 1q-disomic clones. Boxes represent the 25th, 50th, and 75th percentiles of colonies per field, while the whiskers represent the 10th and 90th percentiles. Unpaired t-test, n = 15 fields of view, data from representative trial. Representative images are shown. ***p < 0.0005

Chromosome 1q aneuploidy creates a collateral therapeutic vulnerability

The oncogene addiction hypothesis represents the conceptual foundation for the use of targeted therapies in cancer (Torti and Trusolino 2011). Cancers addicted to driver oncogenes like *BCR-ABL* or $EGFR^{L858R}$ respond to inhibitors of those proteins that otherwise have minimal effect in untransformed tissue. Correspondingly, we sought to uncover whether aneuploidy addictions could also represent a therapeutic vulnerability for certain cancers. Toward that goal, we noted that chromosome 1q harbors the *UCK2* gene, which encodes a kinase involved in the pyrimidine salvage pathway (Fu et al. 2022). *UCK2*-dependent phosphorylation has previously been reported to function as the rate-limiting step in the metabolism of certain nucleotide analogs, including RX-3117 and 3-deazauridine (Fig. 6A) (Van Rompay et al. 2001; van Kuilenburg and Meinsma 2016; Sarkisjan et al. 2016). Phosphorylated RX-3117 and 3-deazauridine can poison cellular nucleotide pools and block DNA and RNA synthesis (Peters 2014). We found that *UCK2* is over-expressed in human cancers that contain extra copies of chromosome 1q, and elimination of the chromosome 1q trisomy consistently decreased *UCK2* protein expression in our engineered cell lines (Fig. 6B-C). We therefore investigated whether gaining chromosome 1q could create a collateral sensitivity to *UCK2*-dependent nucleotide analogs.

First, as the mechanism of many cancer drugs is poorly-understood (Lin et al. 2019; Lin and Sheltzer 2020), we sought to verify that the cytotoxicity of RX-3117 and 3-deazauridine requires *UCK2* expression. We used CRISPR to delete *UCK2* in the haploid HAP1 cell line, and we confirmed that *UCK2*-knockout cells are highly resistant to both compounds (Fig. S16A-C). Next, we tested the effects of RX-3117 and 3-deazauridine in our engineered 1q-trisomic and 1q-disomic cell lines. We found that A2780 and MCF10A cells harboring a trisomy of chromosome 1q were significantly more sensitive to both compounds

compared to isogenic cells containing two copies of chromosome 1q (Fig. 6D). This effect was specific for *UCK2* substrates, as the 1q-trisomic cells did not exhibit greater sensitivity to *UCK2*-independent nucleotide poisons and other cancer drugs (Fig. S16D). Furthermore, ectopic over-expression of *UCK2* cDNA in 1q-disomic clones was sufficient to re-sensitize these cells to RX-3117 (Fig. S16E). Finally, RX-3117 and 3-deazauridine have previously been screened across the NCI-60 cell line panel, and we found that higher *UCK2* expression levels correlate with greater sensitivity to both compounds (Fig. S16F) (Luna et al. 2021). In total, these results indicate that 1q gains induce a collateral sensitivity to specific nucleotide analogs by increasing the expression of the *UCK2* kinase.

We hypothesized that we could use the greater sensitivity of 1q-trisomic cells to *UCK2* substrates to re-direct cellular evolution away from aneuploidy and towards a disomic state with lower malignant potential (Fig. 6E). We mixed fluorescently-labeled 1q-trisomic and 1q-disomic A2780 cells at a ratio of 10:90, and then co-cultured the two cell populations. After three weeks of growth in drug-free media, the trisomic cells had expanded to make up 67% of the culture, consistent with our observation that the extra copy of chromosome 1q enhances cellular fitness (Fig. 6F). In contrast, when the same cell populations were grown in the presence of 400 nM RX-3117, there was no significant increase in the trisomic cell population over time. We conclude that trisomy-selective compounds can be used to manipulate cellular evolution, potentially providing a new strategy to prevent the outgrowth of malignant aneuploid cells in a pre-malignant setting.

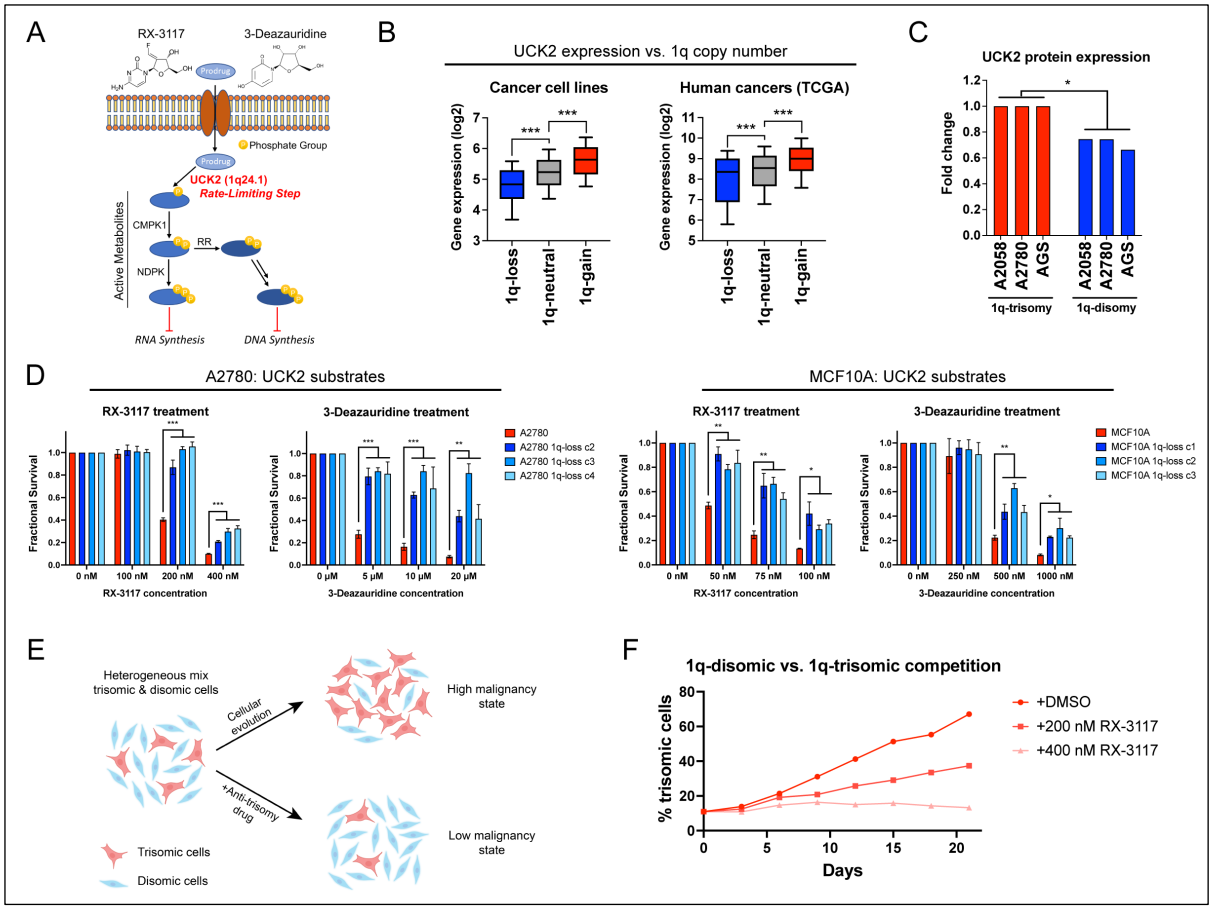

Figure 6. Gaining chromosome 1q increases sensitivity to *UCK2* substrates.
(A) A schematic of the metabolism of two pyrimidine analogs, RX-3117 and 3-deazauridine. *UCK2*, a kinase encoded on chromosome 1q, phosphorylates these compounds to produce cytotoxic derivatives that can poison DNA and RNA synthesis. (B) Boxplots displaying the expression of *UCK2* in cancer cell lines (Barretina et al. 2012) (left) and human cancers (The Cancer Genome Atlas Research Network et al. 2013) (right), divided based on the copy number of chromosome 1q. The boxplots represent the 25th, 50th, and 75th percentiles of the indicated data, while the whiskers represent the 10th and 90th percentiles of the indicated data. (C) Expression of *UCK2* protein in cancer cell lines with 1q trisomies or following aneuploidy-elimination. (D) Cellular sensitivity of A2780 and MCF10A treated with different concentrations of RX-3117 or 3-deazauridine. (E) A schematic displaying cellular competition between trisomic and disomic cells. Under normal conditions, certain trisomies enhance cellular fitness, allowing these cells to overtake the population and enhance malignant growth (top). However, treatment with an "anti-trisomy" compound could selectively impair the growth of the aneuploid cells, keeping the population in a low-malignant state (bottom). (F) A cellular competition between fluorescently-labeled A2780 1q-trisomic and unlabeled 1q-disomic cells. These cells were mixed at a ratio of 10% to 90% and then cultured in either DMSO or RX-3117. While the trisomic cells quickly dominate the population in drug-free media, treatment with RX-3117 prevents the outgrowth of the 1q-trisomy subpopulation. *p < 0.05, ** p < 0.005, *** p < 0.0005

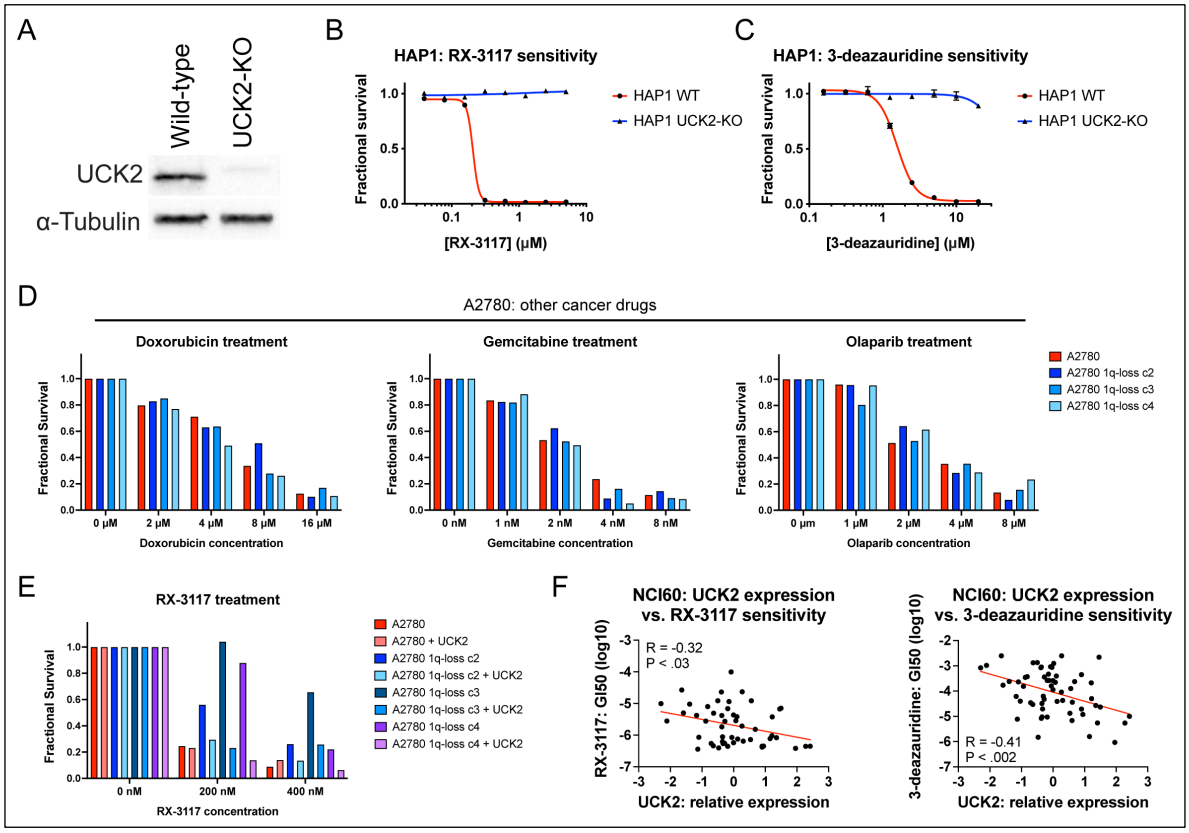

Figure S16. *UCK2* expression sensitizes cancer cells to RX-3117 and 3-deazauridine. (A) Western blotting verifying lack of *UCK2* expression in the HAP1 *UCK2*-KO clone. Tubulin levels were analyzed as a loading control. (B) 7-point dose response curve displaying the viability of HAP1 and HAP1 *UCK2*-KO cells treated with varying concentrations of RX-3117. (C) 7-point dose response curve displaying the viability of HAP1 and HAP1 *UCK2*-KO cells treated with varying concentrations of 3-deazauridine. (D) Viability of A2780 cells treated with different concentrations of the indicated anti-cancer drug. (E) Viability of A2780 cells or A2780 cells transduced with *UCK2* cDNA treated with RX-3117. (F) Correlation between *UCK2* expression and sensitivity to RX-3117 (left) or 3-deazauridine (right) across the NCI-60 panel of cancer cell lines (Luna et al. 2021).

Discussion

Here, we describe ReDACT, a set of tools that can be used to eliminate aneuploid chromosomes from human cell lines. Using ReDACT, we engineered genetically-matched cell lines that have or lack common cancer aneuploidies, and we demonstrate that losing the aneuploidy of chromosome 1q blocks malignant growth in cell lines harboring this alteration. We posit that these phenotypes are due specifically to the loss of the aneuploid chromosome and are not a by-product of CRISPR selection or the elimination of point mutations encoded on the targeted chromosome (discussed in more detail in Supplemental Text 1 and 2, respectively). Due to the similarity between our observations and the previously-described cancer gene addiction phenomenon, we suggest that, in certain circumstances, cancers may also be "addicted" to the aneuploidy found in their genomes.

Historically, cancer aneuploidy has been resistant to close analysis (Vasudevan et al. 2021). While individual cancer driver genes have been studied for several decades using the standard tools of molecular genetics, manipulating chromosome dosage has been technically challenging. Initial insight into the role of aneuploidy in tumorigenesis was gained through the development of genetically-engineered mouse models that harbor mutations in mitotic checkpoint genes (Michel et al. 2001; Schvartzman et al. 2010; Simon et al. 2015). These chromosomal instability-promoting mutations were found to either enhance or suppress tumorigenesis, depending on the oncogenic stimulus and the degree of instability (Weaver et al. 2007; Silk et al. 2013; Baker et al. 2009). However, it is not clear whether these results can be attributed specifically to aneuploidy itself, as chromosome mis-segregation can cause certain phenotypes that are independent of the resulting dosage imbalance (Schukken and Foijer 2018; Bakhoum and Cantley 2018; Bakhoum et al. 2018) and many mitotic checkpoint genes moonlight in other cellular processes (Campbell et al. 2001; Choi et al. 2016; Singh and

Bhalla 2020). Alternately, microcell-mediated chromosome transfer has been used to introduce extra chromosomes into diploid cell lines (Stingele et al. 2012; Doherty and Fisher 2003; Passerini et al. 2016). Cells manipulated to carry trisomic chromosomes were found to exhibit reduced malignant potential compared to their diploid parental cell lines (Sheltzer et al. 2017). These tumor-suppressive effects of aneuploidy have been attributed to the global imbalance in protein stoichiometry caused by the expression of hundreds of extra genes (Santaguida et al. 2015; Donnelly et al. 2014; Donnelly and Storchová 2015; Ohashi et al. 2015).

In this work, we eliminated endogenous aneuploidies from established cancer cell lines, and we revealed that loss of these trisomic chromosomes compromised cancer-like growth. We posit that during tumor evolution, certain aneuploidies can provide context-specific benefits that enhance tumorigenesis. For instance, we showed that chromosome 1q gains are an early event during breast cancer development, and we demonstrated that *MDM4* is a dosage-sensitive gene on 1q that suppresses p53 signaling and enhances cancer growth. In other cancer types or in cells that already harbor *TP53* mutations, the beneficial effects of gaining *MDM4* may be outweighed by the detrimental effects of overexpressing hundreds of additional 1q genes.

We note that *MDM4* and many other genes have been demonstrated to have tumor-promoting properties when highly overexpressed (Santarius et al. 2010). For instance, *MDM4* is focally amplified in ~1% of cancers in the TCGA, and strong overexpression of *MDM4* via retrovirus immortalizes primary cells and renders them sensitive to *RAS*-mediated transformation (Danovi et al. 2004). Our results demonstrate that even a single extra copy of *MDM4* can be oncogenic, and we speculate that there are many genes, both known and unknown, that can promote tumorigenesis when their copy number is increased from two to

three. The overlap between these single-copy dosage-sensitive genes and genes found to have tumor-promoting ability when highly overexpressed is at present unknown.

Finally, our results raise the exciting possibility that "aneuploidy addictions" may represent a new therapeutic vulnerability in cancer. Previous attempts to target aneuploidy have focused on phenotypes that are shared across highly-aneuploid cells, such as alterations in spindle geometry (Quinton et al. 2021; Cohen-Sharir et al. 2021). Here, we sought to develop an approach to take advantage of the genes that are encoded on an aneuploid chromosome, thereby allowing chromosome-specific targeting. In particular, we hypothesized that the over-expression of specific genes – for instance, drug-importer pumps or enzymes required for a pro-drug's activation – could sensitize cancers to compounds that are otherwise better-tolerated in euploid tissue. We demonstrated that gaining chromosome 1q creates a collateral vulnerability to the nucleotide analogs RX-3117 and 3-deazauridine due to the overexpression of the kinase *UCK2*. Notably, RX-3117 has been tested in phase 2A clinical trials, but without the use of any genomic biomarkers for patient selection (Salgia et al. 2019). We speculate that this drug may be particularly effective if given to patients with tumors that harbor gains of chromosome 1q. More broadly, compounds whose anti-cancer function is enhanced by genes encoded on aneuploid chromosomes could be used to direct cellular evolution away from certain aneuploidies and toward the lower-malignancy diploid state.

Acknowledgments

We are grateful to Dr. Tobias Cantz (Hannover Medical School) for providing the TK plasmids used in this work. We thank Peter Andrews (CSHL) for assistance with SMASH-Seq. We thank Yale Flow Cytometry, especially Chao Wang and Lesley Devine, for their assistance with single-cell sorting. Yale Flow Cytometry is supported in part by an NCI Cancer Center Support Grant # NIH P30 CA016359. We thank Al Mennone and the Yale Center for Advanced Light Microscopy Facility for their assistance with soft agar imaging. We thank the Yale Center for Genome Analysis for performing SMASH-Seq. We thank the Yale Center for Research Computing, specifically Robert Bjornson, for guidance and assistance in computation run on the Farnam and Ruddle clusters. We thank the Yale Animal Resources Center Staff for assistance with mouse experiments. This work was performed with assistance from the CSHL Flow Cytometry, Microscopy, Animal, and Sequencing Technologies & Analysis Shared Resources, which are supported in part by the Cancer Center Support Grant 5P30CA045508.

Copy number timing analysis conducted in the Sun Lab uses the computing resources of the Minnesota Supercomputing Institute. The timing analysis was prepared using limited access datasets obtained from the Cancer Genome Project from the Wellcome Sanger Institute and does not necessarily reflect the opinions of the provider institution. Part of the BRCA sequencing data was originally generated by research led by Dr. Masahito Kawazu and is available at the website of the National Bioscience Database Center (NBDC; http://biosciencedbc.jp/en/) of the Japan Science and Technology Agency (JST). We also thank the International Cancer Genome Consortium (ICGC) for providing access to the MEL dataset.

Research in the Sheltzer Lab is supported by NIH grant R01CA237652, Department of Defense grant W81XWH-20-1-068, an American Cancer Society Research Scholar Grant, a Breast Cancer Alliance Young Investigator Award, a Damon Runyon-Rachleff Innovation Award, a sponsored research agreement from Ono Pharmaceuticals, and a sponsored research agreement from Meliora Therapeutics. Research in the Liu Lab is supported by NIH grant R01GM137031.

DECLARATION OF INTERESTS

J.C.S. is a co-founder of Meliora Therapeutics, a member of the advisory board of Surface Ventures, and an employee of Google, Inc. This work was performed outside of her affiliation with Google and used no proprietary knowledge or materials from Google. J.M.S. has received consulting fees from Merck, Pfizer, Ono Pharmaceuticals, and Highside Capital Management, is a member of the advisory board of Tyra Biosciences and the Chemical Probes Portal, and is a co-founder of Meliora Therapeutics.

Materials & Methods

BASIC CELL CULTURE TECHNIQUES

Cell lines and culture conditions

The identities of all cell lines used in this study were confirmed using STR (short tandem repeat) profiling (University of Arizona Genetics Core). A2780 was grown in RPMI 1640 medium (Gibco, cat. no. 11875119) supplemented with 10% fetal bovine serum (FBS) (Sigma-Aldrich, cat. no. F4135), 2 mM glutamine (Lonza, cat. no. 17-605F), and 100 U/mL penicillin-streptomycin (Life Technologies, cat. no. 15140122). A2058, HCT116, HEK-293T, and PLAT-A cells were grown in DMEM (Gibco, cat. no. 11995073) supplemented with 10% FBS, 2 mM glutamine, and 100 U/mL penicillin-streptomycin. AGS was grown in F-12K (ATCC; cat. no. 30-2004) supplemented with 10% FBS, 2 mM glutamine, and 100 U/mL penicillin-streptomycin. HAP1 cells were grown in IMDM (Gibco, cat. no. 12440053) supplemented with 10% FBS, 2 mM glutamine, and 100 U/mL penicillin-streptomycin. MCF-10A was grown in DMEM/F-12 (Gibco, cat. no. 11320082), supplemented with 5% horse serum (Gibco, cat. no. 16050122), 20 ng/mL EGF (PeproTech, cat. no. AF-100-15), 0.5 ng/mL Hydrocortisone (Sigma-Aldrich, cat. no. H0888), 100 ng/mL Cholera Toxin (Sigma-Aldrich, cat. no. C8052), 10 μg/mL Insulin (Sigma-Aldrich, cat. no. I1882), 5 mM Transferrin (Sigma-Aldrich, cat. no. T8158), and 100 U/mL penicillin-streptomycin. All cells were cultured in a humidified environment at 37˚C and 5% CO_2. Sources of the cell lines used in this manuscript are listed in Table S4.

Production of lentivirus and retrovirus

HEK293T (lentivirus) or PLAT-A (retrovirus) cells were transfected using the calcium-phosphate method(Chang et al. 2013). Virus-containing supernatant was harvested 48 to 72

hours post-transfection, filtered through a 0.45 µm syringe, and then frozen at -80˚C for later use or applied directly to cells with 4-10 µg/mL polybrene (Santa Cruz Biotechnology, Inc., cat no. SC-134220). The culture media on target plates was changed 24 hours post-transduction.

PLASMID CLONING METHODS

CRISPR plasmid cloning

Guide RNAs for CRISPR experiments were designed with Benchling (www.benchling.com). Guides were cloned into the Lenti-Cas9-gRNA-GFP vector (Addgene #124770) or LRCherry2.1 (Addgene #108099) using a BsmBI digestion as previously described(Giuliano et al. 2019). Plasmids were transformed in Stbl3 E. coli (Thermo Fisher Scientific, cat. no. C737303) and sequence-verified to confirm the presence of the correct gRNA. CRISPR gRNA sequences are listed in Table S5A.

CRISPRi plasmid cloning

Guide RNAs for CRISPRi experiments were chosen from refs (Horlbeck et al. 2016; Sanson et al. 2018), and two guides per gene were cloned into the LRG2.1 mCherry vector (Addgene #108099) as described above. Plasmids were transformed in Stbl3 *E. coli* and sequenced to confirm the presence of the correct gRNA sequence. CRISPRi gRNA sequences are listed in Table S5B.

Cloning of doxycycline-inducible MDM4

The *MDM4* coding sequence (NM_002393.5) was cloned into Lenti-X™ Tet-One™ Inducible Expression System (Takara Bio, cat. no. 631847). The resulting plasmid was then subject to

whole-plasmid sequencing for verification. A2780 cells were transduced with pLVX-TetOne-MDM4-Puro and selected for with 1.5 µg/mL puromycin (InvivoGen, cat. no. ant-pr-1). Tight inducibility was confirmed through doxycycline (Sigma-Aldrich, cat. no. D3072) titration and quantitative real-time PCR. The final plasmid was deposited on Addgene (#195140).

KARYOTYPING AND DNA COPY NUMBER ANALYSIS

SMASH-seq

Libraries for genomic copy number analysis were prepared as described in ref(Wang et al. 2016). In brief, genomic DNA was enzymatically fragmented to a mean size of ~40bp and ligated to generate long chimeric DNA molecules (~300-700bp) for sequencing. Fragment size selection and purification were done with Agencourt AMPure XP beads (Beckman Coulter, cat. no. A63881). Illumina-compatible NEBNext Multiplex Dual Index primer pairs and adapters (New England Biolabs, cat. no. E6440S) were added to each sample, and the products were pooled for next-generation sequencing (NGS). Libraries were sequenced using an Illumina MiSeq or NovoSeq sequencer. The generated reads were demultiplexed then mapped using a custom Nextflow (Di Tommaso et al. 2017) wrapper running *SMASH* built from MUMdex (Andrews et al. 2016) (commit: 25e1f2f). Plots were generated via a custom script utilizing *tidyverse* (Wickham et al. 2019) (v1.3.1) components run in the R programming environment (R Core Team 2022; v4.2.0).

G-banding karyotyping

A2780 samples were sent to Cell Line Genetics Inc. (www.clgenetics.com), and AGS and A2058 samples were sent to Karyologic Inc. (www.karyologic.com) for G-banding

karyotyping. A minimum of 10 metaphase spreads per sample were counted and analyzed to prepare representative karyotype spreads.

TaqMan copy number analysis

Genomic DNA was extracted and isolated using the Qiagen DNeasy Blood & Tissue kit (Qiagen, cat. no. 69506). Reactions were prepared in quadruplicate, and target probes were duplexed with RNaseP (Applied Biosystems, cat. no. 4316831) or TERT (Applied Biosystems, cat. no. 4403316) as the reference assay. Quantitative PCR was performed using TaqPath ProAmp Master Mix (Applied Biosystems, cat. no. A30867) and quantified using the QuantStudio 6 Flex Real-Time PCR system (Applied Biosystems). Copy number analysis was performed as described in ref (Mayo et al. 2010) and copy number calls were normalized to the near-diploid colorectal cancer cell line DLD1 (Vasudevan et al. 2020). To screen for chromosome arm loss, a minimum of three probes spanning the chromosome of interest were used, and the copy number calls for the individual probes were averaged to determine chromosome arm copy number. To screen for single copy gene deletions, two probes for the gene of interest were used, and the copy number calls for the individual probes were averaged to determine gene copy number. TaqMan copy number probes are listed in Table S6.

GENE EXPRESSION ANALYSIS

RNAseq

Total cellular RNA was extracted using the Qiagen RNeasy Mini Kit (Qiagen, cat. no. 74106) and subjected to on-column DNase digestion (Qiagen, cat. no. 79254). Purified RNA samples were submitted to Novogene for RNAseq and quantification. In brief, mRNA was purified from total cellular RNA using poly-T oligo-attached magnetic beads. After fragmentation,

first strand cDNA was synthesized using random hexamer primers, followed by second strand cDNA synthesis. Subsequently, libraries were prepared with end repair, A-tailing, adapter ligation, size selection, amplification, and purification. Libraries were sequenced on an Illumina platform and paired-end reads were generated. Raw data (raw reads) of fastq format were firstly processed through in-house Novogene Perl scripts. Reference genome and gene model annotation files were downloaded from genome website directly. An index of the reference genome was built using Hisat2 v2.0.5 and paired-end clean reads were aligned to the reference genome using Hisat2 v2.0.5. featureCounts v1.5.0-p3 was used to count the reads numbers mapped to each gene. The FPKM of each gene was calculated based on the length of the gene and reads count mapped to this gene. Gene Set Enrichment analysis was performed with the local version of the GSEA analysis tool http://www.broadinstitute.org/gsea/index.jsp and the predefined Hallmark gene sets.

Mass spectrometry

Proteomic analysis was conducted as previously described (Liu et al. 2019). In short, cell pellets were thawed and a VialTweeter device (Hielscher-Ultrasound Technology) was used to sonicate the samples (4 °C; 1 min; two cycles). The samples were centrifuged at 20,000 g for 1 hour to remove insoluble material. Protein concentration was measured using the Bio-Rad protein assay dye (Bio-Rad, cat. no. 5000006). 800 µg of protein per sample were diluted (final concentration = 2 µg/µL) using a 10 M urea/100 mM ammonium bicarbonate buffer, reduced by 10 mM DTT (1 hour; 56 °C), and alkylated by 20 mM IAA (1 hour; RT). The proteins were subjected to a precipitation-based digestion(Collins et al. 2017). Briefly, five volumes of precooled precipitation solution (50% acetone, 50% ethanol, and 0.1% acetic acid) were added to the samples. After overnight incubation at -20 °C, the samples were centrifuged (20,000 x

g; 4 °C; 40 min). The precipitate was washed with precooled 100% acetone, centrifuged (20,000 x g; 4 °C; 40 min), and the remaining acetone was evaporated in a SpeedVac. For protein digestion, 300 µL of 100 mM NH4HCO3 with sequencing grade porcine trypsin (Promega) at a trypsin-to-protein ratio of 1: 20 were added and incubated overnight at 37 °C. The resulting peptide samples were acidified with formic acid and desalted using a C18 column (MarocoSpin Columns, NEST Group INC.) according to the manufacturer's instructions.

1 µg of the peptide mixture was used for the LC-MS analysis as described previously (Liu et al. 2019; Mehnert et al. 2019). The LC separation was performed using an EASY-nLC 1200 system (Thermo Scientific) using a self-packed PicoFrit column (New Objective, Woburn, MA, USA; 75 µm × 50 cm length) with a ReproSil-Pur 120A C18-Q 1.9 µm resin (Dr. Maisch GmbH, Ammerbuch, Germany). A 120-min gradient length was used to elute peptides from the LC; with buffer B (80% acetonitrile containing 0.1% formic acid) from 5% to 37% and corresponding buffer A (0.1% formic acid in H2O). The flow rate was 300 nL/ min, and the temperature was controlled at 60 °C using a column oven (PRSO-V1, Sonation GmbH, Biberach, Germany). The Orbitrap Fusion Lumos Tribrid mass spectrometer (Thermo Scientific) coupled with a NanoFlex ion source (spray voltage of 2000 V, 275 °C) was used for the MS analysis. The method for DIA-MS consisted of a MS1 survey scan and 33 MS2 scans of variable windows(Bruderer et al. 2017, 2019). The MS1 scan parameters were set as follows: scan range 350–1650 m/z, resolution 120,000 at m/z 200, the AGC target 2.0E6, and the maximum injection time 100 ms. The normalized HCD collision energy was 28%. The MS2 scan parameters were the following: resolution 30,000 at m/z 200, the AGC target 1.5E6, and the maximum injection time 50 ms. The default peptide charge state was set to 2. Both of MS1 and MS2 spectra were recorded in a profile mode.

The DIA-MS data analysis was performed using Spectronaut v15 (Bruderer et al. 2015, 2017) using the library-free DirectDIA workflow (Tsou et al. 2015; Bruderer et al. 2017) and the Swiss-Prot protein database (September 2020, 20,375 entries). The analysis was performed using default Spectronaut settings. Methionine oxidation and N-terminal acetylation were set as variable modifications, where carbamidomethylation at cysteine was set as a fixed modification. Both peptide- and protein-FDR were controlled at 1%, and the resulting data matrix was filtered by "Qvalue". The DIA quantification was performed using the MS2 level peak areas. Protein intensities were exported, log2-transformed and normalized using LOESS normalization (Smyth 2005) prior to the subsequent analysis.

Quantitative real-time PCR

Total cellular RNA was extracted and isolated using the Qiagen RNeasy Mini Kit (Qiagen, cat. no. 74106). cDNA synthesis was performed using SuperScript IV VILO Master Mix (Invitrogen, cat. no. 11756500). Quantitative PCR was performed for the target genes using TaqMan Fast Advanced Master Mix (Applied Biosystems, cat. no. 4444963) and quantified using the QuantStudio 6 Flex Real-Time PCR system (Applied Biosystems). TaqMan gene expression assays are listed in Table S7 and qPCR primers are listed in Table S8.

Western Blotting

One day prior to lysate harvest, 500,000 cells were seeded in a six-well plate. Whole cell lysates were harvested and resuspended in RIPA buffer [25 mM Tris, pH 7.4, 150 mM NaCl, 1% Triton X 100, 0.5% sodium deoxycholate, 0.1% sodium dodecyl sulfate, protease inhibitor cocktail (Sigma, cat. no. 4693159001), and phosphatase inhibitor cocktail (Sigma, cat. no. 4906845001)]. Protein concentration was quantified using the RC DC Protein Assay (Bio-Rad;

cat. no. 500–0119). Equal amounts of lysate were denatured and loaded onto a 10% SDS-PAGE gel. The Trans-Blot Turbo Transfer System (Bio-Rad) and polyvinylidene difluoride membranes were used for protein transfer. Antibody blocking was done with 5% milk in TBST (19 mM Tris base, NaCl 137 mM, KCl 2.7 mM and 0.1% Tween-20) for 1 hour at room temperature. The following antibodies and dilutions were used: p21 (Abcam; cat. no. ab109520) at a dilution of 1:1000 in 5% milk, p53 (Abcam; cat. no. ab1101) at a dilution of 1:1000 in 5% milk, p53 (Abcam; cat. no. ab32389) at a dilution of 1:1000 in 5% milk, Phospho-p53 (Ser15) (Cell Signaling, cat. no. 9284S) at a dilution of 1:1000 in 5% milk, Cleaved-PARP (Asp214) (Cell Signaling; cat. no. 5625S) at a dilution of 1:1000 in 5% milk, and UCK2 (proteinTech; cat. no. 10511-1-AP) at a dilution of 1:1000 in 5% milk. Blots were incubated with the primary antibody overnight at 4°C. Anti-GAPDH (Santa-Cruz; cat. no. sc-365062) at a dilution of 1:20,000 in 5% milk, or Anti-alpha tubulin (Sigma-Aldrich; cat. no. T6199) at a dilution of 1:20,000 in 5% milk was used as a loading control. Membranes were washed at room temperature three times (20 mins each) before they were incubated in secondary antibodies for an hour at room temperature. HRP goat anti-mouse (Bio-Rad; cat. no. 1706516) at 1:20,000 was used for tubulin, p53 (ab1101), MDM4, and GAPDH blots while HRP goat anti-rabbit (Abcam; cat. no. ab6721) at 1:20,000 was used for all other primary antibodies. Membranes were washed three times again (20 min each) and developed using ProtoGlow ECl (National Diagnostics; cat. no. CL-300) and autoradiographic film (Lab Scientific; XAR ALF 2025).

CHROMOSOME ENGINEERING

Chromosome elimination: ReDACT-NS

Generation of selection cassette: A centromere-proximal CRISPR gRNA was designed and cloned into the Lenti-Cas9-gRNA-GFP vector (Addgene #124770) for integration of the selection cassette. Homology arms for cassette integration were designated as the 180bp immediately upstream and downstream of the guide RNA targeting site. Adapters for PCR were added to the 3′ end of the 180bp homology arms (Forward: gacattgattattgactagt; Reverse: ccatagagcccaccgcatcc), and the resulting 200bp ultramers were obtained from IDT. PCR for selection cassette production was performed with SeqAmp DNA Polymerase (Takara Bio, cat. no. 63850) using the ultramers as primers and AAT-PB-CD2APtk (Addgene #86004) or AAT-PB-PG2APtk (Eggenschwiler et al. 2016) (Addgene #195124) as the template. The PCR products were purified and concentrated with the QIAquick PCR Purification kit (Qiagen, cat. no. 28106). Homology arm and ultramer sequences are listed in Table S8.

Knocking-in cassettes with CRISPR-mediated HDR: Cells were transfected with the PCR-purified selection cassette and integration gRNA CRISPR plasmid, using Lipofectamine 3000 (Invitrogen, cat. no. L3000015) for A2780, AGS & HCT116 cells, or FuGENE HD (Promega, cat. no. E2311) for A2058 cells. Integration of the cassette was selected with puromycin (InvivoGen, cat. no. ant-pr-1). Following selection, dsRed positive cells (when using Addgene #86004) or GFP positive cells (when using Addgene #195124) were single cell sorted onto 96-well plates, and clonal cell lines were established. Successful cassette integration was confirmed through PCR and sequencing. PCR check primer sequences are listed in Table S8. Integrant clones were subject to karyotypic validation through SMASH karyotyping prior to inducing chromosome arm loss.

Inducing chromosome arm loss: A centromere targeting CRISPR gRNA was designed and cloned into the Lenti-Cas9-gRNA-GFP vector (Addgene #124770) for targeted chromosome elimination. Integrant clones were transfected with the centromere targeting gRNA CRISPR plasmid using Lipofectamine 3000 or FuGENE HD. Chromosome arm loss was selected for with 10 μM ganciclovir (Sigma Aldrich, cat. no. G2536). Following ganciclovir selection, dsRed or GFP negative cells were single cell sorted onto 96-well plates, and clonal cell lines were established. Clones were screened for targeted chromosome arm loss with TaqMan copy number assays as described below and chromosome elimination was confirmed through SMASH karyotyping. The aneuploidy-loss cell lines generated using this method are listed in Table S3.

Chromosome elimination: ReDACT-TR

Generation of the artificial telomere construct: The ReDACT-TR technique was motivated by the use of a telomere seed sequence to generate monosomic cells as described in ref (Taylor et al. 2018). To enhance the efficacy of this approach, we created new plasmids linking a telomere seed sequence with a puromycin selection marker, which allowed us to enrich for stably-transfected aneuploidy-loss cells using drug selection. These EF1a-Puro-Telo vectors (Addgene #195138 and #195139) were generated by introducing a puromycin selection marker to a telomere seed sequence gifted by Alison Taylor. This vector was digested with FastDigest KpnI (Thermo Fisher Scientific, cat. no. FD0524) and FastDigest BstZ17I (Thermo Fisher Scientific, cat. no. FD0704), and gel purified to obtain the artificial telomere construct.

Inducing chromosome arm-loss with CRISPR-mediated NHEJ: Cells were transfected with the purified artificial telomere construct and centromere targeting gRNA CRISPR plasmids using Lipofectamine 3000 for AGS cells, or Fugene HD for MCF10A cells. Telomere replacement was selected for with puromycin, and puromycin resistant cells were single cell sorted onto 96-well plates. Clonal cell lines were established and screened for targeted chromosome arm loss with TaqMan copy number assays. Chromosome elimination was confirmed through SMASH karyotyping. The aneuploidy-loss cell lines generated using this method are listed in Table S3.

Chromosome elimination: ReDACT-CO

Cells were transfected with centromere targeting gRNA CRISPR plasmids using Lipofectamine 3000 or FuGENE HD. GFP+ cells were single cell sorted onto 96-well plates. Clonal cell lines were established and screened for targeted chromosome arm loss with TaqMan copy number assays. Chromosome elimination was confirmed through SMASH karyotyping. Chr1q_Centromere_Targeting_gRNA (Addgene #195125) and Chr1q_Cassette-Integration_gRNA (Addgene #195126) were used together to target chromosome 1q, Chr7_Centromere-Targeting_gRNA (Addgene #195129) was used to target chromosome 7p, and Chr8q_Centromere-Targeting_gRNA (Addgene #195128) was used to target chromosome 8q (Table S5A). The aneuploidy-loss cell lines generated using this method are listed in Table S3.

Choice of ReDACT techniques for each cell line

No underlying reasons motivated the selection of a specific ReDACT technique for each cell line. Our first approach, ReDACT-NS, was driven by the historical use of thymidine kinase

for genomic modification in embryonic stem cells (Mansour et al. 1988; Li et al. 2012). However, after this project was initiated, several reports were published demonstrating accidental CRISPR-mediated chromosome loss without drug selection (Zuccaro et al. 2020; Papathanasiou et al. 2021), which prompted us to experiment with the ReDACT-TR and ReDACT-CO techniques. Consequently, for most cell lines described in this manuscript, we initiated multiple ReDACT approaches at the same time, and then focused on characterizing the clones in which we were able to verify aneuploidy-loss first. Over time, we discovered that each technique had certain benefits and drawbacks. For instance, with ReDACT-NS, once a clone was isolated containing on-target integration of the HSV-TK cassette, it was relatively straightforward to produce a large number of aneuploidy-loss clones. In contrast, ReDACT-CO required only one round of single-cell cloning and was much faster than ReDACT-NS, but the overall efficiency of ReDACT-CO tended to be lower than ReDACT-NS. Importantly, we obtained consistent results on the effects of aneuploidy-loss regardless of the ReDACT technique that was ultimately used, underscoring our conclusion that aneuploidy-loss itself is the root cause of the observed phenotypes.

PHENOTYPIC CHARACTERIZATION OF ANEUPLOIDY-LOSS CELLS

Proliferation assays

Cells were seeded in 6-well plates at 100,000 cells per well. After 72 hours, cells were harvested, counted, and 100,000 cells were re-plated in fresh media on 6-well plates. Cells were passaged ten times, and population doublings were calculated at each passage.

Soft agar assays

To assay colony formation in soft agar, a solution of 1.0% Difco Agar Noble (VWR Scientific, USA, cat. no. 90000–772) in sterile water was prepared. The 1% agar solution was mixed 1:1 with the base cell culture media supplemented with 20% FBS, 4 mM glutamine, and 200 U/mL penicillin/streptomycin, or for MCF10A, supplemented with 10% horse serum, 40 ng/mL EGF, 1 ng/mL Hydrocortisone, 200 ng/mL Cholera Toxin, 20 μg/mL Insulin, 10 mM Transferrin, and 200U/mL penicillin streptomycin. 1 mL of this mixture was plated on each well of a 6-well plate and allowed to solidify at room temperature to form a base layer of 0.5% agar. Cells were then harvested and counted. For A2780 and A2058, 20,000 cells were seeded in 0.35% agar (1:1 mixture of 0.7% agar in sterile water and 2x supplemented growth medium). For AGS and MCF10A, 10,000 cells were seeded in 0.35% agar. For HCT116, 35,000 cells were seeded in 0.30% agar. Plates were left at room temperature to solidify and then placed in a humidified incubator at 37˚C and 5% CO_2. 1 mL of normal growth media was added the next day, and every three days after. After 10-14 days, cells were fixed with 100% methanol, and stained with 0.01% crystal violet dissolved in 25% methanol. Colony formation was quantified by capturing z-stacks of several fields of view per well from at least three wells on a LSM 710 confocal microscope (Zeiss) or a Cytation5 imaging reader (BioTek Instrument, inc.), under either 4x, 5x, or 6x magnification. The average number of colonies was calculated by counting total number of colonies per field of view from multiple fields of view from at least three wells.

Xenograft assays

To assay tumor formation, cells were harvested and resuspended in cold PBS. For A2780 xenograft experiments, 3 million cells were injected in each flank of NU/J mice (Jackson

Laboratory, cat. no. 002019). For A2058 xenograft experiments, 2 million cells were injected in each flank in NU/J mice. For HCT116 xenograft experiments, 4 million cells were injected in J:NU mice (Jackson Laboratory, cat. no. 007850). For MCF10A cells expressing $HRAS^{G12V}$, 10 million cells were injected in each flank in NU/J mice. For AGS xenograft experiments, the following conditions were tried: 5 million cells resuspended in PBS in each flank of NU/J mice (Jackson Laboratory, cat. no. 002019); 4 million cells resuspended in PBS in each flank of NGS mice (Jackson Laboratory, cat. no. 005557); and 15 million cells resuspended in a 1:1 PBS:Matrigel mixture in each flank of J:NU mice (Jackson Laboratory, cat. no. 007850). Cells were subcutaneously injected using a 1 mL 25G x 5/8 syringe (BD, cat. no. 309626). Mice were visually monitored for tumor formation routinely following injection. Once a tumor was visible, it was measured every three days by calipers. Tumor volume was calculated using the formula V = ½ (longer axis)(shorter axis). All mouse protocols were approved by the CSHL and Yale Institutional Animal Care and Use Committees.

Derivation and characterization of cell lines post-xenograft

To derive post-xenograft cell lines, mice were euthanized at a humane end point, and tumors cut out using a sterilized pair of scissors. The tumors were placed into a chilled conical tube containing 2-3 mL of TrypLE Express Enzyme (Gibco; cat. no. 1260413) and transported on ice to a biosafety hood. The tumors were minced using sterilized scalpels and allowed to dissociate for 20-30 minutes in a 37˚C water bath. Cell culture media was prepared using 2x the regular concentration of penicillin-streptomycin, and TrypLE was neutralized using an equivalent volume of this cell culture media. The mixture was filtered through a cell strainer tube (Corning; cat. no. 352235) and plated onto a tissue culture treated 10 cm dish, with cell culture media added to a total of 10 mL. The following day, upon cell adherence to the dish,

the media was replaced. When cells reached 70-80% confluence, they were frozen down in media containing 2x the regular concentration of FBS and 10% DMSO. Cell pellets were simultaneously taken for downstream analyses, including TaqMan copy number assays and SMASH karyotyping. For subsequent phenotypic characterization, a fresh vial of cells was thawed and used in soft agar assays as previously described.

KRAS genotyping

The sequence of *KRAS* exon 2 was obtained from GRCh38 using Benchling. Primers were designed to amplify the genomic region surrounding exon 2 (Table S8). PCR was performed with SeqAmp DNA Polymerase (Takara Bio; cat. no. 63850), and PCR products purified and concentrated with the QIAquick PCR Purification kit (Qiagen; cat. no. 28106). PCR products were sent for Sanger sequencing with both forward and reverse primers to Azenta Biosciences. The ratio of wild type to mutant base (G to A) to assess allelic ratio of $KRAS^{WT}$ to $KRAS^{G13D}$ was assessed using EditR (Kluesner et al. 2018).

Cell cycle analysis

One day prior to cell cycle analysis, 1.5-2 million cells were plated onto a 10 cm dish. Cells were harvested by trypsinization with TrypLE, followed by centrifugation at 1,000 rpm for 5 minutes, aspiration of the media, and resuspension of the cell pellet in 1 mL PBS. Cells were added dropwise to 4mL of ice cold 100% ethanol and fixed at -20˚C for 5-15 minutes. Fixed cells were pelleted by centrifugation at 1,000 rpm for 5 minutes, resuspended in PBS containing 0.05% Triton X-100, 10 µg/mL RNAse A (Invitrogen, cat no. A32078), and 20 µg/mL propidium iodide (Life Technologies, cat. no. P3566), filtered through a cell strainer

FACS tube cap. Cells were incubated for 30 minutes at room temperature in the dark. Cell cycle analysis was measured by flow cytometry (Miltenyi Biotech).

Senescence assay

Senescence-associated β-galactosidase staining was performed using a senescence β-galactosidase staining kit (Cell Signaling Technology, cat. no. 9860) according to the manufacturer's instructions. Briefly, in a 6-well plate, the medium was discarded, and the cells were rinsed once in PBS. The cells were then fixed in a fixative reagent for 15 minutes at room temperature. The cells were then rinsed twice in PBS and incubated overnight at 37˚C without CO_2 in the β-galactosidase staining solution. The cells were imaged and analyzed under a light microscope (20X magnification, Olympus CKX53).

CRISPRi competition assays

CRISPRi competition assays were performed as described in ref (Girish and Sheltzer 2020). In brief, A2780 cells were transduced with a dCas9-KRAB construct (Addgene #85969). dCas9-KRAB expressing TagBFP+ cells were selected for through bulk sorting, and dCas9-KRAB expression was confirmed through transduction of *MCM2* guides with known biological activity. For competition assays, dCas9-KRAB expressing cells were transduced with guides in vectors co-expressing mCherry that targeted candidate genes, as well as negative control guides targeting the non-coding *AAVS1* locus and positive control guides targeting the essential replication gene *MCM2*. Three days post-transduction, cells were subject to flow cytometry analysis (Miltenyi Biotech) to assess the starting percentage of mCherry+ cells. Cells were re-plated, and timepoints were taken every three days through the conclusion of the assay at the fifth timepoint. To normalize for differences in starting percentages of

mCherry+ cells, fold change, defined as (starting % positive)/(% positive at timepoint), was calculated at each timepoint.

Assessing cellular sensitivity to UCK2 poisons and other chemotherapeutic agents

A 72-hour drug assay was performed to assess cellular sensitivity to the nucleotide analogs RX-3117 (MedChemExpress; cat. no. HY-15228) and 3-deazauridine (Cayman Chemical; cat. no. 23125) in both A2780, A2780 *UCK2*-overexpression, and MCF10A cell lines. One day prior to the addition of the nucleotide analogs, 25,000 cells were plated into individual wells of a 6-well plate. The following day, upon cell adherence to the plate, the media was discarded and replaced with drug-containing media at varying concentrations. The cells were grown in the presence of the drug for 72 hours. Following this, the cells were harvested and counted. A similar protocol was followed to assess the sensitivity of A2780 cells to doxorubicin (Selleck Chemicals; cat. no. S1208), gemcitabine (Selleck Chemicals; cat. no. S1714), and olaparib (Selleck; cat. no. S1060).

OTHER GENETIC MANIPULATIONS

Generation of control clones

Rosa26 gRNA clones: A CRISPR guide was designed to target the noncoding Rosa26 locus and cloned into the Lenti-Cas9-gRNA-GFP vector (Addgene #124770) as described above. Cells were transfected with the Rosa26 targeting gRNA CRISPR plasmid using Lipofectamine 3000, and GFP+ cells were single cell sorted onto 96-well plates. Clonal cell lines were established and subject to karyotypic validation through SMASH karyotyping prior to phenotypic characterization.

1q, 7p, and 8q gRNA clones: Cells were transfected with centromere-targeting gRNA CRISPR plasmids using Lipofectamine 3000 and clonal cell lines were established as described above for ReDACT-CO (Table S5A). Clones that maintained an extra copy of the targeted chromosome, as revealed by TaqMan copy number assays and SMASH-seq, were used as control clones.

Olfactory gene deletions: CRISPR guides were designed to flank the coding sequence of the targeted olfactory gene and cloned into the Lenti-Cas9-gRNA-GFP vector (Addgene #124770) as described above. Cells were transfected with the olfactory gene deletion guides using Lipofectamine 3000, and single GFP+ cells were sorted onto 96-well plates. Clonal cell lines were established and screened for single copy deletions of the targeted olfactory genes with TaqMan copy number assays as described above. To exclude the possibility of a chromosome truncation event, additional TaqMan copy number assays were performed with probes telomeric to the targeted gene. Clones with single copy deletions of the targeted olfactory gene were subject to karyotypic validation through SMASH-seq prior to phenotypic characterization.

Generation of Cassette Deletion Clones: A2780 and AGS integrant clones were co-transfected with a centromere targeting gRNA and a cassette proximal gRNA using Lipofectamine 3000. Cassette deletion was selected for with 10 μM ganciclovir (Sigma Aldrich, cat. no. G2536). Following ganciclovir selection, dsRed or GFP negative cells were single cell sorted onto 96-well plates, and clonal cell lines were established. Clones were screened for cassette loss with PCR primers spanning the deletion region (Table S8) and cassette deletion

independent of any other karyotypic alterations was confirmed through SMASH karyotyping.

Deletion of a single copy of *MDM4*

CRISPR guides were designed to flank the coding sequence of the targeted gene and cloned into the Lenti-Cas9-gRNA-GFP vector (Addgene #124770) as described above. For dual guide plasmids, dual guide gene blocks were ordered from IDT and cloned into the Lenti-Cas9-gRNA-GFP vector using NEBuilder HiFi DNA Assembly (New England Biolabs, cat. no. E2621L). CRISPR gRNA sequences are listed in Table S5A. Cells were transfected with the gene deletion guides using Lipofectamine 3000, and GFP+ cells were single cell sorted onto 96-well plates. Clonal cell lines were established and screened for single copy deletions of targeted genes with TaqMan copy number assays as described above. To exclude the possibility of a chromosome truncation event, additional TaqMan copy number assays were performed with probes telomeric to the targeted gene. Clones with single copy deletions of the targeted genes were subject to karyotypic validation through SMASH karyotyping prior to phenotypic characterization.

Transformation of MCF10A with *HRAS*^{G12V}

pBABE-HRASV12-Hyg (Addgene #195143) was generated by cloning hRASV12 from pBABE-HRASV12-puro (Addgene #9051) into pBABE-hyg (Addgene #1765) by digestion of both plasmids with BamHI and SalI, gel purification of digested DNA, ligation, and transformation into Stbl3 E. coli. The plasmid sequence was verified by sequencing. Viral preparation and transduction were performed as described above.

Derivation of *TP53*-knockout clones

TP53-targeting gRNAs were designed and cloned into the Lenti-Cas9-gRNA-GFP vector (Addgene #124770) for generating *TP53*-KO clones. In parallel, an AAVS1-targeting gRNA was utilized to generate isogenic *TP53*-WT control clones. A2780 cells were transfected with these CRISPR gRNA plasmids and GFP+ cells were single cell sorted onto 96-well plates. Clonal cell lines were established and screened for *TP53*-KO through western blotting. Clones were subject to karyotypic validation through SMASH karyotyping prior to phenotypic characterization.

Generation of HAP1 *UCK2*-KO cells

HAP1 cells harboring a CRISPR-induced frameshift mutation in the *UCK2* gene were purchased from Horizon Discovery (cat. no. HZGHC007067c006). Loss of *UCK2* expression was verified by western blotting.

Generation of *UCK2*-overexpressing cells

A2780 cells were transduced with pLV-Bsd-CMV-hUCK (Addgene #195141) and selected with 4μg/mL blasticidin (InvivoGen; cat. no. ant-bl-1). The plasmid sequence was verified by whole-plasmid sequencing.

COMPUTATIONAL APPROACHES

Copy number timing analysis

Raw whole genome sequencing (WGS) data in Bam or Fastq formats were downloaded from public databases provided by the original publications(Yates et al. 2017; Kawazu et al. 2017; Hayward et al. 2017). We used ith.Variant pipeline

(https://github.com/SunPathLab/ith.Variant) to call somatic copy number alterations (SCNA) and point mutations and to determine the clonality of these somatic variants (Maeser et al. 2023). In total, 38 Breast cancer samples (BRCA) from 21 patients and 37 Melanoma (MEL) primary tumor samples (all paired with normal control samples) passed our WGS data quality control and were included in the analysis. To reconstruct the evolutionary history of SCNAs in patient tumors, we applied BUTTE (Wang et al. 2022) to infer the initiation time of clonal CN gains. We define the initiation time as the time fraction when the first gain occurs for a clonal SCNA. In brief, BUTTE estimates the initiation time of complex gains (or gains involving multiple steps) by modeling the quantitative relationship between point mutations and paths of copy number events. To do so, it first adopts the expectation–maximization (EM) algorithm to find the allele state distribution of point mutations. BUTTE then either directly solves the timing for SCNAs with identifiable CN history matrices (Purdom et al. 2013) or adopts linear programming to calculate the upper bounds of the initiation time if the underlying linear system is underdetermined (e.g., Multiple history matrices exist for an SCNA) (Wang et al. 2022). We identified clustered gains by clustering the inferred timing via nonparametric density estimation (Azzalini and Menardi 2014). Genome doubling was identified as the cluster containing more than 40% of the segments.

Detecting recurrent early gains

To identify genomic regions exhibiting recurrent early gains across patients, we scanned hg38 genome with bins of 1 million bp in size and ranked the bins in each sample according to the timing of respective initiating gain. The timing values are jittered to avoid ties. We then subtract from each bin the middle rank of the respective sample. The middle rank is the expectation value of the ranks under the assumption that the null hypothesis holds: no

regions show recurrent early gain across patients. For each tumor type, we summed the resulting ranks across patients for each bin. Division of the rank sums by its standard deviation yields normalized rank sums which approximately follow a standard normal distribution if the null hypothesis is fulfilled. A large negative normalized rank sum would reject the null hypothesis and indicate recurrent early initiating gains. To evaluate the frequency of gains for each genomic bin across patients, we ranked the segment mean (read depth ratio between the tumor and normal samples) as we did for the timing values, and then performed the same rank sum normalization. A large positive normalized rank sum for the segment mean would suggest frequent gains across patients.

Analysis of mutual exclusivity between aneuploidy and oncogenic mutations

To analyze the mutual exclusivity between aneuploidy and oncogenic mutation, we started from the MSK-MET (Nguyen et al. 2022) dataset available via the public cBioPortal datahub(Gao et al. 2013). In order for a given chromosomal arm and oncogene to be compared, we required that the data pass a set of quality filters. We required all cancer types to have ≥ 25 patients and selected a representative sample for each patient based on available mutation and arm gain data. We built sets of genes and arms by cancer type by applying additional requirements by cancer. The sets of genes we analyzed started from the IMPACT-505 geneset and we required each gene be mutated in ≥ 2% of patients by cancer type. The sets of arms we analyzed started from all previously generated arm gain data by sample and each arm was required to exceed a minimum of 100 patients or ≥ 2% of patients experiencing arm gain by cancer type. Once we had our cleaned sets of genes and arms by cancer, we calculated contingency tables for each combination and conducted a two-sided Fisher's exact test to compute p-values and odds ratios for each gene X arm combination. We converted

these p-values into Z scores for further comparisons and applied the sign of the negative log2 of the odds ratio to represent the direction of the relationship; therefore, a large positive Z would suggest significant mutual exclusivity, while a large negative Z would suggest significant co-occurrence. We repeated this process in a pancancer analysis by utilizing the same cleaned data and pooling all patients, genes, and arms into a single cohort. All mutual exclusivity analysis was automated using Nextflow (Di Tommaso et al. 2017) and Conda, starting from downloading MSK-MET data through to generation of Figures 1D-E and S1.

Analysis of copy number alterations and patient survival

To examine the relationship between copy number gains, mutations, and cancer patient outcomes in TCGA, univariate Cox proportional hazards models were used as described in refs (Smith and Sheltzer 2018, 2022). In brief, TCGA copy number data (broad.mit.edu_PANCAN_Genome_Wide_SNP_6_whitelisted.seg, available at https://gdc.cancer.gov/about-data/publications/pancanatlas) and TCGA mutation data (mc3.v0.2.8.PUBLIC.maf.gz, available at https://gdc.cancer.gov/about-data/publications/pancanatlas) were combined with patient outcomes data described in ref(Liu et al. 2018). Selection of the clinical endpoint for each cancer type was based on the recommendations provided by ref (Liu et al. 2018) based on data quality, cohort size, and the number of events that were observed. TCGA copy number data was generated as relative copy number values for particular chromosomal intervals. This data was translated to produce a single copy number value on a per-gene basis, based on the observed copy number at each gene's transcription start site. This annotation was performed using mapping data from GENCODE v32 (Frankish et al. 2019). Z scores for copy number changes and for mutations in common cancer driver genes were calculated using Cox proportional hazards

regression. For the copy number analysis presented in Figure S2, genes were mapped back to chromosome bands, and the top-scoring gene (based on the pan-cancer Stouffer's Z score) was identified for each band. For the mutation analysis presented in Figure S2, a gene was considered to be mutated if there was a single non-synonymous mutation at any codon within the gene. Non-synonymous mutations included: missense, nonsense, frameshift deletion, splice site, frameshift insertion, inframe deletion, translation start site, nonstop mutation, and in-frame insertion. Additional clinical data presented in Figure S2E were downloaded from cBioportal (Gao et al. 2013).

Analysis of aneuploidy-associated gene expression

Chromosome copy number data for cancers from the TCGA was downloaded from ref (Taylor et al. 2018). Chromosome copy number data for the Cancer Cell Line Encyclopedia was downloaded from ref (Cohen-Sharir et al. 2021). Gene expression data for cancers from the TCGA was downloaded from the TCGA PanCanAtlas (EBPlusPlusAdjustPANCAN_ IlluminaHiSeq_RNASeqV2.geneExp.tsv, available at https://gdc.cancer.gov/about-data/publications/ pancanatlas). Gene expression data for the Cancer Cell Line Encyclopedia was downloaded from DepMap (www.depmap.org) (Barretina et al. 2012).

Data Visualization

Scientific illustrations were generated with Biorender. Most graphs were generated using GraphPad Prism. Boxplots display the 25th, 50th, and 75th percentiles of colonies per field, while the whiskers represent the 10th and 90th percentiles. Unless otherwise indicated, bar graphs and XY plots display the mean ± SEM.

Data and Code Availability

The code used to perform the TCGA survival analysis is available at https://github.com/joan-smith/comprehensive-tcga-survival. The code used to perform the mutual exclusivity analysis is available at github.com/shel tzer-lab/aneuploidy-addictions. The mass spectrometry data have been all deposited to the ProteomeXchange Consortium via the PRIDE PXD037956 (Perez-Riverol et al. 2019). (To review the dataset please go to https://www.ebi.ac.uk/pride/login, and use the following login details: **Username:** reviewer_pxd037956@ebi.ac.uk; **Password: NavbYhDW**). RNA-Seq data has been deposited at GSE222379.

Supplemental Tables

All supplemental tables are available online:

https://www.biorxiv.org/content/10.1101/2023.01.09.523344v1.supplementary-material

Table S1. Mutual exclusivity between chromosome gain events and mutations in cancer-associated genes.

Table S2. Association between chromosome copy number gains and cancer patient outcome.

Table S3. Aneuploidy-loss cell lines generated in this work.

Table S4. Sources of the cell lines used in this work.

Table S5. CRISPR and CRISPRi gRNA sequences used in this work.

Table S6. TaqMan copy number probes used in this work.

Table S7. TaqMan gene expression probes used in this work.

Table S8. Primers and oligonucleotides used in this work.

Supplemental Text 1: Considering alternate explanations for the loss of fitness in engineered 1q-disomic cancer cells

In order to generate isogenic cancer cells that have or lack specific aneuploid chromosomes, we developed and applied a suite of CRISPR tools for chromosome engineering called ReDACT. We discovered that eliminating the trisomy of chromosome 1q severely compromised malignant potential in multiple independent cancer cell lines. We considered and rigorously evaluated the possibility that the loss of fitness observed among the 1q-disomic clones could be a consequence of our chromosome engineering methodologies, rather than the subsequent change in cellular karyotype. However, multiple lines of evidence indicate that this loss of fitness is best explained as a specific outcome of eliminating trisomy-1q and not a consequence of our experimental approach:

<u>The use of CRISPR</u>

All three ReDACT techniques that we applied utilized CRISPR to induce aneuploidy-loss events. In order to assess whether CRISPR itself could compromise malignant growth to the degree that we observed upon elimination of the 1q trisomy, we generated and tested a set of 28 control clones that were subject to various CRISPR manipulations. These clones include:

1) Cell lines harboring a CRISPR-mediated integration of the HSV-TK cassette that were not treated with ganciclovir to select for 1q-loss,
2) Cell lines in which the HSV-TK cassette was deleted by transfecting cells with two gRNAs targeting immediately upstream and downstream of the integrant coupled with ganciclovir selection, which resulted in a segmental deletion of the cassette while leaving the rest of 1q unaffected,

3) Cell lines subjected to CRISPR-mediated cutting with a 1q-targeting gRNA, in which the lesion was repaired without causing chromosome loss,
4) Cell lines subjected to CRISPR-mediated cutting with a gRNA targeting the non-coding Rosa26 locus,
5) Cell lines in which dual CRISPR guides were used to generate segmental deletions on chromosome 1q of a gene encoding a non-expressed olfactory receptor,
6) Cell lines in which CRISPR was used to delete a terminal segment on chromosome 1q, eliminating the telomere and decreasing the copy number of 26 out of 968 protein-coding genes on the chromosome.

Every control clone that we tested exhibited significantly better anchorage-independent growth compared to the 1q-disomic clones that we derived (Fig. S8). Additionally, we note that the control clones generated by the segmental deletion of the HSV-TK gene were subjected to three independent CRISPR-induced DNA breaks (one to integrate HSV-TK and then two to produce the segmental deletion), which is more breaks than all 1q-disomic clones were subjected to.

To further verify that the phenotypes observed upon elimination of the 1q-trisomy are specifically a result of that karyotype alteration, we applied ReDACT-CO to eliminate trisomies of 1q, 7p, and 8q from the same cell line (Fig. 3A). If the use of ReDACT-CO is the cause of the reduced fitness upon 1q-loss, then we would expect that all aneuploidy-loss clones would be impaired to a similar degree. However, we observed that loss of the 7p or 8q trisomies resulted in a significantly milder phenotype compared to the effects of 1q-loss (Fig. 3C-D).

Finally, if an off-target effect of CRISPR is the cause of the reduced fitness upon 1q-loss, then we would not expect to see any selective pressure to restore the 1q trisomy.

However, upon prolonged growth of the 1q-disomic clones *in vitro* or *in vivo*, we observed that many cell populations spontaneously recover an extra copy of chromosome 1q, and these 1q-restored cells exhibit improved colony-formation ability relative to the 1q-disomic clones (Fig. 4A-F). In total, these assays provide multiple independent lines of evidence that the reduced fitness of the 1q-disomic clones cannot be attributed solely to the effects of CRISPR.

Ganciclovir selection

In the ReDACT-NS approach, several 1q-disomic clones were generated by integrating the HSV-TK gene onto chromosome 1q and then selecting for aneuploidy-elimination via treatment with ganciclovir (Fig. 2A). As a specific control for this protocol, we also generated a series of clones in which the HSV-TK-expressing parental cells were transfected with two gRNAs that cut immediately upstream and downstream of the HSV-TK cassette, and then the cells were treated with ganciclovir (Fig. S8A). These clones acquired ganciclovir resistance due to a segmental deletion of the HSV-TK gene, rather than loss of the entire chromosome arm. We subsequently observed that these ganciclovir-resistant control clones exhibited consistently superior anchorage-independent growth compared to clones that had lost the 1q-trisomy (Fig. S8D-E). Additionally, we note that two of our aneuploidy-elimination methods – ReDACT-TR and ReDACT-CO – do not utilize ganciclovir selection, and the phenotypes that we observed across independent 1q-disomic clones were similar regardless of the methods applied to generate them. In total, these findings suggest that any detrimental effects of ganciclovir selection are unable to fully account for the loss of fitness observed in the 1q-disomic clones.

Loss of telomere protection

In the ReDACT-NS and ReDACT-CO approaches, our aneuploidy elimination techniques may result in the loss of telomere protection on the targeted chromosome arm. We therefore investigated whether the loss of telomere protection could be sufficient to explain the phenotypes of our 1q-disomic clones. First, we transfected cells with a gRNA targeting a subtelomeric region on chromosome 1q and we isolated a control clone harboring a terminal chromosomal truncation. This clone maintained the ability to grow under anchorage-independent conditions at wild-type levels (Fig. S8C). Second, if loss of telomere protection on a single chromosome arm is sufficient to inhibit malignant potential, then we would expect this phenotype to be consistent across different chromosomes. However, we applied ReDACT-CO to eliminate the trisomies of chromosome 7p and 8q from A2058 cells, and we observed that the 7p-disomic and 8q-disomic clones exhibited consistently superior fitness compared to 1q-disomic clones obtained using the same techniques in the same cell line (Table S3). Third, a subset of our 1q-disomic clones were created using ReDACT-TR, in which the CRISPR-induced DNA break was repaired with an artificial telomere. As noted above, the phenotypes that we observed across independent 1q-disomic clones were similar regardless of the methods applied to generate them (Fig. 2). In total, these findings suggest that the loss of telomere protection on a single chromosome arm is unable to fully account for the compromised fitness observed in the 1q-disomic clones.

Supplemental Text 2: Considering the loss of specific point mutations on chromosome 1q as an explanation for the loss of fitness in engineered 1q-disomic cancer cells

Deletion of a chromosome not only decreases the dosage of any genes encoded on the targeted chromosome, it may also cause the loss of any point mutations encoded on that chromosome. Correspondingly, we considered the possibility that the effects of 1q-loss could be mediated in part by eliminating unique driver mutations that these cell lines had acquired on chromosome 1q. To explore this possibility, we evaluated all non-synonymous mutations on chromosome 1q in the 1q-trisomic cancer cell lines used in this study. Using data acquired from DepMap, we found 25 1q mutations in A2780, 19 1q mutations in A2058, and 52 1q mutations in AGS. We cross-referenced these mutations with the Catalogue of Somatic Mutations in Cancer (COSMIC) database to examine if any mutations were recurrently observed or causally implicated in human cancers. None of the 96 mutations present on chromosome 1q in A2780, A2058, and AGS were identified as mutational hotspots in the COSMIC database, and none of the genes affected by mutations were included in the Cancer Gene Census. Next, we investigated the list of cancer driver genes identified by Vogelstein et al. (Vogelstein et al. 2013), and we found that none of the 1q genes affected by mutations in these cell lines were annotated as likely drivers. Lastly, we examined MSK-IMPACT, a panel of 505 genes associated with both common and rare cancers. None of the 1q mutated genes are included in this panel. For these reasons, we believe that the mutations found on chromosome 1q in these cell lines likely represent passenger events, rather than cancer drivers. Nonetheless, we do not rule out the possibility that the loss of specific point mutations could influence the effects of aneuploidy-elimination in other experiments. For instance, as described in Figure 4G, we speculate that the effects of gaining chromosome 12 in HCT116 is

mediated in part by the acquisition of an extra copy of the mutant *KRAS*^{G13D} allele, and loss of a chromosome containing mutant *KRAS* may have different consequences than loss of a chromosome containing wild-type *KRAS*.

Chapter 3:

The Complexities of Aneuploidy Research

Overview

Chapter 2 presented compelling evidence for the oncogene-like role of aneuploidy in cancer. Here, I not only provide additional data to support those conclusions, but also highlight the complexities and subtleties involved in understanding this phenomenon.

First, I discuss the differing efficiencies of ReDACT across various cell line models, and indicate cell lines where ReDACT-induced chromosomal manipulation could not be achieved. A comparison of ReDACT with other targeted chromosomal arm loss methods is presented in Chapter 4. Second, I present results showcasing the competitive advantage of trisomy 1q over disomy 1q. Third, I highlight additional dosage-sensitive gene candidates on 1q which may collectively account for its oncogene-like phenotypes. Fourth, I present examples of phenotype rescue, and distinguish between endogenous and exogenous chromosomal regain.

Subsequently, I present findings from a new aneuploidy-loss model: RKO. Because the parental line carries four copies of chromosome 8q, I was able to generate clones with trisomy 8q, disomy 8q, and even pentasomy 8q. This model therefore offers the opportunity to study distinct chromosomal copy number effects. Next, I highlight the importance of 8q aneuploidy in direct comparison to common oncogene drivers. Last, I present results from an ORF overexpression screen conducted to discover dosage-sensitive drivers of 8q loss. Surprisingly, *MYC* overexpression fails to rescue the 8q loss phenotype. However, two genes previously not implicated as oncogenic drivers – *RNF139* and *PEX2* – appear to act in a dosage-sensitive manner to drive the observed phenotype.

Collectively, these results highlight both the challenges and opportunities in dissecting the role of aneuploidy in cancer, and lay the groundwork for future investigations.

The Efficiency of ReDACT

In developing the three different techniques collectively classified as ReDACT, we naturally encountered several hurdles. We first began this project by developing ReDACT-NS. Because this approach required two single cell cloning and verification steps, it took 5-6 months for isolation of aneuploidy loss clones. I subsequently developed ReDACT-TR to achieve the same ends in a single step process, thereby reducing the timeframe to 2-3 months. Inspired by reports suggesting CRISPR-induced double strand breaks could be sufficient for inducing chromosomal arm loss (Zuccaro et al. 2020), we began utilizing ReDACT-CO. This eliminated the drug selection step, thereby shortening the time frame further. Some of these techniques worked better in certain cell lines compared to others. Table 1 summarizes the success rates (or lack thereof) across various cancer backgrounds and targeted chromosomes.

Cell Line	Cell Type	Target Aneuploidy	ReDACT Efficiency			
			NS #1	NS #2	TR	CO
600MPE	Invasive breast carcinoma	1q	0			
A2058	Melanoma	1q			3/54	12/84
		7p				10/54
		8q				25/111
AGS	Gastric Adenocarcinoma	1q	22/101	10/44	2/31	
CAL148	Invasive breast carcinoma	1q			0/24	0
CHP212	Neuroblastoma	1q	0		0/11	0
HCT116	Colorectal Adenocarcinoma	8q				2/18
LoVo	Colorectal Adenocarcinoma	1q				0/43
		7				0/37
LS513	Colorectal Adenocarcinoma	1q				0
		7				0
MCF10A	Breast Epithelial	1q			78/112	3/46
NB69	Neuroblastoma	7				0/25
NCI-H1048	Lung neuroendocrine tumor	1q	1/2	0/5	0/2	0/13
OVK18	Ovarian Epithelial Tumor	1q	3/39	0/45		0/4
RKO	Colorectal Adenocarcinoma	8q			5/153	3/22
SKNSH	Neuroblastoma	7				0/40
SW48	Colorectal Adenocarcinoma	8q	0			

Table 1: A Head-to-Head Comparison of ReDACT Efficiency Across Cell Lines. Efficiency is presented as number of isolated clones with desired alteration / total clones isolated. NS#1 refers to positive selection for cassette integration; NS#2 refers to negative selection for aneuploidy loss. Blank columns indicate those strategies were not tried for that cell line. 0 indicates no clones were successfully grown.

Table 1 highlights several important points. First, efficiency for isolation of single cell clones with the targeted arm alterations varies widely across cell lines. This could be due to several reasons: essentiality of the aneuploidy, such that its elimination renders cells non-viable; poor transfection, i.e., only a small proportion of cells take up the ReDACT constructs, which compounds the low probability of arm loss; poor clonogenicity, i.e., clonal populations are unable to grow from single cells; or poor recovery from drug selection, i.e., the cells enter cell cycle arrest and fail to proliferate following drug selection. While some of these roadblocks could have been resolved with further protocol optimization, our cancer-agnostic approach towards understanding aneuploidy allowed us to switch cell lines in the interest of time. Regardless, these results suggest the same method does not work equally well for any given cell line model. Further investigation into the underlying cellular processes is required to optimally select cell line appropriate methods, and to translate these techniques into organoid and *in vivo* settings.

Second, the process of inducing targeted chromosomal arm loss is labor intensive. For ReDACT-NS, the dual single cell cloning step compounds this inefficiency – first, integration of the selection cassette needs to be verified. Only clones with targeted single-copy integration can then be used for induction of arm loss, and subsequent isolation of aneuploidy loss cells. While ReDACT-TR and ReDACT-NS do not require the cassette integration step, it is nevertheless not uncommon to isolate tens of clones to identify one with targeted chromosomal arm loss.

Additionally, clones may harbor secondary karyotypic alterations. This may not only be due to off-target effects of CRISPR, but also due to cytogenetic organization of the aneuploid chromosome. For example, a number of AGS 1q loss clones showed disruptions of chromosome 8p copy number (data not shown). G-banding analysis revealed the aneuploid

copy of 1q was fused to 8p in this cell line (Chapter 2 Figure S4), thereby suggesting induction of arm loss may have simultaneously disrupted 8p. For the purposes of our work, we restricted experiments to "clean" deletions, i.e., minimal to no secondary karyotypic alterations. This allowed us to study the phenotypic consequences of loss of the targeted chromosome by comparison to an isogenic line with the aneuploid chromosome present. Regardless, to ensure isogenicity beyond karyotypic alterations, whole genome sequencing approaches should be employed. While we have extensively validated our observations through a robust series of controls (Chapter 2 Figures S7-10, Supplemental Text 1), whole genome sequencing could further be used to ensure no mutations in key oncogenes or tumor suppressors have taken place in the process of clonal growth.

A comparison of ReDACT with other chromosomal engineering approaches is presented in Chapter 4. Because most of these techniques have been developed fairly recently, their increased usage across labs throughout the world is ultimately needed to gauge their efficiency and ease of use, and to uncover their context-specific pros and cons.

Trisomy 1q's Competitive Advantage

In Chapter 2, we described a mild proliferative defect upon aneuploidy loss (Figure S6). To assess proliferative differences more directly, I performed competition assays where the parental, trisomy 1q line was competed against a disomy 1q clone or a trisomy 1q control. For both A2780 and A2058, trisomy 1q consistently outcompeted disomy 1q (Figures 1a-d). This was true regardless of starting ratio – even when only 10% of the starting population was trisomic, it overtook the entire population (Figures 1b, 1d). This is perhaps reflective of patient tumor heterogeneity, whereby genomic instability may result in acquisition of aneuploidy.

Due to its fitness advantage, the aneuploid clone can subsequently overtake the tumor population.

Since I had observed karyotype evolution for HCT116 8q-loss cells during the course of tumorigenesis (Chapter 2 Figures 4G-H), I sought to assess karyotypic changes that may arise in A2780 1q loss cells following tumor formation as xenografts. We had previously observed that A2780 1q loss clones were unable to form tumors when subcutaneously injected into immunocompromised mice, contralateral to parental trisomy 1q cells (Chapter 2 Figure 2E). I therefore set up contralateral injections of trisomy 1q cells (parental vs TK+ control) and disomy 1q cells (1q-loss c3 vs 1q-loss c4) (n=5 mice each). I hypothesized that the trisomy 1q cells would form tumors rapidly, and the karyotype would remain stable. In contrast, I expected disomy 1q cells to have a greater latency for tumor formation, and the karyotype to evolve during tumorigenesis. To my surprise, both sets of mice formed tumors and reached the experimental endpoint at similar rates (Figure 1e). Furthermore, no karyotypic alterations were observed for any post-xenograft derived cell lines (Figure 1f). It should be noted that the sample size was small (n = 5 mice only), and this experiment was conducted 2 years after the initial finding that A2780 disomy 1q could not form tumors (Chapter 2 Figure 2E). Therefore, despite a stable karyotype, the cells may nevertheless have acquired somatic mutations to compensate for loss of aneuploidy, such as mutation in *TP53*, either during xenograft formation or over the course of regular tissue culture maintenance (passaging, freezing down, thawing to propagate again) in the intervening years. Alternatively, it is possible that trisomy 1q's competitive advantage may have suppressed growth of disomy 1q tumors within the same mouse (Chapter 2 Figure 2E). Without this competitive suppression, disomy 1q clones could form tumors. Although this experiment has not been repeated, these results merit further investigation.

Anoikis

Anoikis refers to the apoptotic program induced upon cellular detachment from the extracellular matrix (Frisch and Screaton 2001; Chiarugi and Giannoni 2008). Breakdown of anoikis confers a selective advantage upon pre-cancerous cells, allowing increased viability in the absence of matrix attachment and subsequent colonization of secondary sites (Yawata et al. 1998; Shanmugathasan and Jothy 2000). Soft agar assays offer an *in vitro* proxy for cellular propagation in the absence of extracellular attachment, a key hallmark of cancer (Macpherson and Montagnier 1964; Freedman 1974; Horibata et al. 2015). To test whether the strong anchorage-independent phenotype observed across the aneuploidy loss clones (Chapter 2 Figures 2-4) could be explained by changes in anoikis, I investigated whether trisomy 1q had superior viability compared to disomy 1q upon detachment from tissue-culture treated plates. Intriguingly, no consistent difference in apoptosis were observed, as measured using the TUNEL assay to detect DNA fragmentation (Figure 1g). Since the proliferative defect upon aneuploidy loss is mild (Chapter 2 Figure S6), and the apoptotic pathway doesn't appear to be drastically upregulated across 1q loss clones (Figure 1g), these results suggest other cellular mechanisms may be responsible for the stark anchorage-independent growth phenotype. Further investigation of the downstream consequences of aneuploidy loss may therefore pinpoint the exact mechanistic underpinnings of this phenotype, potentially revealing therapeutic vulnerabilities broadly applicable to all aneuploidies.

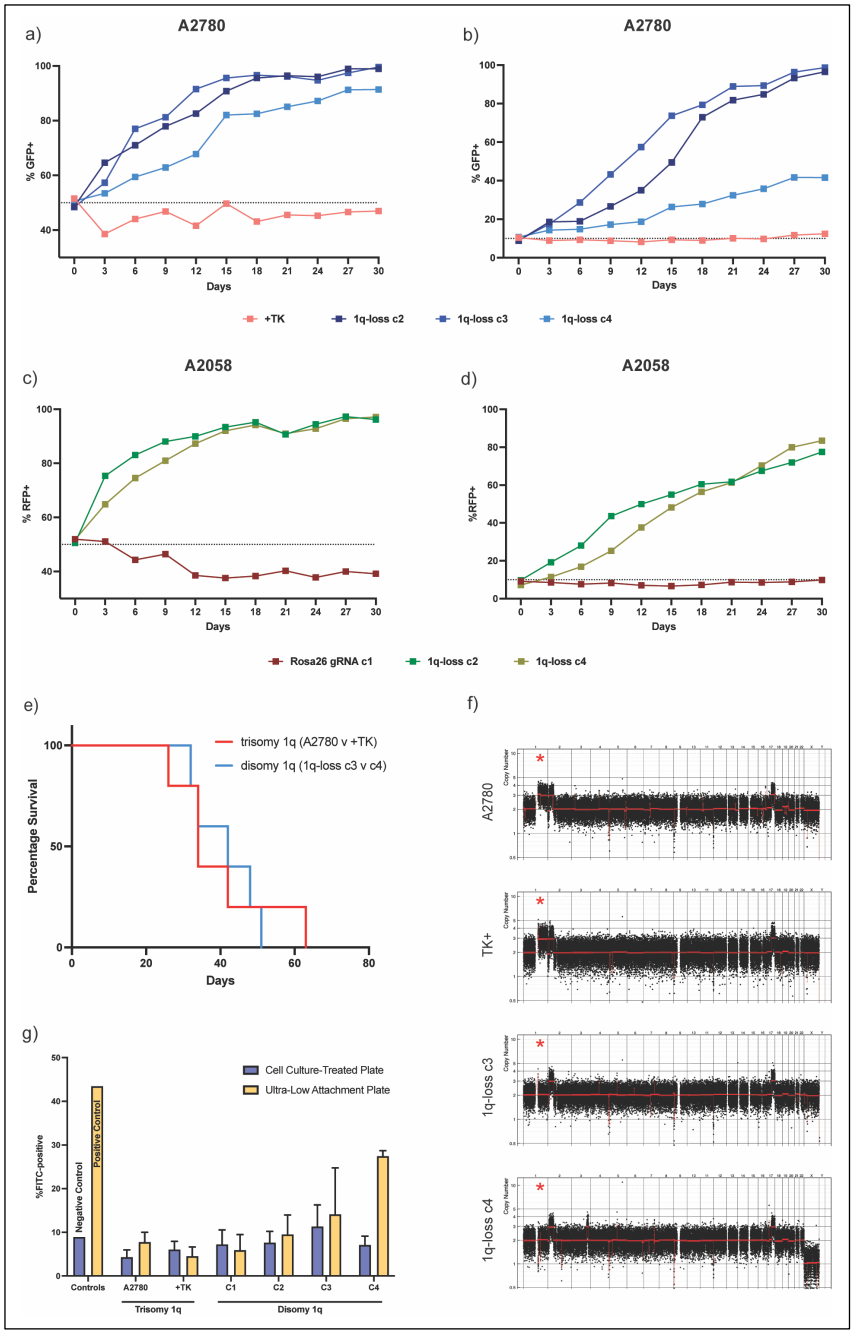

Figure 1: Trisomy 1q Outcompetes Disomy 1q. a-b) GFP-labelled A2780 trisomy 1q (parental) cells outcompete disomy 1q clones but not the TK+ control. c-d) RFP-labelled A2058 trisomy 1q (parental) cells outcompete disomy 1q clones but not the Rosa26 gRNA control. Dotted line indicates the starting percentage of trisomy cells (50% in a & c, 10% in b & d). e) A2780 trisomy 1q and disomy 1q cells injected contralaterally into immunocompromised mice arrive at the experimental endpoint (total tumor burden of 2000 mm^3) at similar rates (n = 5 mice per group). f) Representative SMASH-Seq karyotypes for the indicated A2780 populations following xenografts. Chromosome 1q is highlighted with an asterisk. g) No consistent differences in DNA fragmentation as a measure of apoptosis, measured using the TUNEL assay, are observed between attached and detached trisomy 1q and disomy 1q A2780 cells. n = 3 replicates. Kit positive and negative controls were used.

Dosage-Sensitive Drivers of 1q Gain

In Chapter 2, we posited that *MDM4* was a dosage-sensitive driver of 1q aneuploidy, but highlighted that multiple genes are likely to act in a cooperative manner to fully account for the 1q loss phenotype. To identify these, we nominated several candidates based on their presence in common focally amplified regions of 1q in patient tumors (Beroukhim et al. 2010) and their essentiality across cancer cell lines, as assessed through genome wide CRISPR knockout and RNA interference screens (Behan et al. 2019; Ghandi et al. 2019). We verified that these candidates were indeed transcriptionally downregulated in A2780 disomy 1q clones (Figure 2a). To assess the fitness cost of transcriptional downregulation, we used CRISPR interference (Gilbert et al. 2013) in the parental trisomy 1q cells (Figure 2b). We observed several gene candidates dropped out over successive passages in tissue culture, and these spanned a range of cellular pathways: *PFDN2* is a subunit of the prefoldin complex, a chaperone protein, and has previously been implicated as an oncogene in breast, colon and pancreas cancer (Nami and Wang 2018); *PSMD4* is a component of the 26S proteasome, mediates substrate delivery for degradation of ubiquitinated proteins, and has been implicated in leukemia, colorectal cancer, and hepatocellular carcinoma pathobiology (Cai et al. 2019); *MCL1* is an anti-apoptotic member of the *BCL-2* family, is overexpressed across diverse cancer types, and plays a key role in tumorigenesis (Beroukhim et al. 2010; Wang et al. 2021); *PPP1R15B* promotes dephosphorylation of eukaryotic translation initiation factor 2A to regulate translation under conditions of cellular stress (Kernohan et al. 2015); and *BCL9* promotes ß-catenin dependent transcription, and has causally been implicated in early stages of intestinal tumor development (Brembeck et al. 2011). Collectively, these results suggest that gain of 1q simultaneously suppresses *TP53* signaling, reduces apoptotic signaling, rewires transcription, and mitigates the proteotoxic consequences of an extra chromosome.

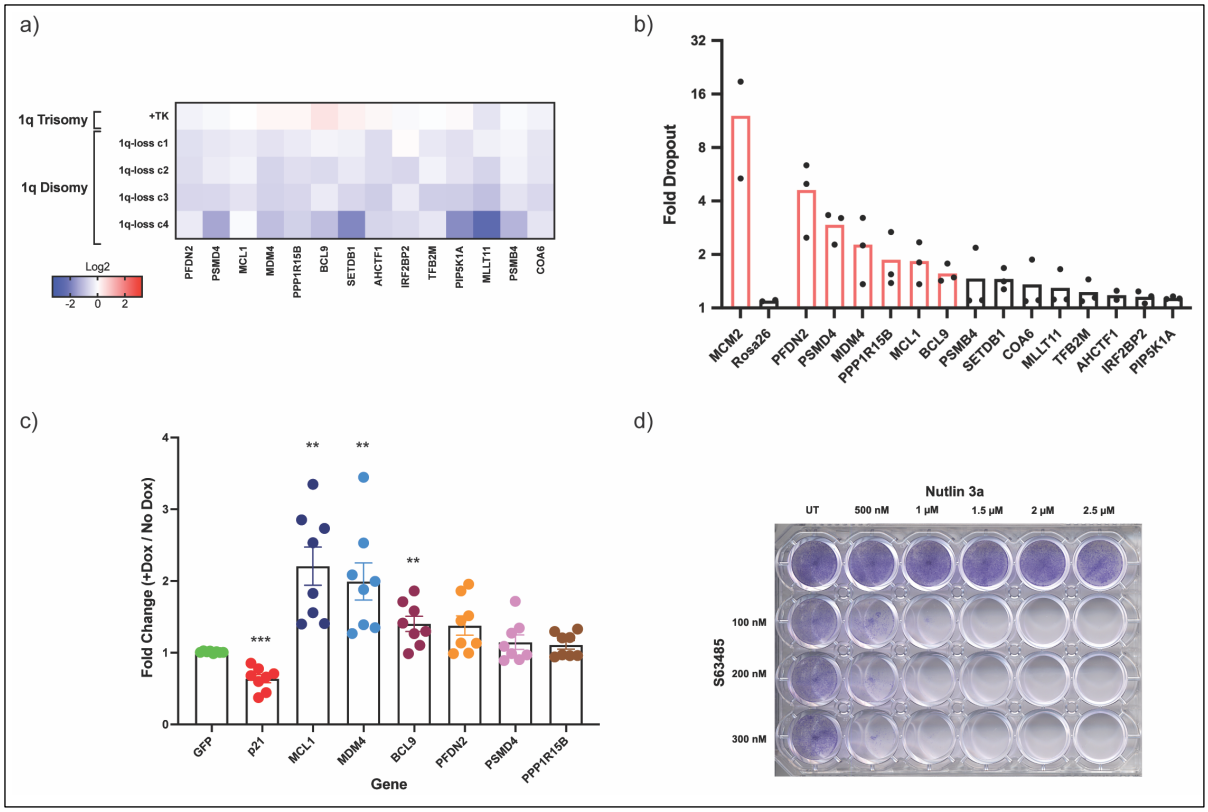

Figure 2: Dosage-Sensitive Genes on 1q. a) Candidate dosage-sensitive genes present on 1q are transcriptionally downregulated in A2780 disomy 1q clones, as assessed by qPCR. b) CRISPR interference screen in A2780 trisomy 1q cells using 3 guides per gene. *MCM2* and Rosa26 serve as positive and negative controls respectively. Highlighted in red are genes that, when downregulated, resulted in 2-fold or greater dropout. c) Inducible upregulation of dosage-sensitive candidates partially rescues the colony formation phenotype in soft agar. Shown are results across 2 biological replicates for 4 A2780 disomy 1q clones, plotted as fold change in colony formation upon induction of gene overexpression. n = 15 fields of view quantified per overexpressed gene for each cell line. ***p< 0.0005 **p < 0.005, Welch's Rank Sum Test. d) Simultaneous inhibition of *MDM4* and *MCL1* using Nutlin 3a and S63485 respectively has an additive effect on A2780 trisomy 1q toxicity. Cells were stained using crystal violet after 5 days of drug treatment. n = 3 replicates.

We subsequently sought to assess whether overexpression of these gene candidates in the disomy 1q clones would rescue their anchorage-independent growth phenotype. Indeed, inducible over-expression of *MCL1* and *MDM4*, and to a lesser extent *BCL9*, partially rescued growth. In contrast, *PFDN2*, *PSMD4*, and *PPP1R15B* overexpression failed to rescue growth (Figure 2c). However, given the cellular roles of these genes described above, this makes intuitive sense. Suppression of apoptosis (*MCL1*) and *TP53* signaling (*MDM4*), as well as

transcriptional reprogramming (*BCL9*), enhance growth of disomy 1q clones. In comparison, mitigation of proteotoxic stress (*PFDN2, PSMD4*) or translation stress (*PPP1R15B*) would not be expected to enhance fitness in an aneuploidy-loss setting, but nevertheless can be important in aneuploid cells. It remains to be seen whether co-overexpression of *MCL1*, *MDM4* and *BCL9* can fully rescue the phenotype of disomy 1q clones.

Finally, I investigated whether simultaneous inhibition of *MDM4* and *MCL1* using small molecule drugs would exert synergistic toxicity against trisomy 1q cells. Nutlin-3a is a small molecule inhibitor of *TP53-MDM2* interaction, and also exerts an inhibitory effect against *MDM4*, albeit to a lower degree (Shen and G. Maki 2011). S63485 inhibits *MCL1*, and has shown anti-tumor activity (Kotschy et al. 2016), but may have off-target activity as well (Yasuda et al. 2020). While combination of the two drugs appeared to have an additive effect on cellular toxicity (Figure 2d), the present experimental setup is insufficient for assessment of synergy. Future studies utilizing more specific inhibitors for both *MDM4* and *MCL1* are needed to comprehensively assess whether they can act synergistically, and whether there exists a therapeutic window for their use in 1q aneuploid tumors. Regardless, the preliminary data presented here suggests simultaneous targeting of multiple dosage-sensitive genes on aneuploid chromosomes may offer a novel therapeutic strategy.

Endogenous 1q Regain Rescues AGS Growth

In Chapter 2, we showed aneuploidy loss clones evolved to regain the lost chromosome during the course of both proliferation assays and subcutaneous xenografts (Figures 5 and S12). We further showed that this chromosomal regain rescued the anchorage-independent growth phenotype (Figure 5C), as did gain of a secondary chromosome in 8q

loss tumors (Figure 5H). However, the provenance of this chromosomal regain was not discussed.

There are two potential sources of chromosomal regain. The first is cell line cross contamination: during the course of regular tissue culture handling, it is possible that the purity of aneuploidy loss clones was compromised by aneuploid parental cells. Relatedly, as both aneuploid and aneuploid loss cells were injected contralaterally within the same mouse for xenograft experiments, aneuploid cells could have seeded tumors on the opposite flank. Given the competitive advantage exhibited by aneuploid cells (Figure 1a-d), they could subsequently overtake the cellular population. These would be examples of exogenous events. While such observations indicate the competitive advantage of aneuploid cells, they are not examples of true phenotypic rescue: it is possible that differences in genetic background between the heterogenous parental cells and the clonal disomy are providing the fitness advantage, independent of aneuploid karyotype.

Alternatively, chromosomal regain could be endogenous: genomic instability could result in chromosomal mis-segregation and acquisition of de-novo aneuploidy. If the aneuploid cell exhibited a fitness advantage, it would come to dominate the population. Not only would this indicate the importance of the observed aneuploidy, but it would also offer the opportunity to assess phenotypic rescue upon chromosomal regain.

To investigate this phenomenon, I utilized Sanger sequencing of single nucleotide polymorphisms (SNPs) on the aneuploid chromosome. In parental, aneuploid cells, SNPs exist at a 2:1 ratio. In the disomy clone, this ratio changes to 2:0 (loss of heterozygosity, or LOH), or to 1:1. Upon chromosomal regain, one of the remaining chromosomes is duplicated. If the ratio of the alleles is flipped in comparison to the parental line, or if homozygosity is maintained, endogenous chromosomal regain has occurred (Figure 3a-b).

Upon subjecting A2058 1q regain tumors to this analysis (Chapter 2 Figure 4A), we determined chromosomal regain was an exogenous event (data not shown). Analysis of A2780 1q regain (Chapter 2 Figure S12) was inconclusive, since no LOH was observed (data not shown). However, for AGS 1q-loss clones c3 and c12, which evolved to regain chromosome 1q during the proliferation assay (Figure 3e), we observed that the regain was endogenous (Figure 3c-d). Moreover, chromosomal regain rescued the anchorage-independent growth phenotype (Figure 3f). Therefore, trisomy 1q is both necessary and sufficient for cancer malignancy.

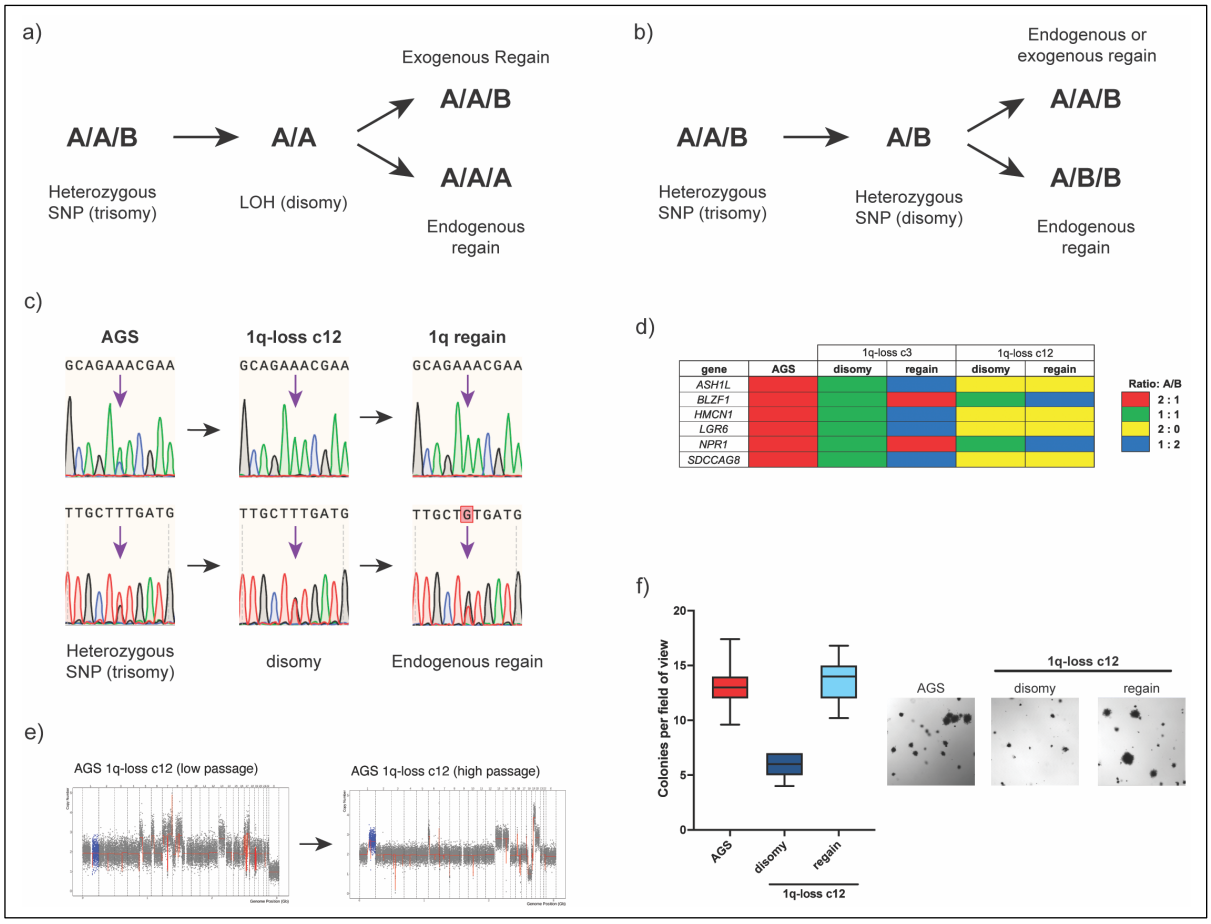

Figure 3: Endogenous Regain Rescues Growth. a-b) Diagrams representing all possible observed patterns of SNPs upon loss of a trisomic chromosome and its regain. Loss of heterozygosity upon chromosome loss and maintenance of homozygosity upon chromosome regain can be used to verify endogenous regain, as can a flipped SNP ratio. c) Sanger sequencing infograms for 1q loci highlight either LOH (top), or a flipped allele ratio (bottom). d) AGS 1q-loss c3 and c12 both exhibit endogenous regain of 1q following prolonged passaging. e) SMASH sequencing confirms high passage AGS 1q-loss c12 has regained the extra copy of chromosome 1q. f) Endogenous regain of chromosome 1q rescues the anchorage-independent growth phenotype. n = 15 fields of view per sample & 2 biological replicates; representative trial shown.

8q Loss in RKO

To further expand our understanding of 8q aneuploidy, I sought to engineer an "allelic series" of 8q loss clones. RKO is a colorectal adenocarcinoma cell line that harbors 4 copies of chromosome 8q. Therefore, it presents an opportunity to study the consequences of both single and dual chromosomal arm loss, without the confounding effects of haploinsufficiency that would be present upon dual arm loss in a trisomic model.

Using ReDACT-TR and ReDACT-CO, I isolated multiple clones with differences in 8q copy number. To my surprise, not only did I isolate clones with single or dual copy 8q loss, but also with 8q gain (Figure 4a). All 8q gain clones also had an extra copy of the X chromosome, indicating 8q is likely translocated onto the X chromosome. RNA Sequencing analysis confirmed transcriptional downregulation of genes on chromosome 8q upon arm loss, particularly in the disomy clones (Figure 4b). While a noticeable decrease in proliferation rate was observed for the disomy 8q clones, with doubling time up to 25h from 20h in the parental tetrasomy 8q, the trisomy and pentasomy clones exhibited a very mild defect, with doubling time up to 21h (Figure 4c). To my surprise, the karyotype for the parental tetrasomy 8q, the 8q gRNA controls, and 3/6 trisomy 8q clones, did not remain stable in tissue culture. SMASH sequencing analysis comparing these cells at the beginning and end of the proliferation assay showed 8q copy number fluctuated between 3 and 4. In contrast, 8q copy number remained stable for 3/6 trisomy 8q clones, the two disomy 8q, and the two pentasomy 8q clones (data not shown). Further cytogenetic analysis is needed to assess what underlies this fluctuation.

I subsequently investigated the consequences of 8q copy number on anchorage independent growth. All trisomy, disomy and pentasomy 8q clones exhibited a deficit in their colony formation ability (Figure 4d). In contrast, the tetrasomy 8q controls formed colonies at

similar rates to the parental cells, suggesting the observed phenotype is not due to CRISPR manipulation (Chapter 2 Supplemental Text 1). This suggests that cells may adapt to precisely tuned levels of gene dosage for aneuploid chromosomes, with any disruption to this balance resulting in a fitness deficit. However, as mentioned above, the stability of the trisomy/tetrasomy 8q karyotype in tissue culture is at present unclear, and the consequences of pentasomy 8q could not be isolated from those of trisomy X.

Finally, I sought to assess whether 8q copy number changes would affect tumor growth. Trisomy 8q clones formed tumors at comparable rates to the parental tetrasomy (Figure 4e), as was observed for HCT116 and A2058 8q loss clones (Chapter 2 Figures 3D, H). To my surprise, disomy 8q clones formed tumors even faster (Figure 4e). Unlike the proliferation assay, the karyotypes of all cells remained stable during the course of the xenograft (data not shown). While further investigation is needed to determine the underlying genetic causes for these phenotypes, these results highlight the variability in aneuploidy contribution to tumorigenesis. Furthermore, they illustrate the distinction between *in vitro* and *in vivo* assays, suggesting phenotypes observed for anchorage independent growth do not necessarily translate to xenografts. Thus, we are once again reminded that aneuploidy can exert context-dependent effects, and must be studied under a rigorous set of conditions to assess true biological function and contribution to tumorigenesis.

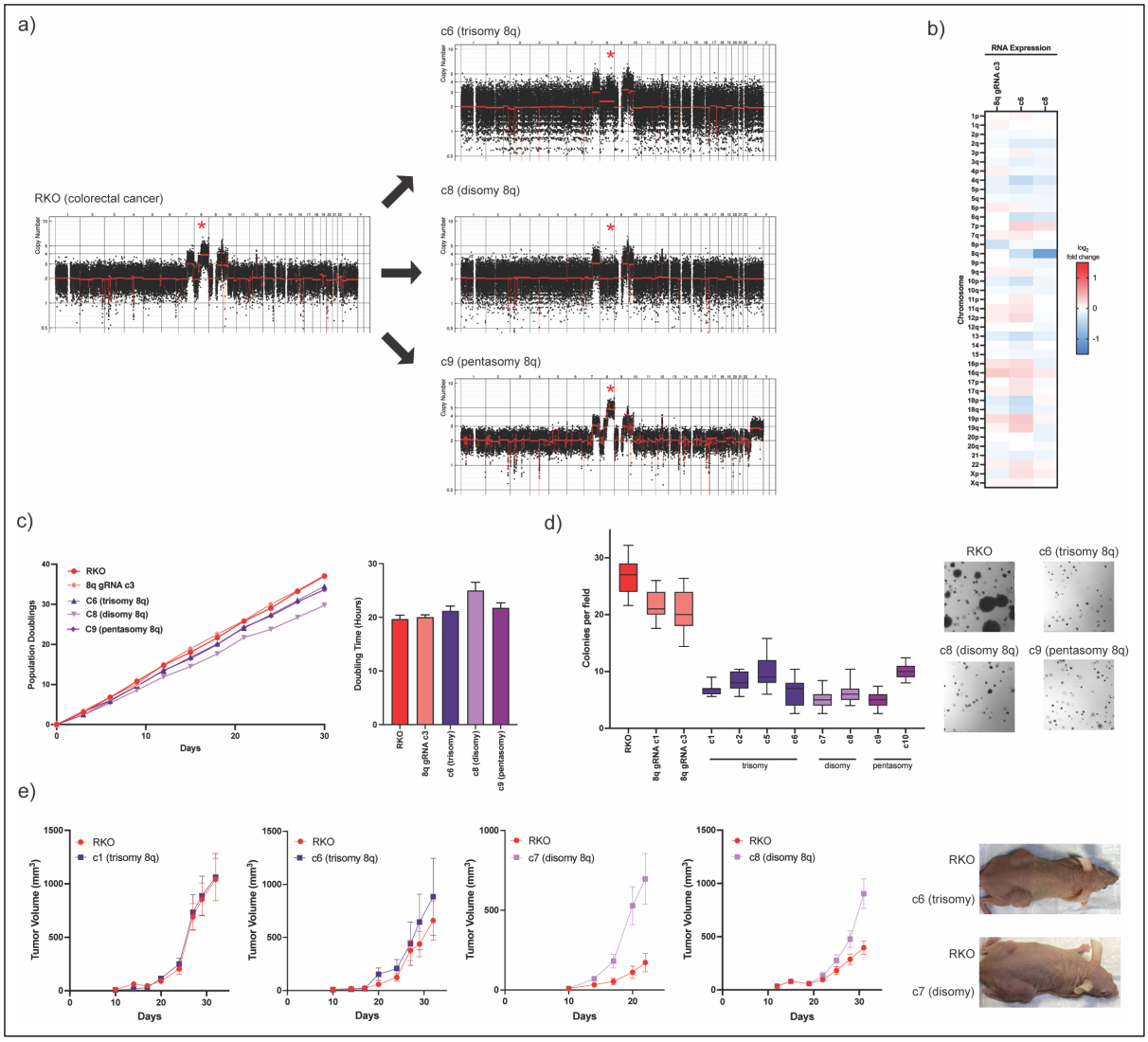

Figure 4: 8q Loss in RKO. a) ReDACT was used to engineer not only single and dual 8q loss clones, but also 8q gain clones. b) RNA sequencing analysis shows transcriptional downregulation of chromosome 8q in the representative disomy 8q clone, and to a lesser extent in the trisomy 8q clone, but not in the 8q gRNA control clone. c) Disomy 8q exhibits a proliferative defect compared to the parental tetrasomy 8q, but not the trisomy or pentasomy 8q clones. d) Variability in 8q copy number compromises anchorage-independent growth in soft agar. n = 15 fields of view per sample & 2 biological replicates; representative trial shown. e) Trisomy 8q clones form tumors at comparable rates to the parental tetrasomy 8q. Disomy 8q clones form tumors even faster. n = 10 mice each for c1, c6 and c7 xenografts; n = 9 mice for c8 xenografts.

Aneuploidy Loss is Comparable to Oncogene Deletion

To assess the magnitude of the fitness deficit observed upon loss of aneuploidy, I investigated the anchorage independent growth capacity of cell lines lacking a driver oncogene. HCT116 colorectal adenocarcinoma cells harbor mutated alleles for both *KRAS* and *CTNNB1*. Loss of the $KRAS^{WT}$ allele increased anchorage-independent colony formation, as the constitutively active $KRAS^{G13D}$ was the only *KRAS* allele present. Loss of the $KRAS^{G13D}$ mutant allele, meanwhile, compromised colony formation (Figure 5a-b), as did loss of $CTNNB1^{pS45del}$ (Figure 5c-d). However, $KRAS^{WT/-}$ and $CTNNB1^{WT/-}$ cells formed only 25% fewer colonies compared to parental $KRAS^{WT/G13D}$ and $CTNNB1^{WT/pS45del}$ cells respectively, whereas 8q-loss clones formed ~67% fewer colonies (Chapter 2 Figure 3G). It should be noted that $KRAS^{WT/-}$ cells do not exhibit complete deletion of the G13D allele, as seen in the Sanger sequencing infogram (Figure 5a). This suggests a fraction of cells still harbor both WT and G13D alleles. It would therefore be expected that a clean $KRAS^{WT/-}$ population may exhibit a greater defect in anchorage independent growth. Regardless, the difference in magnitude between the oncogene deletion and aneuploidy loss phenotypes is notable.

To investigate this further, I also compared the growth phenotype for RKO cells upon loss of the mutant $BRAF^{V600E}$ alleles. RKO cells carry an extra copy of chromosome 7q (Figure 4a), thereby carrying 3 *BRAF* alleles, two V600E mutant and one wild type (Figure 5e). Deletion of both $BRAF^{V600E}$ alleles reduced colony formation by 50% (Figure 5f). In comparison, loss of 8q compromised colony formation by 70-80% (Figure 4d). Therefore, across both cell lines, loss of 8q aneuploidy resulted in loss of malignancy comparable to, and exceeding, loss of driver mutant oncogenes.

It is important to note that 8q loss and oncogene deletion cells cannot be compared directly due to their difference in provenance. The parental HCT116 and RKO lines used to

derive 8q loss clones were obtained from a different source than the parental lines used to engineer oncogene deletion (see Methods and Acknowledgements). Nevertheless, these results highlight the magnitude of the fitness deficit conferred by aneuploidy loss. This lends further support to our proposal of aneuploidy addiction as a relevant paradigm for understanding tumor biology (see Chapters 2 & 4).

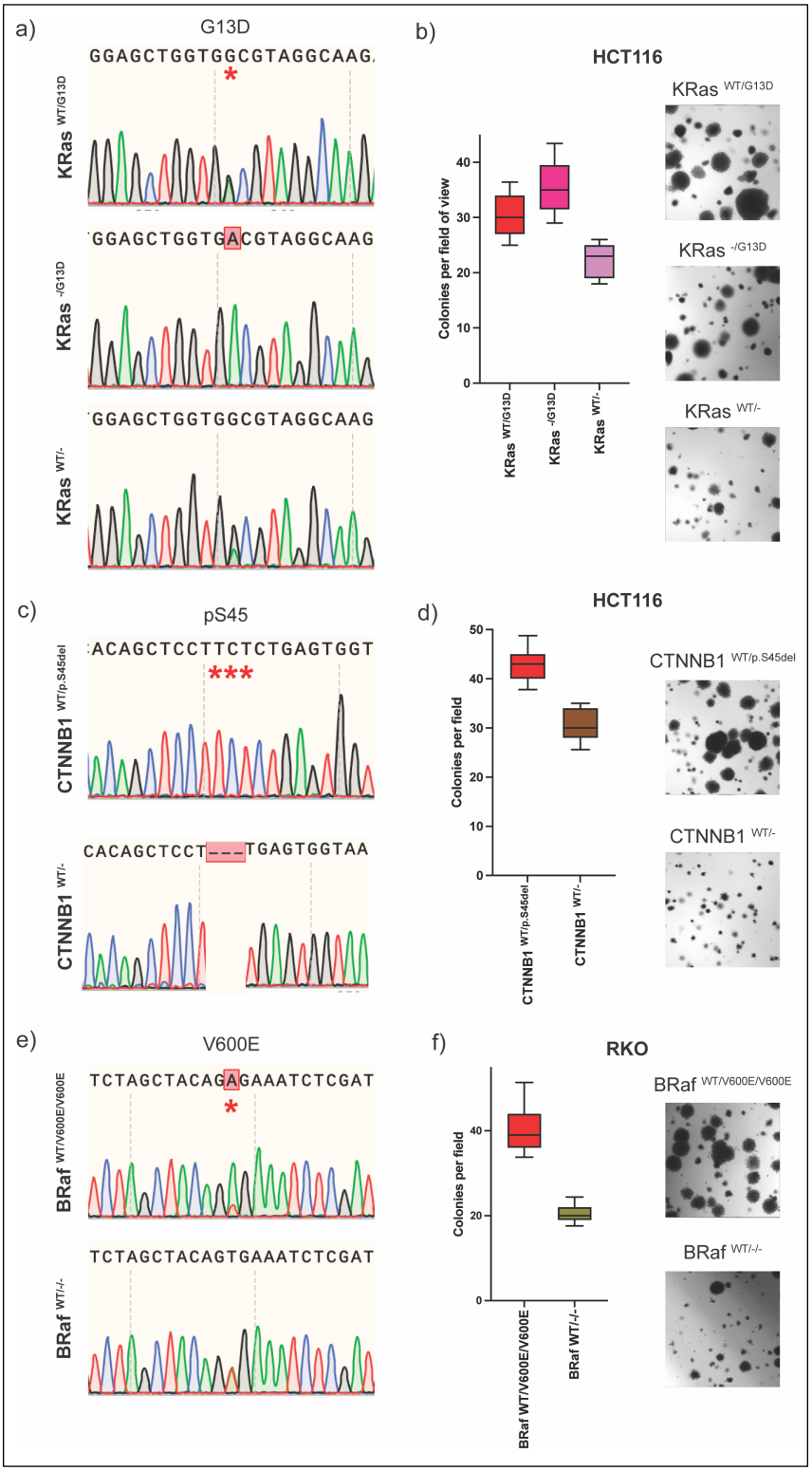

Figure 5: Oncogene Deletions Compromise Anchorage Independent Growth Comparable to Aneuploidy Loss. a, c, e) Sanger sequencing infograms highlight allelic differences among the indicated cell lines. b, d, f) Loss of the mutant oncogene reduces anchorage-independent growth in soft agar. n = 15 fields of view per cell line & 2 biological replicates; representative trials shown.

Unexpected Drivers of 8q Gain

To identify dosage sensitive drivers of 8q gain, I used the same 26-ORF overexpression library as was used for the identification of *RAD21* and *MYC* as cooperative drivers of trisomy 8q in Ewing sarcoma (Su et al. 2021). Briefly, the library contained 20 of the highest expressed genes syntenic between mouse chromosome 15 and human chromosome 8, and 6 controls: 4 genes implicated in connective tissue development, and 2 non-syntenic highly expressed genes. To my surprise, overexpression of only 2 genes partially rescued the 8q-loss phenotype in soft agar: *RNF139* and *PEX2* (Figure 6a). *RNF139* is multi-membrane spanning protein present in the endoplasmic reticulum that possesses ubiquitin ligase activity, and has previously been implicated as a tumor suppressor in hereditary clear cell renal carcinoma (Brauweiler et al. 2007). *PEX2*, meanwhile, encodes an integral peroxisomal membrane protein necessary for peroxisome biogenesis, mutations in which result in Zellweger syndrome (Fedick et al. 2014), one of several peroxisome biogenesis disorders. Neither gene, to my knowledge, has previously been causally implicated in oncogenesis.

Strikingly, overexpression of *MYC* did not rescue the growth deficit (Figure 6b). To ensure this wasn't due to plasmid-specific effects, I utilized a second *MYC* overexpression plasmid (MYC #2), but still failed to observe phenotype rescue. All ORFs were expressed following transduction, as tested by qPCR (data not shown). This is surprising given previous studies that have shown overexpression and downregulation of *MYC* enhance and reduce anchorage-independent growth respectively (Wang et al. 2005; Mori et al. 2009; Wasylishen et al. 2011). However, it is possible that *MYC* overexpression does not directly contribute to the anchorage-independent growth phenotype in the context of HCT116 8q trisomy, but may nevertheless contribute to tumorigenesis through independent cellular mechanisms. Intriguingly, *RAD21* overexpression, previously implicated in Ewing sarcoma and T cell

lymphoma pathobiology (Su et al. 2021; Trakala et al. 2021), also failed to rescue growth (Figure 6b). While comprehensive phenotypic tests have not yet been conducted using 8q-loss *MYC* or *RAD21* overexpression cells, they may offer insight into the underlying mechanisms. For example, *RAD21* overexpression was directly implicated in resolving DNA damage in aneuploid, highly proliferative cells (Su et al. 2021), and assessing DNA damage foci in 8q trisomic and disomic cells could highlight differences (or lack thereof) in baseline levels of DNA replication fork collapse in the context of 8q aneuploid colorectal cancer cells.

RNF139 and *PEX2* potentially represent novel avenues for investigation of 8q aneuploidy. It remains to be seen whether their overexpression rescues xenograft growth independent of chromosome 12 (and $KRAS^{G13D}$) amplification (Figure 4H), and whether such rescue can be observed across diverse models of 8q loss. Regardless, these results highlight the potential of necessity and sufficiency experiments to identify novel dosage-sensitive genes important for aneuploid phenotypes, and warrant further investigation.

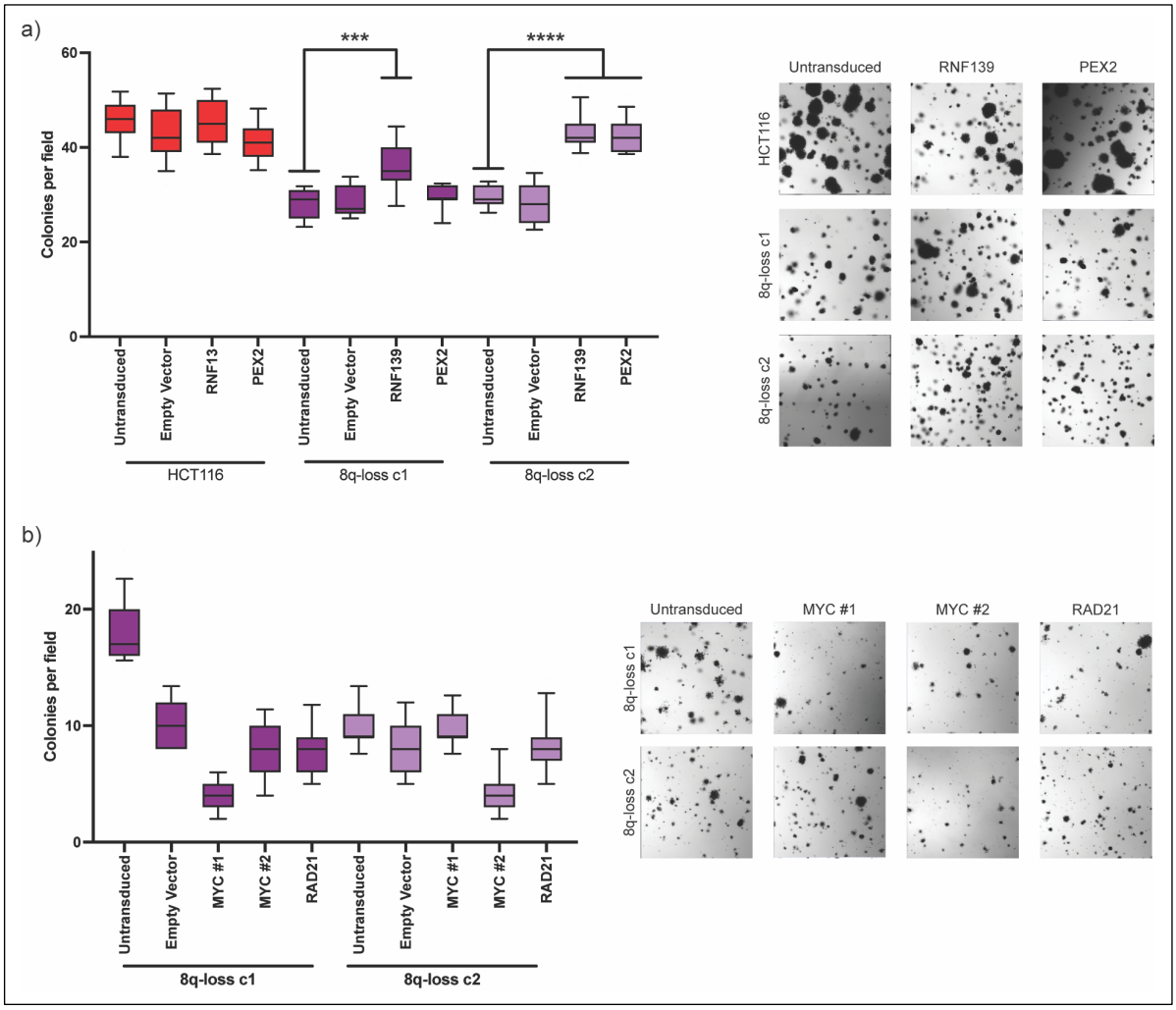

Figure 6: RNF139 and PEX2 Overexpression Partially Rescue 8q-loss Growth. a) *RNF139* and *PEX2* overexpression does not affect anchorage independent growth for parental trisomy 8q HCT116 cells, but does partially rescue the colony formation deficit for 8q-loss c2. *RNF139* overexpression also partially rescues the phenotype for 8q-loss c1. ***$p < 0.005$, ****$p < 0.0001$, Wilcoxon Rank Sum Test. b) Neither *MYC* nor *RAD21* overexpression rescues the 8q-loss phenotype in soft agar. MYC #1 and MYC #2 are two independent *MYC* overexpression constructs. n = 15 fields of view & 3 biological replicates per overexpression line; representative trials shown.

Materials & Methods

All materials and methods are identical to those presented in Chapter 2. Protocols used for RKO cells, competition assays, crystal violet staining following drug treatment, and the anoikis assay are described below.

RKO Culture Conditions

RKO and derived 8q-loss or gain clones were grown in McCoy's 5A medium (Gibco cat no. 16600082), supplemented with 10% fetal bovine serum (FBS) (Sigma-Aldrich, cat. no. F4135), 2 mM glutamine (Lonza, cat. no. 17-605F), and 100 U/mL penicillin-streptomycin (Life Technologies, cat. no. 15140122). RKO *BRAF*$^{WT/V600E/V600E}$ and RKO *BRAF*$^{WT/-}$ lines were obtained from Horizon Discovery (cat. no. HD 106-004), and grown in RPMI 1640 medium (Gibco, cat. no. 11875119) supplemented with 10% fetal bovine serum (FBS) (Sigma-Aldrich, cat. no. F4135), 2 mM glutamine (Lonza, cat. no. 17-605F), and 100 U/mL penicillin-streptomycin (Life Technologies, cat. no. 15140122).

RKO Soft Agar Assays

To assay colony formation in soft agar, a solution of 1.0% Difco Agar Noble (VWR Scientific, USA, cat. no. 90000–772) in sterile water was prepared. The 1% agar solution was mixed 1:1 with the base cell culture media supplemented with 20% FBS, 4 mM glutamine, and 200 U/mL penicillin/streptomycin. 1 mL of this mixture was plated on each well of a 6-well plate and allowed to solidify at room temperature to form a base layer of 0.5% agar. Cells were then harvested and counted. For RKO and derived 8q-loss or gain clones, 20,000 cells were seeded in 0.30% agar (1:1 mixture of 0.6% agar in sterile water and 2x supplemented growth medium). For RKO *BRAF*$^{WT/V600E/V600E}$ and RKO *BRAF*$^{WT/-}$ cells, 40,000 cells were seeded in

0.30% agar. Plates were left at room temperature to solidify and then placed in a humidified incubator at 37˚C and 5% CO2. 1 mL of normal growth media was added the next day, and every three days after. After 11 days, cells were fixed with 100% methanol, and stained with 0.01% crystal violet dissolved in 25% methanol. Colony formation was quantified by capturing z-stacks of three fields of view per well from at least three wells on a LSM 710 confocal microscope (Zeiss) under 5x magnification. The average number of colonies was calculated by counting total number of colonies per field of view from 15 fields of view across three wells.

RKO Xenografts

To assay tumor formation, cells were harvested and resuspended in cold PBS. 3 million cells were injected in each flank of NU/J mice (Jackson Laboratory, cat. no. 002019). Cells were subcutaneously injected using a 1 mL 25G x 5/8 syringe (BD, cat. no. 309626). Mice were visually monitored for tumor formation routinely following injection. Once a tumor was visible, it was measured every three days by calipers. Tumor volume was calculated using the formula V = ½ (longer axis)(shorter axis). The experimental end point was reached and mice were sacrificed when total tumor burden exceeded 2000 mm^3. All mouse protocols were approved by the CSHL Institutional Animal Care and Use Committee.

Competition Assay

A2780 trisomy 1q cells were transduced with retroviral eGFP:P2A:Puro and selected for GFP expression. A2058 trisomy 1q cells were transduced with pMMLV[Exp]-mRFP1(ns):P2A:Puro and selected for RFP expression. Fluorophore expressing trisomy 1q cells were mixed with disomy 1q clones or trisomy 1q controls at a 50:50 or 10:90 ratio, and 100,000 total cells were

plated on day 0. Every 3 days, the intermixed populations were split, percentage fluorophore expression analyzed using flow cytometry, and 100,000 cells replated. Fluorophore expression was normalized to a pure fluorophore expressing population that was simultaneously maintained in tissue culture.

Nutlin-3a + S63485 Drug Combination

30,000 A2780 cells were plated in a 24-well tissue culture treated plate on Day -1. On day 0, Nutlin-3a (Selleckchem cat. no. S8059) and S63485 (Selleckchem cat. no. S8383) were added at the indicated concentrations. On day 5, the cells were washed twice with PBS, fixed with 100% methanol, and stained with 0.5% crystal violet dissolved in 25% methanol.

Anoikis Assay

300,000 cells were plated on tissue-culture treated plates, or on ultra-low attachment plates (Corning cat. no. CLS3474). 72h later, the media was harvested, and any attached cells trypsinized and collected into the same media. The TUNEL assay was performed according to the manufacturer's instructions (Abcam cat. no. ab66108). Briefly, cells were fixed with 1% formaldehyde, washed twice with PBS, resuspended in PBS, and added to 70% ice-cold ethanol. An aliquot of cells was subsequently washed with the kit wash buffer, and resuspended in staining solution. After 60 min, the staining solution was rinsed off using the kit rinse buffer, and cells were resuspended in Propidium Iodide/RNase A solution. Following 30 min in the dark, cells were analyzed for FITC staining (with a PI counter-stain) on a flow cytometer.

Acknowledgments

I would like to thank Dr. Bert Vogelstein (Johns Hopkins University) for generously sharing HCT116 *KRAS* and *CTNNB1* deletion lines. I would also like to thank Dr. Xiaofeng Su (MIT) for generously sharing the 8q ORF expression library.

Chapter 4: Conclusions & Perspectives

"The great discovery that launched the Scientific Revolution was that humans do not know the answers to their most important questions"
Yuval Noah Harari

Summary of Results

Through the course of this thesis, I have highlighted the importance of aneuploidy in tumor biology. Chapter 1 introduces the history of cancer-related aneuploidy research and describes the experimental tools that may be used to distinguish correlational from causative patterns of aneuploidy in tumors. Chapter 2 presents a novel suite of tools for targeted aneuploidy elimination in cells, and uses them to provide compelling evidence for an oncogene-like role of aneuploidy in cancer. Chapter 3 highlights the complexities and subtleties of studying this phenomenon, and provides preliminary evidence for future avenues of research. Below, I expand on the discussion of some key findings and propose frameworks that may be utilized to develop a thorough understanding of the causative role aneuploidy plays in tumorigenesis. I also provide a brief history of the oncogene addiction paradigm, and outline our reasons for suggesting cancers may similarly be addicted to aneuploidy.

Chapter 2: Oncogene-Like Addiction to Aneuploidy in Human Cancers

First, we utilized BUTTE (Bounds of Time Until Expansion) analysis (Wang et al. 2022) to evaluate the developmental timing of aneuploidy in cancer. Previous reports have suggested chromosomal gains occur very early in tumorigenesis, and can dictate subsequent alterations to the tumor genome (PCAWG Evolution & Heterogeneity Working Group et al. 2020). Using multi-sampled tumor sequencing data, we showed chromosome 1q gains tend to occur early in the development of breast cancer and melanoma, and that common aneuploidies arise earlier in tumor development than less common ones (Figure 1A-C). The availability of multi-sampled patient data currently limits expansion of this analysis across cancer types, since assessment of developmental timing for genomic aberrations requires

sequencing across tumor grades for the same patient. As such studies become more common, BUTTE and other methods could be used for mapping the exact trajectory of mutational and aneuploidy acquisition during tumorigenesis.

Second, we added to the repertoire of correlational findings outlining the cancer type-specific patterns of aneuploidy (Taylor et al. 2018; PCAWG Evolution & Heterogeneity Working Group et al. 2020) and their co-occurrence and mutual exclusivity patterns (Davoli et al. 2013; Shukla et al. 2020; Prasad et al. 2022) by analyzing patient datasets for correlations between driver mutations and aneuploidy (Figures 1D-E, S1). For example, we showed chromosome 7p gain tends to co-occur with *TP53* and *EGFR* mutation in non-small cell lung cancer, but is mutually exclusive with *KRAS* mutation. Similarly, chromosome 18q gain in pancreatic cancer is mutually exclusive with *KRAS* mutation, but co-occurs with *MEN1* mutation (Figure S1). Why these patterns exist remains unclear, but future investigations where these driver oncogenes or tumor suppressors are mutated in the presence or absence of the aneuploid chromosome may uncover biomarkers for disease progression as well as potential therapeutic vulnerabilities.

Third, we created a suite of targeted aneuploidy deletion tools called ReDACT: Restoring Disomy in Aneuploid cells using CRISPR Targeting. We used them to engineer isogenic populations of cells differing in copy number of chromosome 1q across different cancer backgrounds (Figure 2A-B). We showed loss of trisomy 1q compromises malignancy for established cancer cell lines (Figure 2D-E), and limits the transformation potential for immortalized breast epithelial cells (Figure 2F-H). We subsequently engineered loss of trisomy 7p and 8q (Figure 3A, E), and demonstrated that the phenotypic consequences of aneuploidy loss vary by targeted chromosome (Figure 3C-D, G-H). Moreover, we showed aneuploidy loss exerts a selective pressure for aneuploidy regain, either for the lost

chromosome (Figure 4A-F), or for a secondary aneuploidy carrying a driver oncogene (Figure 4G-H). While these experiments highlight the necessity of trisomy 1q, and to a lesser extent trisomy 7p and 8q, in cellular models, whether these results hold true in established tumors remains unclear. Utilization of ReDACT and other chromosomal alteration techniques in patient-derived organoids may offer insights into the consequences of aneuploidy loss within tissues. Interrogation of other tumor models and aneuploidies using the same techniques can also outline the generality of aneuploidy addiction as a paradigm. I discuss the efficiency of various targeted aneuploid chromosome deletion techniques and the caveats of a single cell cloning approach below. I also highlight avenues for expanding this analysis to more clinically-relevant models, and approaches for discovering pharmaceutically-targetable biology.

Fourth, we sought to identify the dosage-sensitive gene(s) driving 1q aneuploidy, and uncovered a mutual exclusivity pattern between 1q aneuploidy and *TP53* mutation (Figure 5A-H). We verified *MDM4* as a dosage-sensitive candidate on chromosome 1q, evaluating both its necessity and sufficiency for the trisomy 1q phenotype (Figure 5I-N). However, we note that *MDM4* alone does not fully account for chromosome 1q gain. While I present some other dosage-sensitive gene candidates in Chapter 3, including *MCL1* and *BCL9*, it remains to be seen whether this core subset of genes is solely responsible for the fitness benefits of trisomy 1q. At present, this analysis is limited to a singular cell line. Which genes are necessary and sufficient for 1q aneuploidy in diverse cancer backgrounds, both in the presence and absence of *TP53* mutation, has not yet been evaluated.

Last, we highlight a therapeutic vulnerability conferred by 1q aneuploidy. We demonstrate *UCK2* expression scales with 1q copy number (Figure 6B-C), and this renders 1q trisomic cells more sensitive to *UCK2*-targeted drugs (Figure 6D-F). Thus, 1q trisomy may

serve as a biomarker for *UCK2*-targeted therapy. Again, it remains to be seen whether this is broadly true for all 1q aneuploid models. A comprehensive screen targeting all overexpressed genes on aneuploid chromosomes may reveal further vulnerabilities conferred due to the gained chromosome, which may in turn guide clinical treatment.

Chapter 3: The Complexities of Aneuploidy Research

Chapter 3 brought together several disparate lines of evidence that collectively highlight the challenge of studying aneuploidy. First, I discussed the variability in ReDACT efficiency, and highlighted models where targeted chromosomal loss could not be achieved (Table 1). Further analysis of the cytogenetic organization of chromosomes and the cellular processes immediately following induction of arm loss may aid in optimizing ReDACT for use across all cell lines. Ultimately, translation of the technique into *in vivo* models is needed to yield clinically-relevant insights, including the interplay between spontaneous acquisition or loss of aneuploidy and its interaction with the immune system.

Next, I highlighted the competitive advantage of trisomy 1q over disomy 1q (Figure 1). Even a low percentage of trisomy cells outcompete disomy clones under standard tissue culture conditions, which explains why cells with chromosomal regain rapidly come to dominate the cellular population (Chapter 2 Figure S12). Since aneuploidy loss results in only a mild proliferative defect, this suggests trisomy 1q may confer other unexplored advantages in a competitive setting, such as more efficient nutrient metabolism. The cellular processes underlying this competitive advantage therefore merit further investigation.

I subsequently discussed other dosage-sensitive candidates driving 1q aneuploidy (Figure 2). *MCL1*, an anti-apoptotic protein part of the *BCL2* family of apoptosis regulators, is partially necessary and sufficient for the 1q aneuploid phenotype observed in A2780, similar

to *MDM4* (Figure 2b-c). Multiple other genes, when transcriptionally downregulated, also compromise growth of the parental trisomy, and play roles in protein synthesis, folding, and degradation pathways (Figure 2b). While we were unable to simultaneously overexpress these dosage-sensitive genes to assess whether complete phenotypic rescue could be achieved, our results nevertheless suggest several genes simultaneously contribute to the aneuploid phenotype. Future investigations aimed at identifying the core subset of genes responsible for driving an aneuploidy, and assessing the generality of that phenomenon across diverse cancer models, are likely to yield avenues for synergistic drug combinations (Figure 2d).

An unanswered question from Chapter 2 was whether the chromosomal regain events observed were exogenous (cross-contamination from trisomy cells), or endogenous (de novo chromosomal mis-segregation and acquisition of aneuploidy). I highlighted examples of endogenous regain of 1q aneuploidy for AGS (Figure 3), and showed that this completely rescues the anchorage-independent growth phenotype (Figure 3e). Not only do these results further confirm the validity of our aneuploidy addiction hypothesis, but they also provide additional evidence to negate concerns regarding the observed phenotype being caused by CRISPR manipulation (Chapter 2 Supplemental Text 1).

Another curiosity stimulated by our findings in Chapter 2 was whether differences in copy number of aneuploid chromosomes in the same genetic background would present distinct phenotypes. To this end, I engineered single and dual copy loss, as well as single copy gain, of chromosome 8q in RKO cells, a colorectal adenocarcinoma cell line harboring 8q tetrasomy (Figure 4). Mild proliferative defect and a stronger deficit in colony formation were observed for all 8q copy number variant clones, suggesting any disruption to 8q gene dosage carries a fitness penalty (Figure 4c-d). Surprisingly, disomy 8q clones formed tumors even

faster than the parental tetrasomy (Figure 4e). Whether these phenotypes are unique to RKO or conserved across different 8q tetrasomy models would be an interesting avenue for future research. These results would also be better informed by analysis of the timing of 8q gain in such models. It is possible that 8q aneuploidy is acquired at a critical stage in tumor expansion, when it facilitates anchorage-independent growth (Figure 4d) and expansion of the cancer to secondary sites, but results in slower tumor proliferation (Figure 4e). Investigation into the underlying biology may identify disrupted cellular mechanisms critical for defined phases of tumor growth, and help distinguish aneuploidy contribution to colony formation vs growth as a xenografted tumor.

Remarkably, the magnitude of the fitness defect in anchorage independent growth is greater for loss of an aneuploid chromosome in comparison to loss of a driver oncogene (Figure 5). While these results were only presented for 8q aneuploid cells, and oncogene deletion was engineered in parental cells with a different provenance compared to those used to engineer aneuploidy loss, they nevertheless provide further evidence for an oncogene-like role of aneuploidy in cancer. It remains to be seen whether these findings are consistent across diverse aneuploidies and oncogene drivers.

Finally, I investigated the dosage-sensitive drivers for 8q gain in HCT116 cells. To my surprise, neither *MYC* nor *RAD21* overexpression rescued the 8q loss phenotype (Figure 6b). Instead, overexpression of *PEX2* and *RNF139* partially rescued anchorage-independent growth – two genes previously unimplicated as oncogenes. In fact, *RNF139* has previously been described as a tumor suppressor (Brauweiler et al. 2007), and *PEX2* has most extensively been studied for its role in Zellweger syndrome, a peroxisome biogenesis disorder (Fedick et al. 2014). At present, it is unclear what role these genes may play in cancer development.

However, these findings highlight aneuploidy research as an avenue for discovery of novel cancer biology, which may ultimately yield new drug targets for clinical benefit.

Comparison of Targeted Arm Loss Methods

In chapter 1, I described current methods for targeted chromosomal manipulation, and in Chapter 3, I discussed the efficiency of ReDACT across different cell lines. Due to the recent expansion in techniques available, an analysis of the practical utility of each technique can help guide appropriate use. Table 1 compares the efficiencies, targetable chromosomes, and method of use for each technique.

Technique	Karyocreate	Targeted Mis-segregation	Targeted Mis-segregation	ReDACT	Telomere Truncation	TALENs
Tools	dCas9-KNL1$^{RVSF/AAAA}$ + centromere-specific sgRNAs	dCas9-CENP-TΔC + Mps1i pulse	dCas9-Kinesin14VIb	Centromere-specific Cas9 gRNAs (+ negative selection cassette or artificial telomere)	Cas9 + artifical telomere & drug selection cassette	TALENs spanning intended deletion
Consequence	Arm gain or loss	Arm gain or loss	Arm gain or loss	Arm loss	Arm loss	Arm loss
Method of Delivery	Lentiviral transduction	Liposomal transfection	Lentiviral transduction	Liposomal transfection (+ drug selection)	Liposomal transfection + drug selection	Liposomal transfection
Targetable Chromosomes	Theoretical: 19/24; Demonstrated: 10/24	Chromosomes 1p & 9q	Chromosomes 1p & 9q	Theoretical: all; Demonstrated: 1q, 7p, 8q	Theoretical: all; Demonstrated: 3p	Theoretical: all; Demonstrated: 8p
Efficiency	8% for chromosomal gain; 12% for chromosomal loss	Unreported	Lagging chromosomes in 90% of cells	5 - 15% (cell line-dependent)	Unreported	Unreported
Cell Lines Used	hTERT TP53-KO colon epithelial and retinal pigment epithelial cells	Embryonic kidney and colorectal carcinoma cells	Retinal pigment epithelial cells	Ovarian and gastric carcinoma, melanoma, and breast epithelial cells	Immortalized lung epithelial cells	Mammary epithelial cells
References	(Bosco et al. 2022)	(Tovini et al. 2022)	(Truong et al. 2022)	(Girish*, Lakhani* et al. 2023)	(Taylor et al. 2018)	(Cai et al. 2016)

Table 1: Summary of Practical Use for Targeted Chromosomal Arm Loss Methods

The available methods for chromosomal engineering offer their pros and cons (Table 1). Efficiencies vary widely, and aren't standardized by a singular metric. Therefore, it is unclear how many single cell clones need to be isolated, on average, for each technique to

produce a clone with targeted chromosomal arm gain or loss event. Targeted chromosomal mis-segregation methods using dCas9-CENPT or dCAS9-Kinesin14VIb require chromosomes with repetitive endogenous arrays, limiting their use to chromosomes 1p and 9q. While this range can be expanded by targeting dCas9 to an integrated TetO repeat (Truong et al. 2022), the dual step method will increase length of time required for aneuploidy manipulation, and likely reduce efficiency. A head-to-head comparison of our use of ReDACT-NS, ReDACT-TR, and ReDACT-CO (Girish*, Lakhani* et al. 2023) does favor the latter two techniques for targeted arm loss since they achieve the desired outcome in a single step process, in contrast to the two rounds of cloning and selection required for ReDACT-NS. Additionally, any methods requiring multiple instances of dsDNA break creation increase the likelihood of off-target effects and secondary karyotypic alterations. It is also important to distinguish between methods requiring lentiviral use vs liposomal transfection – the former necessarily involves viral integration into the host genome, which may affect the genome in unexpected ways. Drug selection for expression of exogenous cassettes also exerts selection pressure on the cells, which may manifest in phenotypic consequences. Therefore, it is important to take these aspects into consideration for any experimental design.

Caveats for Single Cell Cloning

It is important to note that all methods outlined above demand single cell cloning for the generation of aneuploidy gain or loss populations of cells, and none have thus far been used with patient-derived organoids. This means that genetic heterogeneity – such as it may be in cell lines isolated from patients decades ago and propagated under non-physiologic tissue culture conditions – is nevertheless lost (Bendall and Nolan 2012). Single cell cloning approaches also frequently utilize flow cytometry for cell sorting, which introduces stresses

that can affect cellular phenotype (Pfister et al. 2020). All studies thus far have utilized less than ten, and often just two or three, clonal populations for assessment of phenotypic consequences of aneuploidy gain or loss, suggesting chromosomal engineering remains an experimental bottleneck. We engineered multiple clonal populations with aneuploidy loss for each cell line, and conducted a wide range of control experiments to ensure the observed phenotypes could only be attributed to aneuploidy loss (Chapters 2 & 3). Regardless, the credibility of this approach relies on strength in numbers – aneuploidy manipulation in diverse and clinically-relevant genetic backgrounds, with large numbers of clones and appropriately matched controls, increases confidence in the results. Chromosomal engineering approaches that can be utilized efficiently for a bulk population of cells need to be developed to mitigate the caveats of single cell cloning, which in turn may allow their use for organoids and mouse models.

Therapeutic Vulnerabilities Created by an Aneuploid Chromosome

Numerous reports have suggested the aneuploid state may confer a therapeutic opportunity (Ben-David and Amon 2020; Vasudevan et al. 2021). The mitotic kinesin *KIF18A,* for example, has been reported as essential in aneuploid cells, which also show an increased sensitivity to proteasome inhibition (Cohen-Sharir et al. 2021). The sensitivity to *KIF18A* inhibition, however, appears to be caused by the high levels of aneuploidy induced after whole genome duplication, as one or two aneuploid chromosomes in a near diploid background do not confer the same sensitivity (Quinton et al. 2021). Inducers of metabolic stress (Tang et al. 2011), increased chromosomal instability (Janssen et al. 2009; Maia et al. 2015), and elevated ceramide levels (Tang et al. 2017), as well as *SRC* kinase inhibitors (Schukken et al. 2020) have all been reported to exert greater toxicity to aneuploid cells.

However, the degree of aneuploidy required to achieve a therapeutic window, and the efficacy of these treatments in pre-clinical models, remains unclear.

In Chapter 2, we reported trisomy 1q as a biomarker for use of *UCK2*-targeting drugs. This suggests that there may exist aneuploidy-specific vulnerabilities. One approach towards exploiting these vulnerabilities is to identify dosage-sensitive genes present on aneuploid chromosomes that are driving tumorigenesis (see below). Another approach would be to conduct high throughput drug screening of genetically matched aneuploid and non-aneuploid cells to identify aneuploidy-specific drug targets. As aneuploid cells have an elevated transcriptional, translational and proteotoxic burden (Schukken and Sheltzer 2022), therapeutic strategies designed to exploit those stresses may yield clinical benefit. Furthermore, since multiple dosage-sensitive genes are likely responsible for the aneuploidy phenotype (Chapter 1), there exists an opportunity for synergistic drug combinations: for example, targeting three dosage-sensitive genes simultaneously in an aneuploid tumor is likely to both minimize the dosage of each individual drug, as well as the likelihood of resistance evolving by re-amplification of any one drug target (Keith et al. 2005; Lehár et al. 2009). Although use of specific aneuploidy patterns as biomarkers for drug treatment remains a relatively unexplored landscape, it presents tremendous opportunity for discovery of both novel drug targets as well as synergistic drug combinations.

Future Approaches for Aneuploidy Dissection

While development of targeted chromosomal mis-segregation and arm loss methods will go a long way towards creating isogenic cellular models for assessment of aneuploid phenotypes, it remains to be seen whether these techniques can be successfully utilized *in vivo*. Although various mouse models for assessment of aneuploidy have been designed, they rely on manipulation of chromosomal instability (CIN), often through deletion or inhibition of spindle assembly checkpoint (SAC) components (Vasudevan et al. 2021). Because SAC gene mutations are extremely rare in cancers and aneuploidy can exist in chromosomally stable backgrounds (Gordon et al. 2012), the relevance of these mouse models to the study of clinically relevant aneuploidy phenotypes is limited. Regardless, new methods for genomic manipulation *in vivo* may allow developmentally-sensitive manipulation of aneuploidy. For example, electroporation-based genetically engineered mouse models (EPO-GEMMs) use CRISPR alongside transposases and *in vivo* organ electroporation to induce somatic mutations in adult mice, and have been used to accelerate development of mouse models that recapitulate human disease (Leibold et al. 2020; Paffenholz et al. 2022). Combining EPO-GEMMs with the chromosomal engineering methods outlined above could allow manipulation of aneuploid chromosomes in tissues (Figure 1a). Targeted deletion of an aneuploid chromosome or induction of chromosomal gain at various stages of tumor development within an organoid or mouse model would provide incredible insight into both the immediate and the longer-term consequences of aneuploidy.

Another useful approach would be chromosomal tiling (Figure 1b). While groups have nominated candidates as dosage-sensitive drivers of aneuploid chromosomes – *SMAD2* and *SMAD4* for chr18q loss (Bosco et al. 2022), *RAD21* and *MYC* for chr8q gain (Su et al. 2021; Trakala et al. 2021), and *MDM4* for chr1q gain (Girish*, Lakhani* et al. 2023) – these genes

only partially explain the observed phenotypes. Therefore, chromosomal tiling approaches, where different segments of aneuploid chromosomes are deleted or overexpressed, could shed light on the importance of focal amplifications and deletions as compared to whole chromosome or chromosomal arm aneuploidy. Both ReDACT-NS (Girish*, Lakhani* et al. 2023) and MACHETE – molecular alteration of chromosomes with engineered tandem elements (Barriga et al. 2022) – are capable of engineering genomic deletions spanning tens of megabases, and could be utilized for this purpose. Meanwhile, human artificial chromosomes (HACs) are progressively overcoming hurdles (Logsdon et al. 2019; Moralli and Monaco 2020) and may soon offer the possibility of introducing entire chromosomal arms stably into cells. These approaches could help assess the simultaneous necessity and sufficiency of chromosomal segments spanning hundreds of genes.

Furthermore, the development of massively parallel screening approaches, if conducted in a chromosome-specific manner, could allow discovery of dosage-sensitive genes. CRISPR interference (CRISPRi) and activation (CRISPRa) screens have already been successfully utilized to discover new facets of oncogene and tumor suppressor biology (Fulco et al. 2016; Klann et al. 2017). Thus, libraries designed to downregulate or overexpress chromosome-specific gene expression in an aneuploid and genetically-matched non-aneuploid setting respectively, could identify dosage-sensitive genes present on aneuploid chromosomes (Figure 1c). It is critical, however, that gene expression be modulated to levels comparable to chromosome gain or loss. For example, CRISPRi in trisomic cells should downregulate targeted gene expression by 33% to assess consequences of chromosome loss, and CRISPRa in disomic cells should upregulate gene expression by 50% to assess consequences of chromosome gain. Although such precise tunability of gene expression is currently difficult, novel techniques are being developed for this purpose, including the use

of chemical epigenetic modifiers to implement dose-dependent gene expression (Chiarella et al. 2020). Furthermore, as mentioned above, it is likely that multiple genes on the aneuploid chromosome contribute to its gain or loss. While efficient use of multiplexed CRISPR arrays (McCarty et al. 2020) and multi-gene overexpression constructs (Patel et al. 2021) remains challenging, their application in aneuploid settings would help uncover the minimal subset of genes necessary and sufficient for the aneuploid phenotypes.

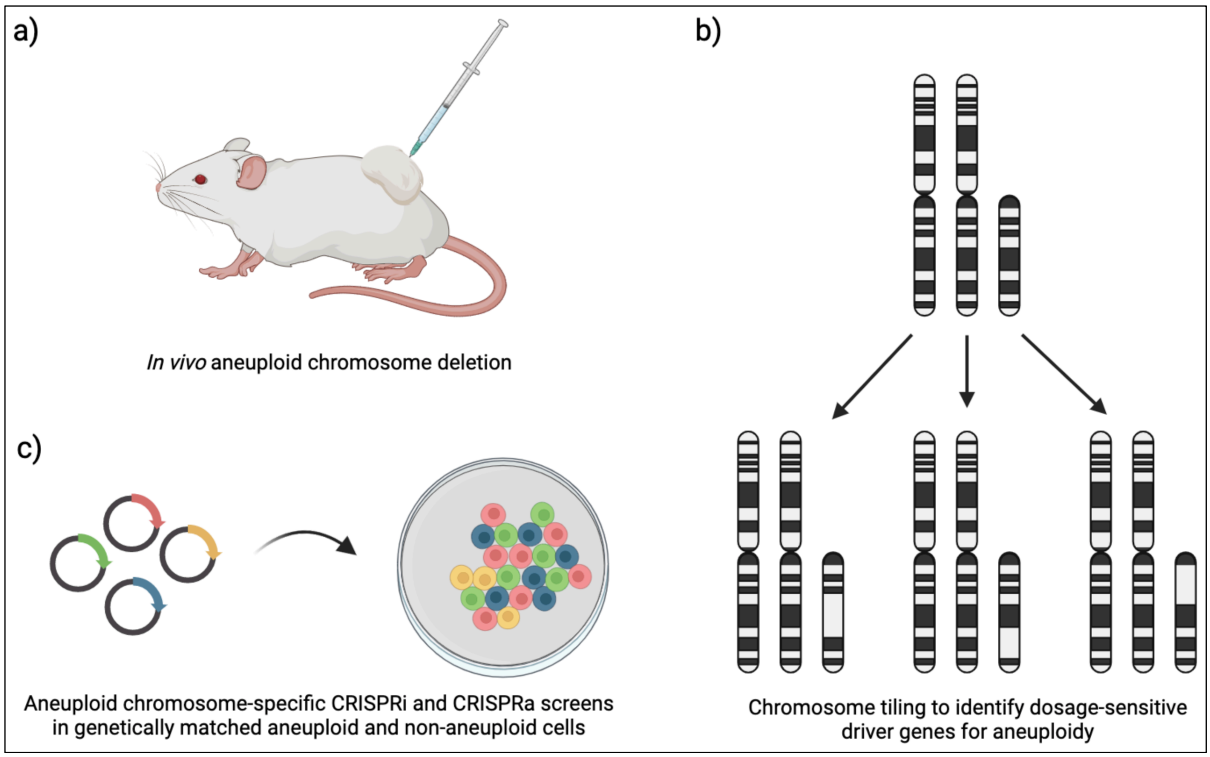

Figure 1: Future Methods to Study Aneuploidy in Cancer
a) Techniques like EPO-GEMM could allow *in vivo* chromosomal manipulation, which may be used to induce chromosome gain or loss at different stages of tumor development. b) Chromosome tiling using tools like MACHETE and ReDACT-NS could pinpoint subsets of genes present on aneuploid chromosomes driving their gain. Human artificial chromosomes and multi-gene overexpression constructs could be used to assess rescue of aneuploid phenotypes in non-aneuploid settings. c) Chromosome-specific libraries for CRISPR interference and activation could evaluate dosage-sensitive genes present on aneuploid chromosomes. Transcriptional downregulation in an aneuploid line would identify genes necessary for fitness. Transcriptional upregulation in a genetically-matched non-aneuploid line would identify genes sufficient for the aneuploid phenotype.

Aneuploidy Addiction: A Novel Clinically-Relevant Cancer Paradigm

In Chapter 2, we presented evidence to suggest recurrently observed aneuploidy may act in a similar manner to oncogenes, thereby introducing the idea of aneuploidy addiction. Below, I provide a brief history of the oncogene addiction paradigm, including early experiments and the subsequent expansion to include non-oncogene addiction. I also distinguish cancer dependencies from drivers, and by placing the results from Chapters 2 and 3 in that context, argue that aneuploidy not only represents a bona fide cancer dependency, but may also act as a driver.

Oncogene Addiction

Oncogene addiction as a paradigm was first introduced in 1997 to describe genes that act as nodes in the rewired molecular networks present in cancer cells (Weinstein et al. 1997), thereby rendering them exploitable targets in cancer therapy. It was shown that Cyclin D was frequently overexpressed in cancers (Weinstein et al. 1997), and antisense cDNA-mediated suppression of Cyclin D in esophageal (Zhou et al. 1995) or colon (Arber et al. 1997) cancer cells resulted in a loss of tumorigenicity. In contrast, ectopic overexpression of Cyclin D in esophageal (Weinstein et al. 1997) or mammary epithelial (Han et al. 1995) cell lines enhanced their malignant potential. These results combined suggested Cyclin D was a cancer addiction.

The proposal of oncogene addiction was motivated by the accumulating body of evidence that highlighted the heavy reliance cancers had on oncogenic mutants. The discovery of the elements driving the transforming potential of Rous sarcoma virus (RSV) in 1970 (Duesberg and Vogt 1970), and the subsequent identification of *SRC* as a homologous human gene (Stehelin et al. 1976), had introduced the concept of oncogenes. The discovery of oncogenic *MYC* and *RAS* followed (Vogt 2012). *c-MYC* expression in Burkitt's lymphoma was

found to be driven by an immunoglobulin enhancer (Dalla-Favera et al. 1982), and *MYCN* was shown to be amplified in neuroblastoma (Schwab et al. 1984). Meanwhile, *RAS* genes from human cancer cells were found to transform mouse bladder cells (Der et al. 1982; Parada et al. 1982), malignant activity of *KRAS* was found to be cancer-specific (Santos et al. 1984), and deletion of *KRAS* in colon cancer cells severely compromised malignancy (Shirasawa et al. 1993). This set the basic experimental design for identification of oncogenes: downregulation of their activity, either by deletion, chemical inhibition or genetic interference, caused a significant reduction in cancer malignancy (Weinstein and Joe 2006, 2008; Pagliarini et al. 2015). Meanwhile, increased expression, either ectopic or endogenous, potentiated malignancy.

A number of seminal studies establishing different oncogenes as addictions in diverse cancer backgrounds followed. These genes could serve as drivers and/or dependencies (see below) – introduction of their aberrant expression in non-malignant backgrounds resulted in oncogenic transformation, and suppression of their activity inflicted a significant fitness cost upon cancers (Weinstein and Joe 2006, 2008; Pagliarini et al. 2015). For example, conditional expression of *BCR-ABL* in a transgenic mouse model resulted in the development of lethal leukemia, whereas suppression of expression resulted in complete remission (Huettner et al. 2000). Meanwhile, breast cancer cells with *HER2* amplification were found to be more sensitive to its inhibition than cells without (Colomer et al. 1994); downregulation of ß-catenin resulted in remission in a mouse model of colon cancer (Verma et al. 2003); and genetic or chemical inhibition of $BRAF^{V600E}$ in melanoma cells either prevented tumor development if induced prior to tumor formation, or prevented further vascular development and enhanced apoptosis in pre-existing tumors (Sharma et al. 2005). These studies set the foundations for oncogene addiction-targeted therapies, which have since transformed clinical practice.

"Lineage addiction" is a related class of oncogene addictions that encompasses genes whose aberrant activity a specific cancer lineage relies on to maintain its lineage programming. For example, the differentiation and survival of melanocytes depends on signaling from the master transcriptional regulator *MITF*. Ectopic *MITF* expression in conjunction with the $BRAF^{V600E}$ mutation can transform primary melanocytes, and reduction of *MITF* activity can sensitize melanoma cells to chemotherapeutic agents (Garraway et al. 2005). Similarly, *FLT3* is a receptor tyrosine kinase that directs myeloid lineage maturation and is frequently mutated in acute myeloid leukemia, resulting in its factor-independent activation. Injection of cells transformed with mutant *Flt3* into syngeneic mice causes a leukemia-like syndrome, whereas disruption of kinase activity causes loss of transformation potential (Gilliland and Griffin 2002). Thus, cancers may adopt aberrant signaling of lineage-specifying regulators, in turn creating an addiction.

Non-Oncogene Addiction

The paradigm of cancer addiction was subsequently expanded to include non-oncogene addiction, thereby encompassing non-mutant proteins that serve rate-limiting steps in cellular pathways. As cancers could rely heavily on the normal cellular function of these genes, their inhibition could be equally as effective in disease treatment as oncogene targeting (Solimini et al. 2007). The concept was proposed in the context of reliance on *HSF-1* activity during tumorigenesis, knockdown of which reduced the viability of multiple cancer cell lines. In contrast, *HSF-1* knockdown in normal cells such as primary mammary epithelial cells and lung fibroblasts had a minimal impact on viability. Furthermore, in a model of skin carcinogenesis, $Hsf1^{(-/-)}$ mice were protected from tumors induced by *Ras* oncogene or *P53*

tumor suppressor mutagenesis in comparison to *Hsf-1*$^{(+/+)}$ littermates (Solimini et al. 2007). *HSF-1*'s regular cellular role therefore rendered it an addiction, but it was not an oncogene.

Numerous examples of non-oncogene addiction have since come to light. These span cellular pathways important for responding to DNA damage (Pilié et al. 2019), mitotic stress (Dominguez-Brauer et al. 2015), proteotoxic stress (Manasanch and Orlowski 2017), metabolic stress (Bader et al. 2020), hypoxia (Rey et al. 2017), autophagy/nutrient stress (Amaravadi et al. 2019), and angiogenesis (Zhao and Adjei 2015). Often, addiction to the non-oncogene is a result of synthetic lethality, whereby a tumor's unique genetic profile creates an increased reliance on non-mutated cellular pathways. For example, human and murine fibroblasts with deficiency in the Fanconi anemia pathway were shown to be reliant on ATM activity, and *FANCG* and *FANCC*-deficient pancreatic tumor cells were more sensitive to ATM inhibition than isogenic corrected cell lines (Kennedy et al. 2007). Similarly, *BRCA1* or *BRCA2* dysfunction results in a deficiency in homologous recombination, increasing the reliance on *PARP* activity to repair collapsed DNA replication forks and creating an acute sensitivity to *PARP* inhibition (Bryant et al. 2005; Farmer et al. 2005). Moreover, the frequency of *TP53* or *RB* mutation in tumors increases reliance on the *CHK1* kinase to maintain cell cycle arrest, allowing inhibition of *CHK1* to potentiate cytotoxicity of topoisomerase inhibitors and radiation in *TP53*-deficient but not in *TP53*-proficient cells of different tissue origins (Chen et al. 2006). Non-oncogene addictions therefore represent therapeutically-targetable cancer dependencies.

Driver or Dependency?

Both oncogene and non-oncogene addictions act as cancer dependencies, such that their genetic or chemical downregulation results in loss of cancer malignancy. These genes

are therefore *necessary* for the cancer phenotype. However, not all dependencies are drivers – inducing their aberrant expression in non-transformed cells is not *sufficient* for oncogenic transformation. In other words, driver oncogenes transform non-malignant cells into malignant ones, but once the malignancy is achieved, their continued activity may or may not be consequential to the cancer.

For example, $KRAS^{G12D}$ serves as both a driver and a dependency in pancreatic cancer: endogenous expression of $KRas^{G12D}$ in progenitor cells of the mouse pancreas induces ductal lesions that fully recapitulate pancreatic intraepithelial neoplasias (PanINs) which can spontaneously progress to invasive and metastatic adenocarcinomas (Hingorani et al. 2003). Meanwhile, inactivation of $KRas^{G12D}$ in lesions or established tumors results in regression (Ying et al. 2012).

In contrast, *ZFP64* is an example of a dependency but not a driver in acute myeloid and lymphoid leukemias that possess *MLL* translocations. *ZFP64* maintains *MLL* expression by binding to its promoter, making it essential for continued *MLL*-driven oncogenic and normal expression (Lu et al. 2018). However, *ZPF64* activity is not the driver for malignancy. Similarly, *OCA-T1* and *OCA-T2* are coactivators of *POU2F3* (Wu et al. 2022), which in turn is a master regulator of chemosensory lineage identity for tuft cells (Huang et al. 2018) – all three have been demonstrated as dependencies in the neuroendocrine^{low} lineage of small cell lunger cancer (SCLC), but not as drivers. Another example is the addiction of the squamous lineage of pancreatic ductal adenocarcinomas (PDA) to the Δ*Np63* isoform of *TP63*: introduction of the isoform into non-squamous PDA lines results in enhancer reprogramming to a squamous state and a powerful addiction to Δ*Np63* (Somerville et al. 2018). Of note, addiction to Δ*Np63* does not occur immediately in PDA models that are already malignant, suggesting Δ*Np63*-driven enhancer reprogramming collaborates with the existing mutational landscape to alter

disease dependency. Furthermore, it has been postulated that the ultimate result of gain-of-function mutations in *IDH1* and *IDH2* is the destabilization of the DNA methylome. Mutations in *IDH1* and *IDH2* appear to be clearly involved in initiating cancer but, because their mutation leads to the mutation of other cancer genes, may not be required for tumor maintenance (Figueroa et al. 2010). This in turn may explain the limited success of *IDH1* inhibitors in the clinic (Wouters 2021). Thus, there are a lot more cancer dependencies than drivers, and these dependencies offer an opportunity for therapeutic exploitation.

Broadly speaking, all non-oncogene addictions, and most oncogenes, therefore represent cancer dependencies. However, only a subset of oncogenes can act as drivers, whereby their aberrant expression in non-malignant contexts is sufficient for oncogenic transformation. This distinction is also important when discussing aneuploidy – we have demonstrated aneuploidy acts as a cancer dependency (Chapters 2 & 3). Whether aneuploidy is also a driver remains unclear. We presented a preliminary line of evidence suggesting this may be so: loss of trisomy 1q in untransformed breast epithelial cells hampers the transformation potential of $HRAS^{G12V}$ (Figure 2F-H). However, future investigations into the temporal order of aneuploidy acquisition and somatic mutation are needed to assess aneuploidy's ability to drive tumorigenesis.

Addiction-Targeting and Evasion of Therapy

Oncogene and non-oncogene addiction inherently represent cancer vulnerability, which has allowed the design of addiction-targeted therapeutic strategies. However, the selective pressure imposed by these therapies has resulted in the evolution of resistance mechanisms that can bypass suppression of the addiction and permit continued cancer growth. Often, these mechanisms include point mutations that prevent drug binding, or

upregulation of multi-drug efflux pumps that minimize drug uptake. In a significant percentage of cases, however, drug resistance can also be achieved by amplification of the drug target to rescue the gene dosage of the addiction. Examples include upregulation of *BCR-ABL* in imatinib-resistant chronic myeloid leukemia cells (Mahon et al. 2000; Gorre et al. 2001), copy number gain of $BRAF^{V600E}$ in melanoma patients treated with vemurafenib (Shi et al. 2012), and amplification of *ALK* in lung cancer patients treated with crizotinib (Katayama et al. 2012).

Similarly, drug resistance can also be achieved by amplification of genes in related cellular pathways. A distinct mechanism of resistance to $BRAF^{V600E}$ targeted therapy is upregulation of *PDGFRß* (Nazarian et al. 2010) or *MAPK3K8* (Johannessen et al. 2010). Meanwhile, resistance to crizotinib can also be caused by activation of *EFGR* or *KIT* (Katayama et al. 2012), and *HER2* (Takezawa et al. 2012) and *MET* (Engelman et al. 2007) amplification are both reported causes of resistance to *EGFR*-targeted therapy.

This highlights an obvious but understated point: cancers aren't addicted to the presence of oncogenic mutations, but rather to their expression. In other words, oncogene and non-oncogene addiction is reliant on the dosage of the addictions, and the effectiveness of addiction-targeted therapies is due to a reduction in gene dosage (i.e., through drug-induced inhibition of the targeted protein). Therefore, perhaps a more appropriate phrase for the phenomenon would be "dosage addiction."

Aneuploidy Addiction

Often, pre-clinical demonstration of oncogene addiction involves several key characteristics: the gene is aberrantly expressed in a significant fraction of patient tumors, downregulation of the gene in malignant models compromises malignancy, and increased

gene expression promotes malignancy, usually in cooperation with other mutations that predispose the model to malignancy. Furthermore, genetic or chemical inhibition of oncogene dosage exerts a selective pressure which results in re-amplification of dosage. The effects of gene downregulation can be observed through phenotypes such as reduction in tumorigenicity in mouse models, reduction in anchorage-independent growth, and decreased proliferation rate (Zhou et al. 1995; Arber et al. 1997; Aoki et al. 1997; Chin et al. 1999; Huettner et al. 2000; Verma et al. 2003). Meanwhile, gene upregulation or ectopic expression presents the opposite phenotypes: increased tumorigenicity in mouse models, higher anchorage-independent growth, and increased proliferative capacity (Weinstein et al. 1997; Han et al. 1995; Wang et al. 1994). As described above, if the addiction is a driver, it also has the capacity to transform non-malignant models into malignant ones. For example, conditional expression of *BCR-ABL* resulted in lethal leukemia (Huettner et al. 2000), and stable overexpression of Cyclin D1 in non-transformed esophageal (Zhou et al. 1995), colon (Arber et al. 1997), and embryonic fibroblasts (Han et al. 1995) enhanced growth and tumorigenicity.

In Chapters 2 & 3, we demonstrated aneuploidies represent a new class of cancer addictions, and termed the phenomenon *aneuploidy addiction*. The phenotypes observed upon aneuploidy-loss and gain, especially for aneuploidy of chromosome 1q, are identical to those observed with oncogene addictions. In Chapter 2, we showed that a significant fraction of cancers exhibits 1q aneuploidy (Figure 1D), and 1q amplification occurs early in tumor development (Figures 1A-C). Elimination of the aneuploid 1q chromosome resulted in a proportional reduction in gene dosage (Figure 1C), compromised tumorigenicity in xenograft models (Figure 1E), reduced anchorage-independent growth (Figure 1D), and hampered proliferative capacity (Figures 6E-F, S6). Furthermore, 1q aneuploidy may act as a driver since it enhanced the malignancy of non-transformed epithelial cells, as evidenced by increased

tumorigenic capacity (Figure 1H) and anchorage-independent growth (Figure 1G) of 1q-aneuploid cells in the presence of *HRAS*^{V12G} mutation. This also meant that elimination of the aneuploid chromosome resulted in a selective pressure to re-establish aneuploidy dosage through chromosome re-gain, as seen in both *in vitro* (Figure S12) and *in vivo* (Figures 4A-B, S11) models. Moreover, we identified one of potentially several dosage-sensitive genes encoded on chromosome 1q: *MDM4*. Reduction in *MDM4* dosage partially phenocopied loss of 1q aneuploidy (Figures 5I-M, S14E), and increase in *MDM4* dosage in a 1q disomy background partially rescued the 1q trisomy phenotype (Figures 5N, S14F). Lastly, we demonstrated that presence of the aneuploidy addiction created a chemically-exploitable vulnerability, whereby small-molecule induced downregulation of a rate-limiting enzyme encoded on chromosome 1q, *UCK2*, differentially affected 1q-aneuploid and isogenic non-aneuploid cells (Figures 6A, 6D-F).

Just as distinct oncogenes may play tumor-specific roles and require cooperative mutations to exert their full malignant potential, so too can distinct aneuploidies exert differential effects. Loss of chromosome 7p or 8q also resulted in loss of tumorigenicity (Figures 3D, 3H) and anchorage-independent growth (Figures 3C, 3G), but to a lesser degree than loss of chromosome 1q. Nevertheless, the pressure induced by triggering loss of the aneuploid chromosome selected for regain of those chromosomes (Figures 4D-F), or amplification of a secondary chromosome that could compensate for loss of the aneuploidy (Figures 4G-H).

These findings were further reinforced in Chapter 3. Trisomy 1q exhibited a clear competitive advantage over disomy 1q (Figure 1), and several other dosage-sensitive drivers were identified (Figure 2). In particular, *MCL1* was shown to be partially necessary and sufficient for the 1q aneuploid phenotype alongside *MDM4* (Figure 2b-d), suggesting

inhibition of apoptosis and downregulation of *TP53* signaling cooperatively drive 1q gain. Endogenous regain of 1q in disomy 1q clones fully rescued the 1q loss phenotype (Figure 3), indicating the importance of this trisomy and the selective advantage it confers. Moreover, loss of 8q in another colorectal cancer cell line supplemented earlier observations, and highlighted the generality of the aneuploidy loss phenomenon (Figure 4). The magnitude of growth defect observed upon aneuploidy loss was also found to exceed the fitness deficit conferred by deletion of a driver oncogene (Figure 5), further emphasizing aneuploidy addiction as a crucial feature of human cancers.

These results combined suggest cancer addiction to recurrently observed aneuploidies represents a bona fide dependency analogous to oncogene, and to a lesser extent non-oncogene, addictions. This body of work is therefore an important advancement in the fundamental understanding of cancer genomes. Future studies will help evaluate the applicability of aneuploidy addiction as a phenomenon across distinct cancer contexts, and assess both the developmental contribution of aneuploid chromosomes as well as their potential to drive tumorigenesis. Ultimately, this will enable discovery of novel aneuploid biomarkers that facilitate improved combination therapies and significantly enhance patient outcomes.

In sum, I hope this thesis effectively communicates not only the profound impact of aneuploidy on cancer genomes, but also the need for further investigation to uncover the molecular underpinnings of this phenomenon.

References

Adell MAY, Klockner TC, Höfler R, Wallner L, Schmid J, Markovic A, Martyniak A, Campbell CS. 2022. *Adaptation to spindle assembly checkpoint inhibition through the selection of specific aneuploidies*. Cell Biology http://biorxiv.org/lookup/doi/10.1101/2022.10.04.510607 (Accessed January 23, 2023).

Amaravadi RK, Kimmelman AC, Debnath J. 2019. Targeting Autophagy in Cancer: Recent Advances and Future Directions. *Cancer Discov* **9**: 1167–1181.

Andrews PA, Iossifov I, Kendall J, Marks S, Muthuswamy L, Wang Z, Levy D, Wigler M. 2016. MUMdex: MUM-based structural variation detection. *bioRxiv* 078261.

Aoki K, Yoshida T, Matsumoto N, Ide H, Sugimura T, Terada M. 1997. Suppression of Ki-ras p21 levels leading to growth inhibition of pancreatic cancer cell lines with Ki-ras mutation but not those without Ki-ras mutation. *Mol Carcinog* **20**: 251–258.

Arber N, Doki Y, Han EK, Sgambato A, Zhou P, Kim NH, Delohery T, Klein MG, Holt PR, Weinstein IB. 1997. Antisense to cyclin D1 inhibits the growth and tumorigenicity of human colon cancer cells. *Cancer Res* **57**: 1569–1574.

Azzalini A, Menardi G. 2014. Clustering via Nonparametric Density Estimation: The R Package pdfCluster. *J Stat Softw* **57**: 1–26.

Bader JE, Voss K, Rathmell JC. 2020. Targeting Metabolism to Improve the Tumor Microenvironment for Cancer Immunotherapy. *Mol Cell* **78**: 1019–1033.

Baker DJ, Jin F, Jeganathan KB, van Deursen JM. 2009. Whole Chromosome Instability Caused by Bub1 Insufficiency Drives Tumorigenesis through Tumor Suppressor Gene Loss of Heterozygosity. *Cancer Cell* **16**: 475–486.

Bakhoum SF, Cantley LC. 2018. The Multifaceted Role of Chromosomal Instability in Cancer and Its Microenvironment. *Cell* **174**: 1347–1360.

Bakhoum SF, Ngo B, Laughney AM, Cavallo J-A, Murphy CJ, Ly P, Shah P, Sriram RK, Watkins TBK, Taunk NK, et al. 2018. Chromosomal instability drives metastasis through a cytosolic DNA response. *Nature* **553**: 467–472.

Barretina J, Caponigro G, Stransky N, Venkatesan K, Margolin AA, Kim S, Wilson CJ, Lehár J, Kryukov GV, Sonkin D, et al. 2012. The Cancer Cell Line Encyclopedia enables predictive modelling of anticancer drug sensitivity. *Nature* **483**: 603–607.

Barriga FM, Tsanov KM, Ho Y-J, Sohail N, Zhang A, Baslan T, Wuest AN, Del Priore I, Meškauskaitė B, Livshits G, et al. 2022. MACHETE identifies interferon-encompassing

chromosome 9p21.3 deletions as mediators of immune evasion and metastasis. *Nat Cancer*. https://www.nature.com/articles/s43018-022-00443-5 (Accessed November 18, 2022).

Behan FM, Iorio F, Picco G, Gonçalves E, Beaver CM, Migliardi G, Santos R, Rao Y, Sassi F, Pinnelli M, et al. 2019. Prioritization of cancer therapeutic targets using CRISPR–Cas9 screens. *Nature* **568**: 511–516.

Bendall SC, Nolan GP. 2012. From single cells to deep phenotypes in cancer. *Nat Biotechnol* **30**: 639–647.

Ben-David U, Amon A. 2020. Context is everything: aneuploidy in cancer. *Nat Rev Genet* **21**: 44–62.

Beroukhim R, Mermel CH, Porter D, Wei G, Raychaudhuri S, Donovan J, Barretina J, Boehm JS, Dobson J, Urashima M, et al. 2010. The landscape of somatic copy-number alteration across human cancers. *Nature* **463**: 899–905.

Bi WL, Horowitz P, Greenwald NF, Abedalthagafi M, Agarwalla PK, Gibson WJ, Mei Y, Schumacher SE, Ben-David U, Chevalier A, et al. 2017. Landscape of Genomic Alterations in Pituitary Adenomas. *Clin Cancer Res* **23**: 1841–1851.

Bielski CM, Zehir A, Penson AV, Donoghue MTA, Chatila W, Armenia J, Chang MT, Schram AM, Jonsson P, Bandlamudi C, et al. 2018. Genome doubling shapes the evolution and prognosis of advanced cancers. *Nat Genet* **50**: 1189–1195.

Bignold L, Coghlan B, Jersmann H. 2006. Hansemann, Boveri, chromosomes and the gametogenesis-related theories of tumours. *Cell Biol Int* **30**: 640–644.

Bister K. 2015. Discovery of oncogenes: The advent of molecular cancer research. *Proc Natl Acad Sci U S A* **112**: 15259–15260.

Bomme L, Bardi G, Pandis N, Fenger C, Kronborg O, Heim S. 1994. Clonal karyotypic abnormalities in colorectal adenomas: Clues to the early genetic events in the adenoma-carcinoma sequence. *Genes Chromosomes Cancer* **10**: 190–196.

Bosco N, Goldberg A, Johnson AF, Zhao X, Mays JC, Cheng P, Bianchi JJ, Toscani C, Katsnelson L, Annuar D, et al. 2022. *KaryoCreate: a new CRISPR-based technology to generate chromosome-specific aneuploidy by targeting human centromeres*. Cell Biology http://biorxiv.org/lookup/doi/10.1101/2022.09.27.509580 (Accessed November 18, 2022).

Boveri T. 2008. Concerning the Origin of Malignant Tumours by Theodor Boveri. Translated and annotated by Henry Harris. *J Cell Sci* **121**: 1–84.

Brauweiler A, Lorick KL, Lee JP, Tsai YC, Chan D, Weissman AM, Drabkin HA, Gemmill RM. 2007. RING-dependent tumor suppression and G2/M arrest induced by the TRC8 hereditary kidney cancer gene. *Oncogene* **26**: 2263–2271.

Brembeck FH, Wiese M, Zatula N, Grigoryan T, Dai Y, Fritzmann J, Birchmeier W. 2011. BCL9-2 Promotes Early Stages of Intestinal Tumor Progression. *Gastroenterology* **141**: 1359-1370.e3.

Bruderer R, Bernhardt OM, Gandhi T, Miladinović SM, Cheng L-Y, Messner S, Ehrenberger T, Zanotelli V, Butscheid Y, Escher C, et al. 2015. Extending the limits of quantitative proteome profiling with data-independent acquisition and application to acetaminophen-treated three-dimensional liver microtissues. *Mol Cell Proteomics MCP* **14**: 1400–1410.

Bruderer R, Bernhardt OM, Gandhi T, Xuan Y, Sondermann J, Schmidt M, Gomez-Varela D, Reiter L. 2017. Optimization of Experimental Parameters in Data-Independent Mass Spectrometry Significantly Increases Depth and Reproducibility of Results. *Mol Cell Proteomics MCP* **16**: 2296–2309.

Bruderer R, Muntel J, Müller S, Bernhardt OM, Gandhi T, Cominetti O, Macron C, Carayol J, Rinner O, Astrup A, et al. 2019. Analysis of 1508 Plasma Samples by Capillary-Flow Data-Independent Acquisition Profiles Proteomics of Weight Loss and Maintenance. *Mol Cell Proteomics MCP* **18**: 1242–1254.

Bryant HE, Schultz N, Thomas HD, Parker KM, Flower D, Lopez E, Kyle S, Meuth M, Curtin NJ, Helleday T. 2005. Specific killing of BRCA2-deficient tumours with inhibitors of poly(ADP-ribose) polymerase. *Nature* **434**: 913–917.

Bunz F, Dutriaux A, Lengauer C, Waldman T, Zhou S, Brown JP, Sedivy JM, Kinzler KW, Vogelstein B. 1998. Requirement for p53 and p21 to sustain G2 arrest after DNA damage. *Science* **282**: 1497–1501.

Burgess MR, Hwang E, Mroue R, Bielski CM, Wandler AM, Huang BJ, Firestone AJ, Young A, Lacap JA, Crocker L, et al. 2017. KRAS Allelic Imbalance Enhances Fitness and Modulates MAP Kinase Dependence in Cancer. *Cell* **168**: 817-829.e15.

Cai M-J, Cui Y, Fang M, Wang Q, Zhang A-J, Kuai J-H, Pang F, Cui X-D. 2019. Inhibition of PSMD4 blocks the tumorigenesis of hepatocellular carcinoma. *Gene* **702**: 66–74.

Cai Y, Crowther J, Pastor T, Abbasi Asbagh L, Baietti MF, De Troyer M, Vazquez I, Talebi A, Renzi F, Dehairs J, et al. 2016. Loss of Chromosome 8p Governs Tumor Progression and Drug Response by Altering Lipid Metabolism. *Cancer Cell* **29**: 751–766.

Cairncross G, Wang M, Shaw E, Jenkins R, Brachman D, Buckner J, Fink K, Souhami L, Laperriere N, Curran W, et al. 2013. Phase III Trial of Chemoradiotherapy for

Anaplastic Oligodendroglioma: Long-Term Results of RTOG 9402. *J Clin Oncol* **31**: 337–343.

Campbell MS, Chan GK, Yen TJ. 2001. Mitotic checkpoint proteins HsMAD1 and HsMAD2 are associated with nuclear pore complexes in interphase. *J Cell Sci* **114**: 953–963.

Chang K, Marran K, Valentine A, Hannon GJ. 2013. Packaging shRNA retroviruses. *Cold Spring Harb Protoc* **2013**: 734–737.

Chapman PB, Hauschild A, Robert C, Haanen JB, Ascierto P, Larkin J, Dummer R, Garbe C, Testori A, Maio M, et al. 2011. Improved Survival with Vemurafenib in Melanoma with BRAF V600E Mutation. *N Engl J Med* **364**: 2507–2516.

Chen Z, Xiao Z, Gu W, Xue J, Bui MH, Kovar P, Li G, Wang G, Tao Z-F, Tong Y, et al. 2006. Selective Chk1 inhibitors differentially sensitize p53-deficient cancer cells to cancer therapeutics. *Int J Cancer* **119**: 2784–2794.

Chiarella AM, Butler KV, Gryder BE, Lu D, Wang TA, Yu X, Pomella S, Khan J, Jin J, Hathaway NA. 2020. Dose-dependent activation of gene expression is achieved using CRISPR and small molecules that recruit endogenous chromatin machinery. *Nat Biotechnol* **38**: 50–55.

Chiarugi P, Giannoni E. 2008. Anoikis: A necessary death program for anchorage-dependent cells. *Biochem Pharmacol* **76**: 1352–1364.

Chin L, Tam A, Pomerantz J, Wong M, Holash J, Bardeesy N, Shen Q, O'Hagan R, Pantginis J, Zhou H, et al. 1999. Essential role for oncogenic Ras in tumour maintenance. *Nature* **400**: 468–472.

Choi E, Zhang X, Xing C, Yu H. 2016. Mitotic Checkpoint Regulators Control Insulin Signaling and Metabolic Homeostasis. *Cell* **166**: 567–581.

Chunduri NK, Storchová Z. 2019. The diverse consequences of aneuploidy. *Nat Cell Biol* **21**: 54–62.

Cimini D, Tanzarella C, Degrassi F. 1999. Differences in malsegregation rates obtained by scoring ana-telophases or binucleate cells. *Mutagenesis* **14**: 563–568.

Cisowski J, Bergo MO. 2017. What makes oncogenes mutually exclusive? *Small GTPases* **8**: 187–192.

Clarke DJ, Giménez-Abián JF, Tönnies H, Neitzel H, Sperling K, Downes CS, Johnson RT. 1998. Creation of monosomic derivatives of human cultured cell lines. *Proc Natl Acad Sci* **95**: 167–171.

Cohen-Sharir Y, McFarland JM, Abdusamad M, Marquis C, Bernhard SV, Kazachkova M, Tang H, Ippolito MR, Laue K, Zerbib J, et al. 2021. Aneuploidy renders cancer cells vulnerable to mitotic checkpoint inhibition. *Nature* **590**: 486–491.

Collins BC, Hunter CL, Liu Y, Schilling B, Rosenberger G, Bader SL, Chan DW, Gibson BW, Gingras A-C, Held JM, et al. 2017. Multi-laboratory assessment of reproducibility, qualitative and quantitative performance of SWATH-mass spectrometry. *Nat Commun* **8**: 291.

Colomer R, Lupu R, Bacus S, Gelmann E. 1994. erbB-2 antisense oligonucleotides inhibit the proliferation of breast carcinoma cells with erbB-2 oncogene amplification. *Br J Cancer* **70**: 819–825.

Cong L, Ran FA, Cox D, Lin S, Barretto R, Habib N, Hsu PD, Wu X, Jiang W, Marraffini LA, et al. 2013. Multiplex Genome Engineering Using CRISPR/Cas Systems. *Science* **339**: 819–823.

Cuneo A, Bigoni R, Roberti MG, Bardi A, Rigolin GM, Piva N, Mancini M, Nanni M, Alimena G, Mecucci C, et al. 1998. Detection and monitoring of trisomy 8 by fluorescence in situ hybridization in acute myeloid leukemia: a multicentric study. *Haematologica* **83**: 21–26.

Dalla-Favera R, Bregni M, Erikson J, Patterson D, Gallo RC, Croce CM. 1982. Human c-myc onc gene is located on the region of chromosome 8 that is translocated in Burkitt lymphoma cells. *Proc Natl Acad Sci* **79**: 7824–7827.

Danovi D, Meulmeester E, Pasini D, Migliorini D, Capra M, Frenk R, de Graaf P, Francoz S, Gasparini P, Gobbi A, et al. 2004. Amplification of Mdmx (or Mdm4) Directly Contributes to Tumor Formation by Inhibiting p53 Tumor Suppressor Activity. *Mol Cell Biol* **24**: 5835–5843.

Davoli T, Uno H, Wooten EC, Elledge SJ. 2017. Tumor aneuploidy correlates with markers of immune evasion and with reduced response to immunotherapy. *Science* **355**: eaaf8399.

Davoli T, Xu AW, Mengwasser KE, Sack LM, Yoon JC, Park PJ, Elledge SJ. 2013. Cumulative Haploinsufficiency and Triplosensitivity Drive Aneuploidy Patterns and Shape the Cancer Genome. *Cell* **155**: 948–962.

Der CJ, Krontiris TG, Cooper GM. 1982. Transforming genes of human bladder and lung carcinoma cell lines are homologous to the ras genes of Harvey and Kirsten sarcoma viruses. *Proc Natl Acad Sci* **79**: 3637–3640.

Di Tommaso P, Chatzou M, Floden EW, Barja PP, Palumbo E, Notredame C. 2017. Nextflow enables reproducible computational workflows. *Nat Biotechnol* **35**: 316–319.

Dieken ES, Fournier REK. 1996. Homologous Modification of Human Chromosomal Genes in Chicken B-Cell × Human Microcell Hybrids. *Methods* **9**: 56–63.

Doherty AMO, Fisher EMC. 2003. Microcell-mediated chromosome transfer (MMCT): small cells with huge potential. *Mamm Genome* **14**: 583–592.

Dominguez-Brauer C, Thu KL, Mason JM, Blaser H, Bray MR, Mak TW. 2015. Targeting Mitosis in Cancer: Emerging Strategies. *Mol Cell* **60**: 524–536.

Donnelly N, Passerini V, Dürrbaum M, Stingele S, Storchová Z. 2014. HSF1 deficiency and impaired HSP90-dependent protein folding are hallmarks of aneuploid human cells. *EMBO J* **33**: 2374–2387.

Donnelly N, Storchová Z. 2015. Aneuploidy and proteotoxic stress in cancer. *Mol Cell Oncol* **2**: e976491.

Duesberg PH, Vogt PK. 1970. Differences between the Ribonucleic Acids of Transforming and Nontransforming Avian Tumor Viruses. *Proc Natl Acad Sci* **67**: 1673–1680.

Dutrillaux B, Gerbault-Seureau M, Zafrani B. 1990. Characterization of chromosomal anomalies in human breast cancer. *Cancer Genet Cytogenet* **49**: 203–217.

Ege T, Ringertz NR. 1974. Preparation of microcells by enucleation of micronucleate cells. *Exp Cell Res* **87**: 378–382.

Eggenschwiler R, Moslem M, Fráguas MS, Galla M, Papp O, Naujock M, Fonfara I, Gensch I, Wähner A, Beh-Pajooh A, et al. 2016. Improved bi-allelic modification of a transcriptionally silent locus in patient-derived iPSC by Cas9 nickase. *Sci Rep* **6**: 38198.

El Tekle G, Bernasocchi T, Unni AM, Bertoni F, Rossi D, Rubin MA, Theurillat J-P. 2021. Co-occurrence and mutual exclusivity: what cross-cancer mutation patterns can tell us. *Trends Cancer* **7**: 823–836.

Engelman JA, Zejnullahu K, Mitsudomi T, Song Y, Hyland C, Park JO, Lindeman N, Gale C-M, Zhao X, Christensen J, et al. 2007. *MET* Amplification Leads to Gefitinib Resistance in Lung Cancer by Activating ERBB3 Signaling. *Science* **316**: 1039–1043.

Farmer H, McCabe N, Lord CJ, Tutt ANJ, Johnson DA, Richardson TB, Santarosa M, Dillon KJ, Hickson I, Knights C, et al. 2005. Targeting the DNA repair defect in BRCA mutant cells as a therapeutic strategy. *Nature* **434**: 917–921.

Fedick A, Jalas C, Treff NR. 2014. A deleterious mutation in the *PEX2* gene causes Zellweger syndrome in individuals of Ashkenazi Jewish descent: A deleterious mutation in the *PEX2* gene. *Clin Genet* **85**: 343–346.

Figueroa ME, Abdel-Wahab O, Lu C, Ward PS, Patel J, Shih A, Li Y, Bhagwat N, Vasanthakumar A, Fernandez HF, et al. 2010. Leukemic IDH1 and IDH2 Mutations Result in a Hypermethylation Phenotype, Disrupt TET2 Function, and Impair Hematopoietic Differentiation. *Cancer Cell* **18**: 553–567.

Fillat C, Carrio M, Cascante A, Sangro B. 2003. Suicide Gene Therapy Mediated by the Herpes Simplex Virus Thymidine Kinase Gene / Ganciclovir System: Fifteen Years of Application. *Curr Gene Ther* **3**: 13–26.

Fischer M. 2017. Census and evaluation of p53 target genes. *Oncogene* **36**: 3943–3956.

Fito-Lopez B, Salvadores M, Alvarez M-M, Supek F. 2022. Prevalence, causes and impact of TP53-loss phenocopying events in human tumors. 2022.11.01.514743. https://www.biorxiv.org/content/10.1101/2022.11.01.514743v1 (Accessed November 20, 2022).

Fournier RE, Ruddle FH. 1977. Microcell-mediated transfer of murine chromosomes into mouse, Chinese hamster, and human somatic cells. *Proc Natl Acad Sci* **74**: 319–323.

Frankish A, Diekhans M, Ferreira A-M, Johnson R, Jungreis I, Loveland J, Mudge JM, Sisu C, Wright J, Armstrong J, et al. 2019. GENCODE reference annotation for the human and mouse genomes. *Nucleic Acids Res* **47**: D766–D773.

Freedman V. 1974. Cellular tumorigenicity in nude mice: Correlation with cell growth in semi-solid medium. *Cell* **3**: 355–359.

Frisch SM, Screaton RA. 2001. Anoikis mechanisms. *Curr Opin Cell Biol* **13**: 555–562.

Fu Y, Wei X, Guo L, Wu K, Le J, Ma Y, Kong X, Tong Y, Wu H. 2022. The Metabolic and Non-Metabolic Roles of UCK2 in Tumor Progression. *Front Oncol* **12**: 904887.

Fulco CP, Munschauer M, Anyoha R, Munson G, Grossman SR, Perez EM, Kane M, Cleary B, Lander ES, Engreitz JM. 2016. Systematic mapping of functional enhancer–promoter connections with CRISPR interference. *Science* **354**: 769–773.

Gao J, Aksoy BA, Dogrusoz U, Dresdner G, Gross B, Sumer SO, Sun Y, Jacobsen A, Sinha R, Larsson E, et al. 2013. Integrative Analysis of Complex Cancer Genomics and Clinical Profiles Using the cBioPortal. *Sci Signal* **6**: pl1.

Garraway LA, Widlund HR, Rubin MA, Getz G, Berger AJ, Ramaswamy S, Beroukhim R, Milner DA, Granter SR, Du J, et al. 2005. Integrative genomic analyses identify MITF as a lineage survival oncogene amplified in malignant melanoma. *Nature* **436**: 117–122.

Ghandi M, Huang FW, Jané-Valbuena J, Kryukov GV, Lo CC, McDonald ER, Barretina J, Gelfand ET, Bielski CM, Li H, et al. 2019. Next-generation characterization of the Cancer Cell Line Encyclopedia. *Nature* **569**: 503–508.

Gilbert LA, Horlbeck MA, Adamson B, Villalta JE, Chen Y, Whitehead EH, Guimaraes C, Panning B, Ploegh HL, Bassik MC, et al. 2014. Genome-Scale CRISPR-Mediated Control of Gene Repression and Activation. *Cell* **159**: 647–661.

Gilbert LA, Larson MH, Morsut L, Liu Z, Brar GA, Torres SE, Stern-Ginossar N, Brandman O, Whitehead EH, Doudna JA, et al. 2013. CRISPR-Mediated Modular RNA-Guided Regulation of Transcription in Eukaryotes. *Cell* **154**: 442–451.

Gilliland DG, Griffin JD. 2002. Role of FLT3 in leukemia: *Curr Opin Hematol* **9**: 274–281.

Girish V, Lakhani AA, Scaduto CM, Thompson SL, Brown LM, Hagenson RA, Sausville EL, Mendelson BE, Lukow DA, Yuan ML, et al. 2023. *Oncogene-like addiction to aneuploidy in human cancers*. Cancer Biology http://biorxiv.org/lookup/doi/10.1101/2023.01.09.523344 (Accessed January 12, 2023).

Girish V, Sheltzer JM. 2020. A CRISPR Competition Assay to Identify Cancer Genetic Dependencies. *Bio-Protoc* **10**: e3682–e3682.

Giuliano CJ, Lin A, Girish V, Sheltzer JM. 2019. Generating Single Cell–Derived Knockout Clones in Mammalian Cells with CRISPR/Cas9. *Curr Protoc Mol Biol* **128**: e100.

Gorden A, Osman I, Gai W, He D, Huang W, Davidson A, Houghton AN, Busam K, Polsky D. 2003. Analysis of BRAF and N-RAS Mutations in Metastatic Melanoma Tissues. *Cancer Res* **63**: 3955–3957.

Gordon DJ, Resio B, Pellman D. 2012. Causes and consequences of aneuploidy in cancer. *Nat Rev Genet* **13**: 189–203.

Gorre ME, Mohammed M, Ellwood K, Hsu N, Paquette R, Rao PN, Sawyers CL. 2001. Clinical Resistance to STI-571 Cancer Therapy Caused by BCR-ABL Gene Mutation or Amplification. *Science* **293**: 876–880.

Hamburger AW, Salmon SE. 1977. Primary bioassay of human tumor stem cells. *Science* **197**: 461–463.

Han EK, Sgambato A, Jiang W, Zhang YJ, Santella RM, Doki Y, Cacace AM, Schieren I, Weinstein IB. 1995. Stable overexpression of cyclin D1 in a human mammary epithelial cell line prolongs the S-phase and inhibits growth. *Oncogene* **10**: 953–961.

Hannon GJ, Rossi JJ. 2004. Unlocking the potential of the human genome with RNA interference. *Nature* **431**: 371–378.

Hansemann D. 1890. Ueber asymmetrische Zelltheilung in Epithelkrebsen und deren biologische Bedeutung. *Arch Für Pathol Anat Physiol Für Klin Med* **119**: 299–326.

Hardy PA, Zacharias H. 2005. Reappraisal of the Hansemann-Boveri hypothesis on the origin of tumors. *Cell Biol Int* **29**: 983–992.

Hasle H, Friedman JM, Olsen JH, Rasmussen SA. 2016. Low risk of solid tumors in persons with Down syndrome. *Genet Med* **18**: 1151–1157.

Hayward NK, Wilmott JS, Waddell N, Johansson PA, Field MA, Nones K, Patch A-M, Kakavand H, Alexandrov LB, Burke H, et al. 2017. Whole-genome landscapes of major melanoma subtypes. *Nature* **545**: 175–180.

Heselmeyer K, Macville M, Schröck E, Blegen H, Hellström A-C, Shah K, Auer G, Ried T. 1997. Advanced-stage cervical carcinomas are defined by a recurrent pattern of chromosomal aberrations revealing high genetic instability and a consistent gain of chromosome arm 3q. *Genes Chromosomes Cancer* **19**: 233–240.

Heselmeyer K, Schrock E, du Manoir S, Blegen H, Shah K, Steinbeck R, Auer G, Ried T. 1996. Gain of chromosome 3q defines the transition from severe dysplasia to invasive carcinoma of the uterine cervix. *Proc Natl Acad Sci* **93**: 479–484.

Hieronymus H, Murali R, Tin A, Yadav K, Abida W, Moller H, Berney D, Scher H, Carver B, Scardino P, et al. 2018. Tumor copy number alteration burden is a pan-cancer prognostic factor associated with recurrence and death eds. M.R. Green, J. Settleman, C. Abate-Shen, and M.A. Rubin. *eLife* **7**: e37294.

Hingorani SR, Petricoin EF, Maitra A, Rajapakse V, King C, Jacobetz MA, Ross S, Conrads TP, Veenstra TD, Hitt BA, et al. 2003. Preinvasive and invasive ductal pancreatic cancer and its early detection in the mouse. *Cancer Cell* **4**: 437–450.

Horibata S, Vo TV, Subramanian V, Thompson PR, Coonrod SA. 2015. Utilization of the Soft Agar Colony Formation Assay to Identify Inhibitors of Tumorigenicity in Breast Cancer Cells. *J Vis Exp* 52727.

Horlbeck MA, Gilbert LA, Villalta JE, Adamson B, Pak RA, Chen Y, Fields AP, Park CY, Corn JE, Kampmann M, et al. 2016. Compact and highly active next-generation libraries for CRISPR-mediated gene repression and activation. *eLife* **5**: e19760.

Hu X, Zhang Z. 2016. Understanding the Genetic Mechanisms of Cancer Drug Resistance Using Genomic Approaches. *Trends Genet* **32**: 127–137.

Huang Y-H, Klingbeil O, He X-Y, Wu XS, Arun G, Lu B, Somerville TDD, Milazzo JP, Wilkinson JE, Demerdash OE, et al. 2018. POU2F3 is a master regulator of a tuft cell-like variant of small cell lung cancer. *Genes Dev* **32**: 915–928.

Huettner CS, Zhang P, Van Etten RA, Tenen DG. 2000. Reversibility of acute B-cell leukaemia induced by BCR–ABL1. *Nat Genet* **24**: 57–60.

Hung J. 1995. Allele-Specific Chromosome 3p Deletions Occur at an Early Stage in the Pathogenesis of Lung Carcinoma. *JAMA J Am Med Assoc* **273**: 558.

Hwang S, Williams JF, Kneissig M, Lioudyno M, Rivera I, Helguera P, Busciglio J, Storchova Z, King MC, Torres EM. 2019. Suppressing Aneuploidy-Associated Phenotypes Improves the Fitness of Trisomy 21 Cells. *Cell Rep* **29**: 2473-2488.e5.

Inoue J, Mitsuya K, Maegawa S, Kugoh H, Kadota M, Okamura D, Shinohara T, Nishihara S, Takehara S, Yamauchi K, et al. 2001. Construction of 700 human/mouse A9 monochromosomal hybrids and analysis of imprinted genes on human chromosome 6. *J Hum Genet* **46**: 137–145.

Ippolito MR, Martis V, Martin S, Tijhuis AE, Hong C, Wardenaar R, Dumont M, Zerbib J, Spierings DCJ, Fachinetti D, et al. 2021. Gene copy-number changes and chromosomal instability induced by aneuploidy confer resistance to chemotherapy. *Dev Cell* **56**: 2440-2454.e6.

Irion S, Luche H, Gadue P, Fehling HJ, Kennedy M, Keller G. 2007. Identification and targeting of the ROSA26 locus in human embryonic stem cells. *Nat Biotechnol* **25**: 1477–1482.

Janssen A, Kops GJPL, Medema RH. 2009. Elevating the frequency of chromosome mis-segregation as a strategy to kill tumor cells. *Proc Natl Acad Sci* **106**: 19108–19113.

Johannessen CM, Boehm JS, Kim SY, Thomas SR, Wardwell L, Johnson LA, Emery CM, Stransky N, Cogdill AP, Barretina J, et al. 2010. COT drives resistance to RAF inhibition through MAP kinase pathway reactivation. *Nature* **468**: 968–972.

Joung J, Kirchgatterer PC, Singh A, Cho JH, Nety SP, Larson RC, Macrae RK, Deasy R, Tseng Y-Y, Maus MV, et al. 2022. CRISPR activation screen identifies BCL-2 proteins and B3GNT2 as drivers of cancer resistance to T cell-mediated cytotoxicity. *Nat Commun* **13**: 1606.

Karni-Schmidt O, Lokshin M, Prives C. 2016. The Roles of MDM2 and MDMX in Cancer. *Annu Rev Pathol Mech Dis* **11**: 617–644.

Katayama R, Shaw AT, Khan TM, Mino-Kenudson M, Solomon BJ, Halmos B, Jessop NA, Wain JC, Yeo AT, Benes C, et al. 2012. Mechanisms of Acquired Crizotinib Resistance in ALK-Rearranged Lung Cancers. *Sci Transl Med* **4**. https://www.science.org/doi/10.1126/scitranslmed.3003316 (Accessed December 20, 2022).

Kawazu M, Kojima S, Ueno T, Totoki Y, Nakamura H, Kunita A, Qu W, Yoshimura J, Soda M, Yasuda T, et al. 2017. Integrative analysis of genomic alterations in triple-negative breast cancer in association with homologous recombination deficiency. *PLoS Genet* **13**: e1006853.

Keith CT, Borisy AA, Stockwell BR. 2005. Multicomponent therapeutics for networked systems. *Nat Rev Drug Discov* **4**: 71–78.

Kennedy RD, Chen CC, Stuckert P, Archila EM, De la Vega MA, Moreau LA, Shimamura A, D'Andrea AD. 2007. Fanconi anemia pathway–deficient tumor cells are hypersensitive to inhibition of ataxia telangiectasia mutated. *J Clin Invest* **117**: 1440–1449.

Kernohan KD, Tétreault M, Liwak-Muir U, Geraghty MT, Qin W, Venkateswaran S, Davila J, Care4Rare Canada Consortium, Holcik M, Majewski J, et al. 2015. Homozygous mutation in the eukaryotic translation initiation factor 2alpha phosphatase gene, *PPP1R15B* , is associated with severe microcephaly, short stature and intellectual disability. *Hum Mol Genet* **24**: 6293–6300.

Kimura M, Cao X, Skurnick J, Cody M, Soteropoulos P, Aviv A. 2005. Proliferation dynamics in cultured skin fibroblasts from Down syndrome subjects. *Free Radic Biol Med* **39**: 374–380.

Klann TS, Black JB, Chellappan M, Safi A, Song L, Hilton IB, Crawford GE, Reddy TE, Gersbach CA. 2017. CRISPR–Cas9 epigenome editing enables high-throughput screening for functional regulatory elements in the human genome. *Nat Biotechnol* **35**: 561–568.

Kluesner MG, Nedveck DA, Lahr WS, Garbe JR, Abrahante JE, Webber BR, Moriarity BS. 2018. EditR: A Method to Quantify Base Editing from Sanger Sequencing. *CRISPR J* **1**: 239–250.

Kneissig M, Keuper K, de Pagter MS, van Roosmalen MJ, Martin J, Otto H, Passerini V, Campos Sparr A, Renkens I, Kropveld F, et al. 2019. Micronuclei-based model system reveals functional consequences of chromothripsis in human cells. *eLife* **8**: e50292.

Knouse KA, Davoli T, Elledge SJ, Amon A. 2017. Aneuploidy in Cancer: Seq-ing Answers to Old Questions. *Annu Rev Cancer Biol* **1**: 335–354.

Kotschy A, Szlavik Z, Murray J, Davidson J, Maragno AL, Le Toumelin-Braizat G, Chanrion M, Kelly GL, Gong J-N, Moujalled DM, et al. 2016. The MCL1 inhibitor S63845 is tolerable and effective in diverse cancer models. *Nature* **538**: 477–482.

Larson MH, Gilbert LA, Wang X, Lim WA, Weissman JS, Qi LS. 2013. CRISPR interference (CRISPRi) for sequence-specific control of gene expression. *Nat Protoc* **8**: 2180–2196.

Lehár J, Krueger AS, Avery W, Heilbut AM, Johansen LM, Price ER, Rickles RJ, Short III GF, Staunton JE, Jin X, et al. 2009. Synergistic drug combinations tend to improve therapeutically relevant selectivity. *Nat Biotechnol* **27**: 659–666.

Leibold J, Ruscetti M, Cao Z, Ho Y-J, Baslan T, Zou M, Abida W, Feucht J, Han T, Barriga FM, et al. 2020. Somatic Tissue Engineering in Mouse Models Reveals an Actionable Role for WNT Pathway Alterations in Prostate Cancer Metastasis. *Cancer Discov* **10**: 1038–1057.

Lens SMA, Medema RH. 2019. Cytokinesis defects and cancer. *Nat Rev Cancer* **19**: 32–45.

Li LB, Chang K-H, Wang P-R, Hirata RK, Papayannopoulou T, Russell DW. 2012. Trisomy Correction in Down Syndrome Induced Pluripotent Stem Cells. *Cell Stem Cell* **11**: 615–619.

Li X, Pu W, Zheng Q, Ai M, Chen S, Peng Y. 2022. Proteolysis-targeting chimeras (PROTACs) in cancer therapy. *Mol Cancer* **21**: 99.

Lin A, Giuliano CJ, Palladino A, John KM, Abramowicz C, Yuan ML, Sausville EL, Lukow DA, Liu L, Chait AR, et al. 2019. Off-target toxicity is a common mechanism of action of cancer drugs undergoing clinical trials. *Sci Transl Med* **11**.

Lin A, Sheltzer JM. 2020. Discovering and validating cancer genetic dependencies: approaches and pitfalls. *Nat Rev Genet* **21**: 671–682.

Liu J, Lichtenberg T, Hoadley KA, Poisson LM, Lazar AJ, Cherniack AD, Kovatich AJ, Benz CC, Levine DA, Lee AV, et al. 2018. An Integrated TCGA Pan-Cancer Clinical Data Resource to Drive High-Quality Survival Outcome Analytics. *Cell* **173**: 400-416.e11.

Liu Y, Chen C, Xu Z, Scuoppo C, Rillahan CD, Gao J, Spitzer B, Bosbach B, Kastenhuber ER, Baslan T, et al. 2016. Deletions linked to TP53 loss drive cancer through p53-independent mechanisms. *Nature* **531**: 471–475.

Liu Y, Mi Y, Mueller T, Kreibich S, Williams EG, Van Drogen A, Borel C, Frank M, Germain P-L, Bludau I, et al. 2019. Multi-omic measurements of heterogeneity in HeLa cells across laboratories. *Nat Biotechnol* **37**: 314–322.

Logsdon GA, Gambogi CW, Liskovykh MA, Barrey EJ, Larionov V, Miga KH, Heun P, Black BE. 2019. Human Artificial Chromosomes that Bypass Centromeric DNA. *Cell* **178**: 624-639.e19.

Lu B, Klingbeil O, Tarumoto Y, Somerville TDD, Huang Y-H, Wei Y, Wai DC, Low JKK, Milazzo JP, Wu XS, et al. 2018. A Transcription Factor Addiction in Leukemia Imposed by the MLL Promoter Sequence. *Cancer Cell* **34**: 970-981.e8.

Lukow DA, Sausville EL, Suri P, Chunduri NK, Wieland A, Leu J, Smith JC, Girish V, Kumar AA, Kendall J, et al. 2021. Chromosomal instability accelerates the evolution of resistance to anti-cancer therapies. *Dev Cell* **56**: 2427-2439.e4.

Lukow DA, Sheltzer JM. 2022. Chromosomal instability and aneuploidy as causes of cancer drug resistance. *Trends Cancer* **8**: 43–53.

Luna A, Elloumi F, Varma S, Wang Y, Rajapakse VN, Aladjem MI, Robert J, Sander C, Pommier Y, Reinhold WC. 2021. CellMiner Cross-Database (CellMinerCDB) version 1.2: Exploration of patient-derived cancer cell line pharmacogenomics. *Nucleic Acids Res* **49**: D1083–D1093.

Luo J, Solimini NL, Elledge SJ. 2009. Principles of Cancer Therapy: Oncogene and Non-oncogene Addiction. *Cell* **136**: 823–837.

Mackenzie KJ, Carroll P, Martin C-A, Murina O, Fluteau A, Simpson DJ, Olova N, Sutcliffe H, Rainger JK, Leitch A, et al. 2017. cGAS surveillance of micronuclei links genome instability to innate immunity. *Nature* **548**: 461–465.

Macpherson I, Montagnier L. 1964. Agar suspension culture for the selective assay of cells transformed by polyoma virus. *Virology* **23**: 291–294.

Maeser N, Khan A, Sun R. 2023. Somatic variant detection from multi-sampled genomic sequencing data of tumor specimens using the ith.Variant pipeline. *STAR Protoc* **4**: 101927.

Mahon FX, Deininger MW, Schultheis B, Chabrol J, Reiffers J, Goldman JM, Melo JV. 2000. Selection and characterization of BCR-ABL positive cell lines with differential sensitivity to the tyrosine kinase inhibitor STI571: diverse mechanisms of resistance. *Blood* **96**: 1070–1079.

Maia ARR, de Man J, Boon U, Janssen A, Song J-Y, Omerzu M, Sterrenburg JG, Prinsen MBW, Willemsen-Seegers N, de Roos JADM, et al. 2015. Inhibition of the spindle assembly checkpoint kinase TTK enhances the efficacy of docetaxel in a triple-negative breast cancer model. *Ann Oncol* **26**: 2180–2192.

Manasanch EE, Orlowski RZ. 2017. Proteasome inhibitors in cancer therapy. *Nat Rev Clin Oncol* **14**: 417–433.

Mansour SL, Thomas KR, Capecchi MR. 1988. Disruption of the proto-oncogene int-2 in mouse embryo-derived stem cells: a general strategy for targeting mutations to non-selectable genes. *Nature* **336**: 348–352.

Mayo P, Hartshorne T, Li K, McMunn-Gibson C, Spencer K, Schnetz-Boutaud N. 2010. CNV Analysis Using TaqMan Copy Number Assays. *Curr Protoc Hum Genet* **67**: 2.13.1-2.13.10.

McCarty NS, Graham AE, Studená L, Ledesma-Amaro R. 2020. Multiplexed CRISPR technologies for gene editing and transcriptional regulation. *Nat Commun* **11**: 1281.

McGranahan N, Favero F, de Bruin EC, Birkbak NJ, Szallasi Z, Swanton C. 2015. Clonal status of actionable driver events and the timing of mutational processes in cancer evolution. *Sci Transl Med* **7**: 283ra54-283ra54.

McKusick VA. 1985. Marcella O'Grady Boveri (1865-1950) and the chromosome theory of cancer. *J Med Genet* **22**: 431–440.

McShane E, Sin C, Zauber H, Wells JN, Donnelly N, Wang X, Hou J, Chen W, Storchova Z, Marsh JA, et al. 2016. Kinetic Analysis of Protein Stability Reveals Age-Dependent Degradation. *Cell* **167**: 803-815.e21.

Mehnert M, Li W, Wu C, Salovska B, Liu Y. 2019. Combining Rapid Data Independent Acquisition and CRISPR Gene Deletion for Studying Potential Protein Functions: A Case of HMGN1. *Proteomics* **19**: e1800438.

Meijer GA, Hermsen MA, Baak JP, van Diest PJ, Meuwissen SG, Belien JA, Hoovers JM, Joenje H, Snijders PJ, Walboomers JM. 1998. Progression from colorectal adenoma to carcinoma is associated with non- random chromosomal gains as detected by comparative genomic hybridisation. *J Clin Pathol* **51**: 901–909.

Michel LS, Liberal V, Chatterjee A, Kirchwegger R, Pasche B, Gerald W, Dobles M, Sorger PK, Murty VVVS, Benezra R. 2001. MAD2 haplo-insufficiency causes premature anaphase and chromosome instability in mammalian cells. *Nature* **409**: 355–359.

Moralli D, Monaco ZL. 2020. Gene expressing human artificial chromosome vectors: Advantages and challenges for gene therapy. *Exp Cell Res* **390**: 111931.

Mori S, Chang JT, Andrechek ER, Matsumura N, Baba T, Yao G, Kim JW, Gatza M, Murphy S, Nevins JR. 2009. Anchorage-independent cell growth signature identifies tumors with metastatic potential. *Oncogene* **28**: 2796–2805.

Mueller S, Engleitner T, Maresch R, Zukowska M, Lange S, Kaltenbacher T, Konukiewitz B, Öllinger R, Zwiebel M, Strong A, et al. 2018. Evolutionary routes and KRAS dosage define pancreatic cancer phenotypes. *Nature* **554**: 62–68.

Muleris M, Zafrani B, Validire P, Girodet J, Salmon R-J, Dutrillaux B. 1994. Cytogenetic study of 30 colorectal adenomas. *Cancer Genet Cytogenet* **74**: 104–108.

Nami B, Wang Z. 2018. Genetics and Expression Profile of the Tubulin Gene Superfamily in Breast Cancer Subtypes and Its Relation to Taxane Resistance. *Cancers* **10**: 274.

Nazarian R, Shi H, Wang Q, Kong X, Koya RC, Lee H, Chen Z, Lee M-K, Attar N, Sazegar H, et al. 2010. Melanomas acquire resistance to B-RAF(V600E) inhibition by RTK or N-RAS upregulation. *Nature* **468**: 973–977.

Nguyen B, Fong C, Luthra A, Smith SA, DiNatale RG, Nandakumar S, Walch H, Chatila WK, Madupuri R, Kundra R, et al. 2022. Genomic characterization of metastatic patterns from prospective clinical sequencing of 25,000 patients. *Cell* **185**: 563-575.e11.

Ohashi A, Ohori M, Iwai K, Nakayama Y, Nambu T, Morishita D, Kawamoto T, Miyamoto M, Hirayama T, Okaniwa M, et al. 2015. Aneuploidy generates proteotoxic stress and DNA damage concurrently with p53-mediated post-mitotic apoptosis in SAC-impaired cells. *Nat Commun* **6**: 7668.

O'Loughlin TA, Gilbert LA. 2019. Functional Genomics for Cancer Research: Applications In Vivo and In Vitro. *Annu Rev Cancer Biol* **3**: 345–363.

Ono M, Hirata A, Kometani T, Miyagawa M, Ueda S, Kinoshita H, Fujii T, Kuwano M. 2004. Sensitivity to gefitinib (Iressa, ZD1839) in non-small cell lung cancer cell lines correlates with dependence on the epidermal growth factor (EGF) receptor/extracellular signal-regulated kinase 1/2 and EGF receptor/Akt pathway for proliferation. *Mol Cancer Ther* **3**: 465–472.

Orth JD, Loewer A, Lahav G, Mitchison TJ. 2012. Prolonged mitotic arrest triggers partial activation of apoptosis, resulting in DNA damage and p53 induction ed. S. Doxsey. *Mol Biol Cell* **23**: 567–576.

Oudat R, Khan Z, Glassman AB. 2001. Detection of trisomy 8 in philadelphia chromosome-positive CML patients using conventional cytogenetic and interphase fluorescence in situ hybridization techniques and its relation to c-myc involvement. *Ann Clin Lab Sci* **31**: 68–74.

Paffenholz SV, Salvagno C, Ho Y-J, Limjoco M, Baslan T, Tian S, Kulick A, de Stanchina E, Wilkinson JE, Barriga FM, et al. 2022. Senescence induction dictates response to chemo- and immunotherapy in preclinical models of ovarian cancer. *Proc Natl Acad Sci* **119**: e2117754119.

Pagliarini R, Shao W, Sellers WR. 2015. Oncogene addiction: pathways of therapeutic response, resistance, and road maps toward a cure. *EMBO Rep* **16**: 280–296.

Pandis N, Heim S, Bardi G, Idvall I, Mandahl N, Mitelman F. 1992. Whole-arm t(1;16) and i(1q) as sole anomalies identify gain of 1 q as a primary chromosomal abnormality in breast cancer. *Genes Chromosomes Cancer* **5**: 235–238.

Papathanasiou S, Markoulaki S, Blaine LJ, Leibowitz ML, Zhang C-Z, Jaenisch R, Pellman D. 2021. Whole chromosome loss and genomic instability in mouse embryos after CRISPR-Cas9 genome editing. *Nat Commun* **12**: 5855.

Parada LF, Tabin CJ, Shih C, Weinberg RA. 1982. Human EJ bladder carcinoma oncogene is homologue of Harvey sarcoma virus ras gene. *Nature* **297**: 474–478.

Passerini V, Ozeri-Galai E, de Pagter MS, Donnelly N, Schmalbrock S, Kloosterman WP, Kerem B, Storchová Z. 2016. The presence of extra chromosomes leads to genomic instability. *Nat Commun* **7**: 10754.

Patel YD, Brown AJ, Zhu J, Rosignoli G, Gibson SJ, Hatton D, James DC. 2021. Control of Multigene Expression Stoichiometry in Mammalian Cells Using Synthetic Promoters. *ACS Synth Biol* **10**: 1155–1165.

Paterson C, Clevers H, Bozic I. 2020. Mathematical model of colorectal cancer initiation. *Proc Natl Acad Sci* **117**: 20681–20688.

Patkar S, Heselmeyer-Haddad K, Auslander N, Hirsch D, Camps J, Bronder D, Brown M, Chen W-D, Lokanga R, Wangsa D, et al. 2021. Hard wiring of normal tissue-specific chromosome-wide gene expression levels is an additional factor driving cancer type-specific aneuploidies. *Genome Med* **13**: 93.

PCAWG Evolution & Heterogeneity Working Group, PCAWG Consortium, Gerstung M, Jolly C, Leshchiner I, Dentro SC, Gonzalez S, Rosebrock D, Mitchell TJ, Rubanova Y, et al. 2020. The evolutionary history of 2,658 cancers. *Nature* **578**: 122–128.

Perez-Riverol Y, Csordas A, Bai J, Bernal-Llinares M, Hewapathirana S, Kundu DJ, Inuganti A, Griss J, Mayer G, Eisenacher M, et al. 2019. The PRIDE database and related tools and resources in 2019: improving support for quantification data. *Nucleic Acids Res* **47**: D442–D450.

Peters GJ. 2014. Novel Developments in the Use of Antimetabolites. *Nucleosides Nucleotides Nucleic Acids* **33**: 358–374.

Pfister G, Toor SM, Sasidharan Nair V, Elkord E. 2020. An evaluation of sorter induced cell stress (SICS) on peripheral blood mononuclear cells (PBMCs) after different sort conditions - Are your sorted cells getting SICS? *J Immunol Methods* **487**: 112902.

Pilié PG, Tang C, Mills GB, Yap TA. 2019. State-of-the-art strategies for targeting the DNA damage response in cancer. *Nat Rev Clin Oncol* **16**: 81–104.

Prasad K, Bloomfield M, Levi H, Keuper K, Bernhard SV, Baudoin NC, Leor G, Eliezer Y, Giam M, Wong CK, et al. 2022. Whole-Genome Duplication Shapes the Aneuploidy Landscape of Human Cancers. *Cancer Res* **82**: 1736–1752.

Privitera AP, Barresi V, Condorelli DF. 2021. Aberrations of Chromosomes 1 and 16 in Breast Cancer: A Framework for Cooperation of Transcriptionally Dysregulated Genes. *Cancers* **13**: 1585.

Purdom E, Ho C, Grasso CS, Quist MJ, Cho RJ, Spellman P. 2013. Methods and challenges in timing chromosomal abnormalities within cancer samples. *Bioinforma Oxf Engl* **29**: 3113–3120.

Qian X, McDonald A, Zhou H-J, Adams ND, Parrish CA, Duffy KJ, Fitch DM, Tedesco R, Ashcraft LW, Yao B, et al. 2010. Discovery of the First Potent and Selective Inhibitor of Centromere-Associated Protein E: GSK923295. *ACS Med Chem Lett* **1**: 30–34.

Quinton RJ, DiDomizio A, Vittoria MA, Kotýnková K, Ticas CJ, Patel S, Koga Y, Vakhshoorzadeh J, Hermance N, Kuroda TS, et al. 2021. Whole-genome doubling confers unique genetic vulnerabilities on tumour cells. *Nature* **590**: 492–497.

Rey S, Schito L, Wouters BG, Eliasof S, Kerbel RS. 2017. Targeting Hypoxia-Inducible Factors for Antiangiogenic Cancer Therapy. *Trends Cancer* **3**: 529–541.

Ross-Innes CS, Becq J, Warren A, Cheetham RK, Northen H, O'Donovan M, Malhotra S, di Pietro M, Ivakhno S, He M, et al. 2015. Whole-genome sequencing provides new insights into the clonal architecture of Barrett's esophagus and esophageal adenocarcinoma. *Nat Genet* **47**: 1038–1046.

Roy DM, Walsh LA, Desrichard A, Huse JT, Wu W, Gao J, Bose P, Lee W, Chan TA. 2016. Integrated Genomics for Pinpointing Survival Loci within Arm-Level Somatic Copy Number Alterations. *Cancer Cell* **29**: 737–750.

Sack LM, Davoli T, Li MZ, Li Y, Xu Q, Naxerova K, Wooten EC, Bernardi RJ, Martin TD, Chen T, et al. 2018. Profound Tissue Specificity in Proliferation Control Underlies Cancer Drivers and Aneuploidy Patterns. *Cell* **173**: 499-514.e23.

Salgia N, Pal SK, Chung V, Tagawa ST, Picus J, Babiker HM, Gupta S, Wadlow RC, Poore J, Peterson C, et al. 2019. Activity of RX-3117, an oral antimetabolite nucleoside, in subjects with advanced urothelial cancer: Preliminary results of a phase IIa study. *J Clin Oncol* **37**: 455–455.

Sanson KR, Hanna RE, Hegde M, Donovan KF, Strand C, Sullender ME, Vaimberg EW, Goodale A, Root DE, Piccioni F, et al. 2018. Optimized libraries for CRISPR-Cas9 genetic screens with multiple modalities. *Nat Commun* **9**. https://www.ncbi.nlm.nih.gov/pmc/articles/PMC6303322/ (Accessed May 20, 2020).

Santaguida S, Amon A. 2015. Short- and long-term effects of chromosome mis-segregation and aneuploidy. *Nat Rev Mol Cell Biol* **16**: 473–485.

Santaguida S, Vasile E, White E, Amon A. 2015. Aneuploidy-induced cellular stresses limit autophagic degradation. *Genes Dev* **29**: 2010–2021.

Santarius T, Shipley J, Brewer D, Stratton MR, Cooper CS. 2010. A census of amplified and overexpressed human cancer genes. *Nat Rev Cancer* **10**: 59–64.

Santos E, Martin-Zanca D, Reddy EP, Pierotti MA, Della Porta G, Barbacid M. 1984. Malignant Activation of a K- *ras* Oncogene in Lung Carcinoma But Not in Normal Tissue of the Same Patient. *Science* **223**: 661–664.

Sarkisjan D, Julsing JR, Smid K, Klerk D de, Kuilenburg ABP van, Meinsma R, Lee YB, Kim DJ, Peters GJ. 2016. The Cytidine Analog Fluorocyclopentenylcytosine (RX-3117) Is Activated by Uridine-Cytidine Kinase 2. *PLOS ONE* **11**: e0162901.

Satgé D, Sommelet D, Geneix A, Nishi M, Malet P, Vekemans M. 1998. A tumor profile in Down syndrome. *Am J Med Genet* **78**: 207–216.

Schmidt TM, Fonseca R, Usmani SZ. 2021. Chromosome 1q21 abnormalities in multiple myeloma. *Blood Cancer J* **11**: 83.

Schukken KM, Foijer F. 2018. CIN and Aneuploidy: Different Concepts, Different Consequences. *BioEssays* **40**: 1700147.

Schukken KM, Lin Y-C, Bakker PL, Schubert M, Preuss SF, Simon JE, van den Bos H, Storchova Z, Colomé-Tatché M, Bastians H, et al. 2020. Altering microtubule dynamics is synergistically toxic with spindle assembly checkpoint inhibition. *Life Sci Alliance* **3**: e201900499.

Schukken KM, Sheltzer J. 2022. Extensive protein dosage compensation in aneuploid human cancers. *Genome Res* gr.276378.121.

Schvartzman J-M, Sotillo R, Benezra R. 2010. Mitotic chromosomal instability and cancer: mouse modelling of the human disease. *Nat Rev Cancer* **10**: 102–115.

Schwab M, Ellison J, Busch M, Rosenau W, Varmus HE, Bishop JM. 1984. Enhanced expression of the human gene N-myc consequent to amplification of DNA may contribute to malignant progression of neuroblastoma. *Proc Natl Acad Sci* **81**: 4940–4944.

Shanmugathasan M, Jothy S. 2000. Apoptosis, anoikis and their relevance to the pathobiology of colon cancer. *Pathol Int* **50**: 273–279.

Sharma A, Trivedi NR, Zimmerman MA, Tuveson DA, Smith CD, Robertson GP. 2005. Mutant V599EB-Raf Regulates Growth and Vascular Development of Malignant Melanoma Tumors. *Cancer Res* **65**: 2412–2421.

Sharma SV, Settleman J. 2007. Oncogene addiction: setting the stage for molecularly targeted cancer therapy. *Genes Dev* **21**: 3214–3231.

Sheltzer JM, Amon A. 2011. The aneuploidy paradox: costs and benefits of an incorrect karyotype. *Trends Genet TIG* **27**: 446–453.

Sheltzer JM, Ko JH, Replogle JM, Habibe Burgos NC, Chung ES, Meehl CM, Sayles NM, Passerini V, Storchova Z, Amon A. 2017. Single-chromosome Gains Commonly Function as Tumor Suppressors. *Cancer Cell* **31**: 240–255.

Shen H, G. Maki C. 2011. Pharmacologic Activation of p53 by Small-Molecule MDM2 Antagonists. *Curr Pharm Des* **17**: 560–568.

Shi H, Moriceau G, Kong X, Lee M-K, Lee H, Koya RC, Ng C, Chodon T, Scolyer RA, Dahlman KB, et al. 2012. Melanoma whole-exome sequencing identifies V600EB-RAF amplification-mediated acquired B-RAF inhibitor resistance. *Nat Commun* **3**: 724.

Shin SI, Freedman VH, Risser R, Pollack R. 1975. Tumorigenicity of virus-transformed cells in nude mice is correlated specifically with anchorage independent growth in vitro. *Proc Natl Acad Sci* **72**: 4435–4439.

Shirasawa S, Furuse M, Yokoyama N, Sasazuki T. 1993. Altered Growth of Human Colon Cancer Cell Lines Disrupted at Activated Ki- *ras*. *Science* **260**: 85–88.

Shukla A, Nguyen THM, Moka SB, Ellis JJ, Grady JP, Oey H, Cristino AS, Khanna KK, Kroese DP, Krause L, et al. 2020. Chromosome arm aneuploidies shape tumour evolution and drug response. *Nat Commun* **11**: 449.

Silk AD, Zasadil LM, Holland AJ, Vitre B, Cleveland DW, Weaver BA. 2013. Chromosome missegregation rate predicts whether aneuploidy will promote or suppress tumors. *Proc Natl Acad Sci* **110**: E4134–E4141.

Simon JE, Bakker B, Foijer F. 2015. CINcere Modelling: What Have Mouse Models for Chromosome Instability Taught Us? In *Chromosomal Instability in Cancer Cells* (eds. B.M. Ghadimi and T. Ried), *Recent Results in Cancer Research*, pp. 39–60, Springer International Publishing, Cham https://doi.org/10.1007/978-3-319-20291-4_2 (Accessed December 23, 2022).

Singh N, Bhalla N. 2020. Moonlighting Proteins. *Annu Rev Genet* **54**: 265–285.

Siwko SK, Bu W, Gutierrez C, Lewis B, Jechlinger M, Schaffhausen B, Li Y. 2008. Lentivirus-Mediated Oncogene Introduction into Mammary Cells In Vivo Induces Tumors. *Neoplasia* **10**: 653-IN1.

Smith JC, Sheltzer JM. 2022. Genome-wide identification and analysis of prognostic features in human cancers. *Cell Rep* **38**: 110569.

Smith JC, Sheltzer JM. 2018. Systematic identification of mutations and copy number alterations associated with cancer patient prognosis ed. J. Settleman. *eLife* **7**: e39217.

Smyth GK. 2005. limma: Linear Models for Microarray Data. In *Bioinformatics and Computational Biology Solutions Using R and Bioconductor* (eds. R. Gentleman, V.J. Carey, W. Huber, R.A. Irizarry, and S. Dudoit), *Statistics for Biology and Health*, pp. 397–420, Springer, New York, NY https://doi.org/10.1007/0-387-29362-0_23 (Accessed January 3, 2023).

Solimini NL, Luo J, Elledge SJ. 2007. Non-Oncogene Addiction and the Stress Phenotype of Cancer Cells. *Cell* **130**: 986–988.

Somerville TDD, Xu Y, Miyabayashi K, Tiriac H, Cleary CR, Maia-Silva D, Milazzo JP, Tuveson DA, Vakoc CR. 2018. TP63-Mediated Enhancer Reprogramming Drives the Squamous Subtype of Pancreatic Ductal Adenocarcinoma. *Cell Rep* **25**: 1741-1755.e7.

Soto M, García-Santisteban I, Krenning L, Medema RH, Raaijmakers JA. 2018. Chromosomes trapped in micronuclei are liable to segregation errors. *J Cell Sci* jcs.214742.

Soule HD, Maloney TM, Wolman SR, Peterson WD, Brenz R, McGrath CM, Russo J, Pauley RJ, Jones RF, Brooks SC. 1990. Isolation and characterization of a spontaneously immortalized human breast epithelial cell line, MCF-10. *Cancer Res* **50**: 6075–6086.

Stehelin D, Varmus HE, Bishop JM, Vogt PK. 1976. DNA related to the transforming gene(s) of avian sarcoma viruses is present in normal avian DNA. *Nature* **260**: 170–173.

Stingele S, Stoehr G, Peplowska K, Cox J, Mann M, Storchova Z. 2012. Global analysis of genome, transcriptome and proteome reveals the response to aneuploidy in human cells. *Mol Syst Biol* **8**: 608.

Stopsack KH, Whittaker CA, Gerke TA, Loda M, Kantoff PW, Mucci LA, Amon A. 2019. Aneuploidy drives lethal progression in prostate cancer. *Proc Natl Acad Sci* **116**: 11390–11395.

Su XA, Ma D, Parsons JV, Replogle JM, Amatruda JF, Whittaker CA, Stegmaier K, Amon A. 2021. *RAD21* is a driver of chromosome 8 gain in Ewing sarcoma to mitigate replication stress. *Genes Dev* **35**: 556–572.

Sugrue MM, Shin DY, Lee SW, Aaronson SA. 1997. Wild-type p53 triggers a rapid senescence program in human tumor cells lacking functional p53. *Proc Natl Acad Sci* **94**: 9648–9653.

Sundaresan V, Ganly P, Hasleton P, Rudd R, Sinha G, Bleehen NM, Rabbitts P. 1992. p53 and chromosome 3 abnormalities, characteristic of malignant lung tumours, are detectable in preinvasive lesions of the bronchus. *Oncogene* **7**: 1989–1997.

Suzuki T, Kazuki Y, Hara T, Oshimura M. 2020. Current advances in microcell-mediated chromosome transfer technology and its applications. *Exp Cell Res* **390**: 111915.

Takezawa K, Pirazzoli V, Arcila ME, Nebhan CA, Song X, de Stanchina E, Ohashi K, Janjigian YY, Spitzler PJ, Melnick MA, et al. 2012. *HER2* Amplification: A Potential Mechanism of Acquired Resistance to EGFR Inhibition in *EGFR* -Mutant Lung Cancers That Lack the Second-Site *EGFR* T790M Mutation. *Cancer Discov* **2**: 922–933.

Tang Y-C, Williams BR, Siegel JJ, Amon A. 2011. Identification of Aneuploidy-Selective Antiproliferation Compounds. *Cell* **144**: 499–512.

Tang Y-C, Yuwen H, Wang K, Bruno PM, Bullock K, Deik A, Santaguida S, Trakala M, Pfau SJ, Zhong N, et al. 2017. Aneuploid Cell Survival Relies upon Sphingolipid Homeostasis. *Cancer Res* **77**: 5272–5286.

Taylor AM, Shih J, Ha G, Gao GF, Zhang X, Berger AC, Schumacher SE, Wang C, Hu H, Liu J, et al. 2018. Genomic and Functional Approaches to Understanding Cancer Aneuploidy. *Cancer Cell* **33**: 676-689.e3.

Taylor-Weiner A, Zack T, O'Donnell E, Guerriero JL, Bernard B, Reddy A, Han GC, AlDubayan S, Amin-Mansour A, Schumacher SE, et al. 2016. Genomic evolution and chemoresistance in germ-cell tumours. *Nature* **540**: 114–118.

The Cancer Genome Atlas Research Network, Weinstein JN, Collisson EA, Mills GB, Shaw KRM, Ozenberger BA, Ellrott K, Shmulevich I, Sander C, Stuart JM. 2013. The Cancer Genome Atlas Pan-Cancer analysis project. *Nat Genet* **45**: 1113–1120.

Thompson SL, Compton DA. 2008. Examining the link between chromosomal instability and aneuploidy in human cells. *J Cell Biol* **180**: 665–672.

Torres EM, Williams BR, Amon A. 2008. Aneuploidy: Cells Losing Their Balance. *Genetics* **179**: 737–746.

Torti D, Trusolino L. 2011. Oncogene addiction as a foundational rationale for targeted anti-cancer therapy: promises and perils. *EMBO Mol Med* **3**: 623–636.

Tovini L, Johnson SC, Andersen AM, Spierings DCJ, Wardenaar R, Foijer F, McClelland SE. 2022. *Inducing Specific Chromosome Mis-Segregation in Human Cells*. Cell Biology http://biorxiv.org/lookup/doi/10.1101/2022.04.19.486691 (Accessed November 18, 2022).

Trakala M, Aggarwal M, Sniffen C, Zasadil L, Carroll A, Ma D, Su XA, Wangsa D, Meyer A, Sieben CJ, et al. 2021. Clonal selection of stable aneuploidies in progenitor cells drives high-prevalence tumorigenesis. *Genes Dev* **35**: 1079–1092.

Truong MA, Cané-Gasull P, de Vries SG, Nijenhuis W, Wardenaar R, Kapitein LC, Foijer F, Lens SMA. 2022. *A motor-based approach to induce chromosome-specific mis-segregations in human cells*. Cell Biology http://biorxiv.org/lookup/doi/10.1101/2022.04.19.488790 (Accessed November 18, 2022).

Tsou C-C, Avtonomov D, Larsen B, Tucholska M, Choi H, Gingras A-C, Nesvizhskii AI. 2015. DIA-Umpire: comprehensive computational framework for data-independent acquisition proteomics. *Nat Methods* **12**: 258–264, 7 p following 264.

Uno N, Hiramatsu K, Uno K, Komoto S, Kazuki Y, Oshimura M. 2017. CRISPR/Cas9-induced transgene insertion and telomere-associated truncation of a single human chromosome for chromosome engineering in CHO and A9 cells. *Sci Rep* **7**: 12739.

van Jaarsveld RH, Kops GJPL. 2016. Difference Makers: Chromosomal Instability versus Aneuploidy in Cancer. *Trends Cancer* **2**: 561–571.

van Kuilenburg ABP, Meinsma R. 2016. The pivotal role of uridine-cytidine kinases in pyrimidine metabolism and activation of cytotoxic nucleoside analogues in neuroblastoma. *Biochim Biophys Acta BBA - Mol Basis Dis* **1862**: 1504–1512.

Van Rompay AR, Norda A, Lindén K, Johansson M, Karlsson A. 2001. Phosphorylation of uridine and cytidine nucleoside analogs by two human uridine-cytidine kinases. *Mol Pharmacol* **59**: 1181–1186.

Vasudevan A, Baruah PS, Smith JC, Wang Z, Sayles NM, Andrews P, Kendall J, Leu J, Chunduri NK, Levy D, et al. 2020. Single-Chromosomal Gains Can Function as Metastasis Suppressors and Promoters in Colon Cancer. *Dev Cell* **52**: 413-428.e6.

Vasudevan A, Schukken KM, Sausville EL, Girish V, Adebambo OA, Sheltzer JM. 2021. Aneuploidy as a promoter and suppressor of malignant growth. *Nat Rev Cancer* **21**: 89–103.

Veomett G, Prescott DM, Shay J, Porter KR. 1974. Reconstruction of Mammalian Cells from Nuclear and Cytoplasmic Components Separated by Treatment with Cytochalasin B. *Proc Natl Acad Sci* **71**: 1999–2002.

Verma UN, Surabhi RM, Schmaltieg A, Becerra C, Gaynor RB. 2003. Small interfering RNAs directed against beta-catenin inhibit the in vitro and in vivo growth of colon cancer cells. *Clin Cancer Res Off J Am Assoc Cancer Res* **9**: 1291–1300.

Vogelstein B, Papadopoulos N, Velculescu VE, Zhou S, Diaz LA, Kinzler KW. 2013. Cancer Genome Landscapes. *Science* **339**: 1546–1558.

Vogt PK. 2012. Retroviral oncogenes: a historical primer. *Nat Rev Cancer* **12**: 639–648.

Wang H, Guo M, Wei H, Chen Y. 2021. Targeting MCL-1 in cancer: current status and perspectives. *J Hematol OncolJ Hematol Oncol* **14**: 67.

Wang TC, Cardiff RD, Zukerberg L, Lees E, Arnold A, Schmidt EV. 1994. Mammary hyperplasia and carcinoma in MMTV-cyclin D1 transgenic mice. *Nature* **369**: 669–671.

Wang Y, Liu S, Zhang G, Zhou C, Zhu H, Zhou X, Quan L, Bai J, Xu N. 2005. Knockdown of c-Myc expression by RNAi inhibits MCF-7 breast tumor cells growth in vitro and in vivo. *Breast Cancer Res* **7**: R220.

Wang Z, Andrews P, Kendall J, Ma B, Hakker I, Rodgers L, Ronemus M, Wigler M, Levy D. 2016. SMASH, a fragmentation and sequencing method for genomic copy number analysis. *Genome Res* **26**: 844–851.

Wang Z, Xia Y, Mills L, Nikolakopoulos AN, Maeser N, Sheltzer JM, Sun R. 2022. *Evolving copy number gains promote tumor expansion and bolster mutational diversification*. Genomics http://biorxiv.org/lookup/doi/10.1101/2022.06.14.495959 (Accessed November 18, 2022).

Wasylishen AR, Stojanova A, Oliveri S, Rust AC, Schimmer AD, Penn LZ. 2011. New model systems provide insights into Myc-induced transformation. *Oncogene* **30**: 3727–3734.

Waters AM, Der CJ. 2018. KRAS: The Critical Driver and Therapeutic Target for Pancreatic Cancer. *Cold Spring Harb Perspect Med* **8**. https://www.ncbi.nlm.nih.gov/pmc/articles/PMC5995645/ (Accessed December 26, 2019).

Watkins TBK, Lim EL, Petkovic M, Elizalde S, Birkbak NJ, Wilson GA, Moore DA, Grönroos E, Rowan A, Dewhurst SM, et al. 2020. Pervasive chromosomal instability and karyotype order in tumour evolution. *Nature* **587**: 126–132.

Weaver BAA, Cleveland DW. 2006. Does aneuploidy cause cancer? *Curr Opin Cell Biol* **18**: 658–667.

Weaver BAA, Silk AD, Montagna C, Verdier-Pinard P, Cleveland DW. 2007. Aneuploidy Acts Both Oncogenically and as a Tumor Suppressor. *Cancer Cell* **11**: 25–36.

Weinstein IB. 2002. Addiction to Oncogenes--the Achilles Heal of Cancer. *Science* **297**: 63–64.

Weinstein IB, Begemann M, Zhou P, Han EK, Sgambato A, Doki Y, Arber N, Ciaparrone M, Yamamoto H. 1997. Disorders in cell circuitry associated with multistage carcinogenesis: exploitable targets for cancer prevention and therapy. *Clin Cancer Res Off J Am Assoc Cancer Res* **3**: 2696–2702.

Weinstein IB, Joe A. 2008. Oncogene Addiction. *Cancer Res* **68**: 3077–3080.

Weinstein IB, Joe AK. 2006. Mechanisms of Disease: oncogene addiction—a rationale for molecular targeting in cancer therapy. *Nat Clin Pract Oncol* **3**: 448–457.

Westover D, Zugazagoitia J, Cho BC, Lovly CM, Paz-Ares L. 2018. Mechanisms of acquired resistance to first- and second-generation EGFR tyrosine kinase inhibitors. *Ann Oncol* **29**: i10–i19.

Wickham H, Averick M, Bryan J, Chang W, McGowan LD, François R, Grolemund G, Hayes A, Henry L, Hester J, et al. 2019. Welcome to the Tidyverse. *J Open Source Softw* **4**: 1686.

Wistuba II, Behrens C, Virmani AK, Mele G, Milchgrub S, Girard L, Fondon JW, Garner HR, McKay B, Latif F, et al. 2000. High resolution chromosome 3p allelotyping of human lung cancer and preneoplastic/preinvasive bronchial epithelium reveals multiple, discontinuous sites of 3p allele loss and three regions of frequent breakpoints. *Cancer Res* **60**: 1949–1960.

Wouters BJ. 2021. Targeting IDH1 and IDH2 Mutations in Acute Myeloid Leukemia: Emerging Options and Pending Questions. *HemaSphere* **5**: e583.

Wu XS, He X-Y, Ipsaro JJ, Huang Y-H, Preall JB, Ng D, Shue YT, Sage J, Egeblad M, Joshua-Tor L, et al. 2022. OCA-T1 and OCA-T2 are coactivators of POU2F3 in the tuft cell lineage. *Nature* **607**: 169–175.

Xue W, Kitzing T, Roessler S, Zuber J, Krasnitz A, Schultz N, Revill K, Weissmueller S, Rappaport AR, Simon J, et al. 2012. A cluster of cooperating tumor-suppressor gene candidates in chromosomal deletions. *Proc Natl Acad Sci* **109**: 8212–8217.

Yasuda Y, Ozasa H, Kim YH, Yamazoe M, Ajimizu H, Yamamoto Funazo T, Nomizo T, Tsuji T, Yoshida H, Sakamori Y, et al. 2020. MCL1 inhibition is effective against a subset of small-cell lung cancer with high MCL1 and low BCL-XL expression. *Cell Death Dis* **11**: 177.

Yates LR, Knappskog S, Wedge D, Farmery JHR, Gonzalez S, Martincorena I, Alexandrov LB, Van Loo P, Haugland HK, Lilleng PK, et al. 2017. Genomic Evolution of Breast Cancer Metastasis and Relapse. *Cancer Cell* **32**: 169-184.e7.

Yawata A, Adachi M, Okuda H, Naishiro Y, Takamura T, Hareyama M, Takayama S, Reed JC, Imai K. 1998. Prolonged cell survival enhances peritoneal dissemination of gastric cancer cells. *Oncogene* **16**: 2681–2686.

Ying H, Kimmelman AC, Lyssiotis CA, Hua S, Chu GC, Fletcher-Sananikone E, Locasale JW, Son J, Zhang H, Coloff JL, et al. 2012. Oncogenic Kras Maintains Pancreatic Tumors through Regulation of Anabolic Glucose Metabolism. *Cell* **149**: 656–670.

Zack TI, Schumacher SE, Carter SL, Cherniack AD, Saksena G, Tabak B, Lawrence MS, Zhang C-Z, Wala J, Mermel CH, et al. 2013. Pan-cancer patterns of somatic copy number alteration. *Nat Genet* **45**: 1134–1140.

Zhao Y, Adjei AA. 2015. Targeting Angiogenesis in Cancer Therapy: Moving Beyond Vascular Endothelial Growth Factor. *The Oncologist* **20**: 660–673.

Zhong L, Li Y, Xiong L, Wang W, Wu M, Yuan T, Yang W, Tian C, Miao Z, Wang T, et al. 2021. Small molecules in targeted cancer therapy: advances, challenges, and future perspectives. *Signal Transduct Target Ther* **6**: 201.

Zhou P, Bogacki R, McReynolds L, Howley PM. 2000. Harnessing the Ubiquitination Machinery to Target the Degradation of Specific Cellular Proteins. *Mol Cell* **6**: 751–756.

Zhou P, Jiang W, Zhang YJ, Kahn SM, Schieren I, Santella RM, Weinstein IB. 1995. Antisense to cyclin D1 inhibits growth and reverses the transformed phenotype of human esophageal cancer cells. *Oncogene* **11**: 571–580.

Zhu PJ, Khatiwada S, Cui Y, Reineke LC, Dooling SW, Kim JJ, Li W, Walter P, Costa-Mattioli M. 2019. Activation of the ISR mediates the behavioral and neurophysiological abnormalities in Down syndrome. *Science* **366**: 843–849.

Zimonjic D, Brooks MW, Popescu N, Weinberg RA, Hahn WC. 2001. Derivation of Human Tumor Cells in Vitro without Widespread Genomic Instability. *Cancer Res* **61**: 8838–8844.

Zuccaro MV, Xu J, Mitchell C, Marin D, Zimmerman R, Rana B, Weinstein E, King RT, Palmerola KL, Smith ME, et al. 2020. Allele-Specific Chromosome Removal after Cas9 Cleavage in Human Embryos. *Cell* **183**: 1650-1664.e15.